CHARACTERIZATION OF THE PROTEIN-PROTEIN INTERACTIONS AND CATALYTIC MECHANISM OF HEME A SYNTHASE

By

Elise Dawn Rivett

A DISSERTATION

Submitted to
Michigan State University
in partial fulfillment of the requirements
for the degree of

Biochemistry and Molecular Biology — Doctor of Philosophy

2021

ABSTRACT

CHARACTERIZATION OF THE PROTEIN-PROTEIN INTERACTIONS AND CATALYTIC MECHANISM OF HEME A SYNTHASE

By

Elise Dawn Rivett

Aerobic respiration is a key energy-producing pathway in many prokaryotes and virtually all eukaryotes. The final step of aerobic respiration is most commonly catalyzed by heme-copper oxidases embedded in the cytoplasmic or mitochondrial membrane. The majority of these terminal oxidases are aa_3 cytochrome *c* oxidases, meaning that the heme cofactor is a modified heme known as heme *a*. Despite the critical role of heme *a* in aerobic respiration, many details of the catalytic mechanism by which heme *b*, the prototypical cellular heme, is converted to heme *o* (a biosynthetic intermediate) and then to heme *a* have yet to be elucidated. The mechanism of heme transfer among the enzymes in the heme *a* biosynthetic pathway also remains unclear. In this dissertation, I report on my investigation of the protein-protein interactions of heme *a* synthase and the catalytic mechanism of this enzyme. Chapter 1 provides an overview of the structural and biochemical data that is currently available for heme *o* synthase and heme *a* synthase and also summarizes what is currently known about prenylated heme trafficking. Chapter 2 reports on our investigations of the protein-protein interactions of heme *a* synthase in *Saccharomyces cerevisiae*, a model eukaryote. Surprisingly, we found that heme *a* synthase can interact with the cytochrome bc_1 complex even in the absence of cytochrome *c* oxidase. Finally, Chapter 3 summarizes our study of the catalytic mechanism of heme *a* synthase using both prokaryotic and eukaryotic heme *a* synthase variants. Our data suggest that a conserved glutamate stabilizes a carbocation that is proposed to form during catalysis. Overall, this dissertation contributes to our understanding of how heme *a* synthase functions at the catalytic level and as a participant in intracellular heme trafficking.

ACKNOWLEDGEMENTS

I thank Dr. Lim Heo and Prof. Michael Feig (Michigan State University) for constructing the model of heme *o* synthase presented in Chapter 1 and for helpful discussion. I gratefully acknowledge Prof. Robert Hausinger (Michigan State University) for his critical reading of the manuscript that formed the basis for Chapter 1. I thank Jon Dietz and Prof. Oleh Khalimonchuk (Univeristy of Nebraska-Lincoln) and Prof. Jennifer Fox (College of Charleston) for helpful discussion about Cox15. Dr. Oleh Khalimonchuck also kindly provided the pRS415 plasmids used in Chapter 2 and the pRS426 plasmids used in Chapter 3. I gratefully acknowledge Dr. Emily Herwaldt, who designed the studies presented in Chapter 2 and wrote the published manuscript. Finally, I would like to thank Prof. Eric Hegg for his mentorship.

TABLE OF CONTENTS

LIST OF TABLES

LIST OF FIGURES

KEY TO ABBREVIATIONS

co-IP	Co-immunoprecipitation
BN-PAGE	Blue native polyacrylamide gel electrophoresis
Cryo-EM	Cryo electron microscopy
DDM	*n*-dodecyl-β-D-maltopyranoside
HA	Hemagglutinin
HAS	Heme *a* synthase
HOS	Heme *o* synthase
HL	Helix-loop
IMM	Inner mitochondrial membrane
IMS	Intermembrane space
MBP	Maltose binding protein
N-side	Negative side (of a membrane)
Ni-NTA	Nickel-nitrilotriacetic acid
P-side	Positive side (of a membrane)
PBS	Phosphate-buffered saline
PMSF	Phenylmethylsulfonyl fluoride
PPIX	Protoporphyrin IX
PP_i	Pyrophosphate
PVDF	Polyvinylidene difluoride
TBS	Tris-buffered saline
TFA	Trifluoracetic acid
TM	Transmembrane
WT	Wild-type

XPP	Polyprenyl diphosphate
YPD	Liquid medium: 1% yeast extract, 2% peptone, and 2% glucose

Chapter 1: Biosynthesis and trafficking of heme *o* and heme *a*: New structural insights and their implications for reaction mechanisms and prenylated heme transfer[1]

[1] This chapter is adapted from Rivett, E. D, Heo, L., Feig. M., and Hegg, E. L. Biosynthesis and trafficking of heme *o* and heme *a*: New structural insights and their implications for reaction mechanisms and prenylated heme transfer. *Critical reviews in biochemistry and molecular biology* (In preparation). E. D. Rivett wrote the paper. L. Heo and M. Feig prepared the structural model shown in Figure 1.3.

Abstract

Aerobic respiration is a key energy-producing pathway in many prokaryotes and virtually all eukaryotes. The final step of aerobic respiration is most commonly catalyzed by heme-copper oxidases embedded in the cytoplasmic or mitochondrial membrane. The majority of these terminal oxidases contain a prenylated heme (typically heme *a* or occasionally heme *o*) in the bimetallic active site. In addition, many heme-copper oxidases, including mitochondrial cytochrome *c* oxidases, also possess a second heme *a* molecule that serves in an electron transfer capacity. Despite the critical role of heme *a* in the electron transport chain, the details of the mechanism by which heme *b*, the prototypical cellular heme, is converted to heme *o* and then to heme *a* remain poorly understood. The mechanism of heme transfer between enzymes in this pathway is also unclear. Recent investigations, however, have helped clarify some elements of heme *a* biosynthesis. These new studies include structural determination of heme *o* synthase (HOS) homologs and of bacterial heme *a* synthase (HAS). In this review, I discuss the insight gained from these structural advances. In particular, I present a new structural model of HOS based on distance restraints from inferred coevolutionary relationships and refined by molecular dynamics simulations that is in good agreement with the experimentally determined structures of HOS homologs. I also analyze the two structures of HAS that have recently been solved by other groups. For both HOS and HAS, I discuss the proposed catalytic mechanisms and highlight how new insights into the heme binding site locations shed light on previously obtained biochemical data. Finally, I explore the implications of the new structural data in the broader context of heme trafficking in the heme *a* biosynthetic pathway and heme-copper oxidase assembly.

Introduction

For practically all aerobic forms of life, respiration is a key pathway for producing useable cellular energy in the form of ATP. Aerobic respiration is the metabolic process in which electrons are transferred from intermediate redox cofactors (such as NADH and $FADH_2$) to a membrane-localized electron transport chain and finally to O_2, the terminal electron acceptor.

The flow of electrons through the electron transport chain is coupled to movement of protons across the membrane from the N-side (negative side) to the P-side (positive side), generating the chemiosmotic gradient that drives ATP production. To allow for continued flow of electrons through the electron transport chain, the terminal oxidase accepts electrons from the chain while catalyzing the four-electron reduction of O_2 to H_2O (1). Two unrelated superfamilies of terminal oxidases are known, the *bd* quinol oxidases and the heme-copper oxidases. As their respective names suggest, the *bd* oxidases use hemes *b* and *d* as cofactors, while the heme-copper oxidases have a bimetallic heme-copper active site, as well as additional heme and copper cofactors. While *bd* oxidases are only found in certain bacterial and archaeal phyla, heme-copper oxidases are found in all three domains of life (2-6).

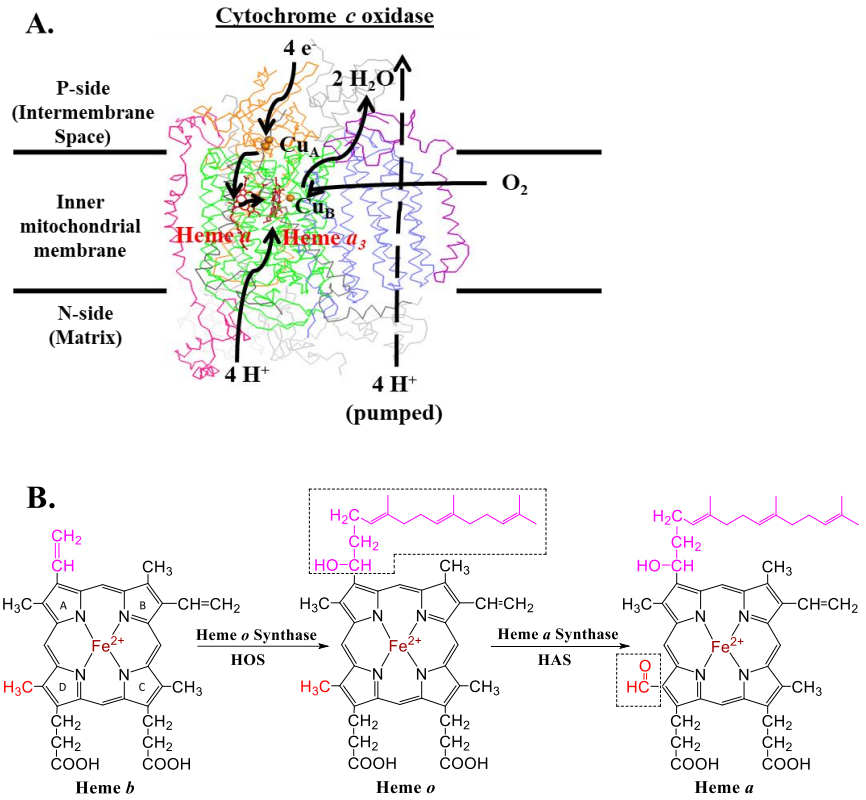

Figure 1.1 Heme *a*, a cofactor of cytochrome *c* oxidase, is synthesized from heme *b* via two enzymatically catalyzed steps

A. Heme-copper oxidases catalyze the 4-electron reduction of O_2 to H_2O with concomitant proton pumping. The 11-subunit *S. cerevisiae* cytochrome *c* oxidase (a mitochondrial-type aa_3 oxidase) is shown. Subunit I (which binds low-spin heme *a*, high-spin heme a_3, and Cu_B) is shown in green. Subunit II (which includes the binuclear Cu_A site) is shown in orange, and subunit III is shown in slate. Nuclear-encoded subunits Cox5a and Cox13 are shown in hot pink and purple, respectively. The remaining 5 nuclear-encoded subunits are shown in gray. Electrons are transferred from cytochrome *c* (not shown) to the Cu_A site, then to heme *a*, and finally to the binuclear active site (heme a_3 and Cu_B) where O_2 is reduced to H_2O. Although varied proton pumping stoichiometries have been observed for isolated heme-copper oxidases from different families, family A oxidases (such as the one shown) have the greatest proton pumping capacities, with pumped H^+/e^- ratios approaching 1 (7). This figure was prepared using a previously published homology model of *S. cerevisiae* cytochrome *c* oxidase based on the bovine crystal structure (8). B. Summary of heme *o* and heme *a* biosynthesis. Heme *o* is synthesized from heme *b* by the conversion of the vinyl group from pyrrole ring A (C2 position) to a hydroxyethylfarnesyl moiety (both shown in pink). Heme *a* is synthesized from heme *o* by the oxidation of the pyrrole ring D formyl group (C8 position) to an aldehyde (shown in red).

Heme-copper oxidases have two heme cofactors with different axial ligand coordination and spin states (Figure 1.1A). One of these hemes is a low-spin, *bis*-histidine axially ligated heme that transfers electrons to the active site. In contrast, the active site heme is high-spin and only has one axial histidine ligand (1,4,9). Depending on the specific heme-copper oxidase, different types of hemes with different porphyrin ring substituents occupy the low-spin and high-spin heme binding sites. The low-spin heme binding site may be occupied by heme *a* or *b*, while the high-spin site may be occupied by heme *a*, *b*, or *o* (4). In addition to the low-spin and high-spin heme binding sites that are common to all heme-copper oxidases, some oxidases have additional heme binding sites that precede the low-spin and high-spin hemes in the oxidase's electron transfer pathway. The heme type found in these sites is invariably heme *c* (heme *b* that is covalently crosslinked to the protein via thioether linkages to cysteine residues) (10). By convention, when naming oxidases, the hemes are listed in the order of electron flow through the oxidase: heme *c* (where present) is listed first, followed by the low-spin heme, and ending with the high-spin (active site) heme, which is designated with a subscript "3." Although the heme-copper oxidase superfamily can be divided into three phylogenetically distinct families (A, B, and C), heme types do not strictly correlate with phylogeny: All family-C oxidases are cbb_3 cytochrome *c* oxidases, while family A includes mitochondrial-like aa_3 oxidases and bo_3 oxidases, and family B includes ba_3 oxidases as well as a different subset of aa_3 oxidases (7,10). While C-type oxidases and B-type oxidases have only been identified in bacteria or bacteria and archaea, respectively, A-type oxidases are present in all three domains of life and account for the majority of the heme-copper oxidase sequences that have been identified thus far (2-6,11). Furthermore, although many prokaryotes have branched electron transport chains with multiple types of terminal oxidases, the only type of terminal oxidase present in eukaryotic mitochondria is an aa_3 cytochrome *c* oxidase from family A (6,7,10). Given the widespread role of heme *a* as a

cofactor for terminal heme-copper oxidases, heme *a* biosynthesis is a critical component of primary metabolism for many aerobic organisms, and is essential for energy production in higher eukaryotes.

Hemes *a* and *o* are chemically modified derivatives of the prototypical heme, heme *b*. Hemes *o* and *a* can be synthesized from heme *b* via sequential enzyme-catalyzed reactions (Figure 1.1B). First, heme *b*'s vinyl group from pyrrole ring A (the C2 position in Fischer nomenclature) is converted to a hydroxyethylfarnesyl moiety, producing heme *o* (12). This reaction is catalyzed by heme *o* synthase (HOS), a prenyltransferase (13-19). Then, in organisms requiring heme *a*, heme *a* synthase (HAS) catalyzes the oxidation of the pyrrole ring D methyl (C8 position) to a formyl group (15,18-25). The only known function for heme *a* is to serve as a cofactor for heme-copper terminal oxidases, and, in some acidophilic archaea, as a cofactor for the cytochrome *b*-like subunit of quinol reductases (analogous to mitochondrial complex III) (4,26-29). Heme *o* serves either as a precursor for heme *a* synthesis or as a terminal oxidase cofactor (or both, in some prokaryotic species) (4,30-37).

Organism	Prenylated heme(s)	HOS		HAS		References
		Gene[a]	TM#[b]	Gene[a]	TM#[b]	
Bacteria						
Bacillus subtilis	a	*ctaB1*	9			(19,21,38,39)
		ctaB2	9			
				ctaA	8	
Thermus thermophilus	a_S	*ctaAB*	17[c]	*ctaAB*	17[c]	(26,40)
Archaea						
Sulfolobus acidocaldarius	a_S	*ctaB*	9[d]	Unknown		(26,27)
Acidianus ambivalens (Desulfurolobus ambivalens)	a_S	D1866_00335	9[d]	Unknown		(26,29)
Halobacterium salinarum	a_S	*ctaAB*	13[d]	*ctaAB*	13[d]	(26)
				ctaA	8[d]	
Natronomonas phaoronis	a_S	*ctaAB1*	13[e]	*ctaAB1*	13[e]	(26,41)
		ctaAB2	13[e]	*ctaAB2*	13[e]	
				ctaA	8[d]	
Thermoplasma acidophilum	o_T	*ctaB*	9	NA		(26)
Pyrobaculum aerophilum	o_{P1}, o_{P2}, a_S	*ctaB1*	9	Unknown		(26)
		ctaB2	9			

Table 1.1: Genes encoding HOS and HAS from selected prokaryotic species that synthesize alternate prenylated hemes

The genes for *B. subtilis* HOS and HAS (which have been biochemically characterized and which synthesize standard heme *o* and heme *a*, respectively) are included for reference. All genes encoding HOS listed include highly conserved residues that are expected to be required for activity. The archaeal HAS sequences predicted to have 8 TM helices are missing one or both of the highly conserved C-terminal histidines, but these species also contain a 4-TM version of HAS fused to HOS.

Table 1.1 (cont'd)

[a]Gene names are taken from Uniprot with the exception of the fused genes encoding HAS and HOS from *T. thermophilus*, *H. salinarum*, *and N. phaoronis*, which were renamed *ctaAB*.
[b]The number (or predicted number) of transmembrane (TM) helices (TM#) is listed.
[c]The gene encoding HAS (TM1-8) is fused to the gene encoding HOS (TM9-17). The HAS sequence is missing both of the C-terminal highly conserved histidines.
[d]The predicted number of TM helices from Uniprot has been corrected by the authors after manual inspection of sequence alignments.
[e]The gene encoding a shortened HAS variant (TM1-4) is fused to the gene encoding HOS (TM5-13).

The biosynthesis of hemes *o* and *a* appears to be a universally conserved process that uses heme *b* as the initial porphyrin substrate. All known genes encoding HOS belong to the same sub-family of the aromatic intramembrane prenyltransferase (UbiA) superfamily (15,42). Similarly, all identified HAS-encoding genes belong to one family (Cox15/CtaA family) (43,44). Although alternate forms of heme *o* (hemes o_T, o_{P1}, o_{P2}) and heme *a* (heme a_S) have been identified in archaea and one bacterial species, the deviations from the "normal" prenylated heme structures are minimal and are located on pyrrole ring A at the C2 position (26-28,40,43,45). In most cases, genes for canonical HOS and HAS can be identified within the genomes of the species in question (Table 1.1) (43,46). This association suggests that the modified hemes are synthesized by a canonical HOS that uses an alternate prenyl donor or a slightly different reaction mechanism instead of by an unrelated enzyme (see the section entitled "Heme *o* synthase"). Oxidation of the methyl group on pyrrole ring D of the heme *o* variant would then be catalyzed by a canonical HAS.

While the structures and biochemical reactions of all eight enzymes that catalyze the steps of the most common heme *b* biosynthetic pathway have been studied extensively (47,48), prenylated heme biosynthesis is not as well understood. This is partly due to the fact that HOS and HAS are both integral membrane proteins that can be difficult to overexpress and purify. However, recent progress has been made in the structural characterization of both enzymes. The first crystal structures from the prenyltransferase superfamily that HOS belongs to have been solved (49,50), and we have used these new structural data and a

coevolution-based machine learning technique to model the structure of HOS. The structure of HAS from two different species has also been determined independently by X-ray crystallography and cryo-electron microscopy (cryo-EM), and the substrate-bound structure of HAS was modelled on the basis of the crystal structure (51,52). The new structural information about HOS and HAS provides fresh insights into the structure-function paradigm and mechanism of these enzymes, and also raises new questions about intracellular transfer of hemes *b*, *o*, and *a*.

Heme* o *synthase

Heme o *properties and function*

Heme *o* is synthesized from heme *b* by the conversion of the vinyl group of pyrrole ring A (C2 vinyl) to a hydroxyethylfarnesyl group (Figures 1B, 2) (12,14,15,53). While the reduction potentials of hemes *b* and *o* are similar, the addition of the lipid tail produces a porphyrin that can bind a protein more tightly. A direct comparison of these two hemes binding to the same synthetic heme protein maquette shows the hydroxyethylfarnesyl moiety increases the binding affinity of heme *o* by a factor of 700 (ferrous state) and 40,000 (ferric state) relative to heme *b* (54). The hydroxyl group of the hydroxyethylfarnesyl moiety for the high-spin (active site) heme is located in one of the proton channels in family-A heme-copper oxidases and has been proposed to participate in proton delivery to the active site (55-57). In addition, this hydroxyl group forms a hydrogen bond with the tyrosine residue that is crosslinked to one of the histidine ligands of copper in the oxidase's binuclear active site, possibly allowing for modulation of the tyrosine pK_a in aa_3 oxidases (9,58,59). Interestingly, in cbb_3 oxidases, a slightly different arrangement of the active site may compensate for the absence of this hydroxyl group (9,58). Thus, the hydroxyethylfarnesyl tail of heme *o* (and heme *a*) seems to play a major role in enhancing the heme's affinity for its oxidase and may also play a role in catalysis.

HOS mechanism

Heme *o* synthase (HOS) catalyzes the conversion of a vinyl group from heme *b* (located on pyrrole ring A) to a hydroxyethylfarnesyl moiety, producing heme *o* (Figure 1.2). HOS, which is located either in the prokaryotic cytoplasmic membrane or the eukaryotic inner mitochondrial membrane, belongs to the UbiA superfamily of intramembrane aromatic prenyltransferases (14,60). These integral membrane proteins transfer polyprenyl groups from polyprenyl diphosphates of varying chain length (XPP) to a variety of aromatic (and some non-aromatic) substrates, including heme *b*, chlorophyll, and the ubiquinone precursor *p*-hydroxybenzoate (42). In the general catalytic mechanism for this superfamily, the XPP substrate is cleaved to generate a polyprenyl carbocation, followed by condensation with the aromatic substrate and elimination of a proton to generate the prenylated product. For example, *p*-hydroxybenzoate octaprenyltransferase (UbiA) catalyzes the transfer of an octaprenyl group from octaprenyldiphosphate to the *meta* position of *p*-hydroxybenzoate. This reaction requires the presence of divalent metal cofactors, presumably to facilitate phosphoester bond cleavage by making the pyrophosphate a better leaving group (42,61-63). The proposed ionization-condensation-elimination mechanism for the UbiA superfamily is based on biochemical characterization of the structurally related soluble isoprenyl pyrophosphate synthases (IPPS), which also rely on divalent metal cations for pyrophosphate ionization (64-66). While this mechanism is often drawn as three distinct steps, the available experimental data for IPPS would also be consistent with the first two steps occurring in a concerted fashion, without the formation of a distinct carbocation intermediate (64). There is, however, evidence for a carbocation intermediate in an unrelated family of soluble aromatic prenyltransferases, where the cation intermediate appears to be stabilized by interactions with active site tyrosine residues and with the aromatic substrate via cation-π interactions (67-71). Regardless of whether phosphoester bond cleavage and C-C bond formation occur

sequentially or concurrently, the final step in the general catalytic mechanism of intramembrane aromatic prenyltransferases is elimination of a proton and rearomatization of the prenyl acceptor. One key difference between the prototypical UbiA reaction and the reaction catalyzed by HOS is that instead of proton abstraction, HOS catalyzes hydroxylation at the C1 position of the attacking vinyl. At present, the mechanism for this hydroxylation is unknown, although simultaneous hydroxylation and condensation has been proposed (14,15).

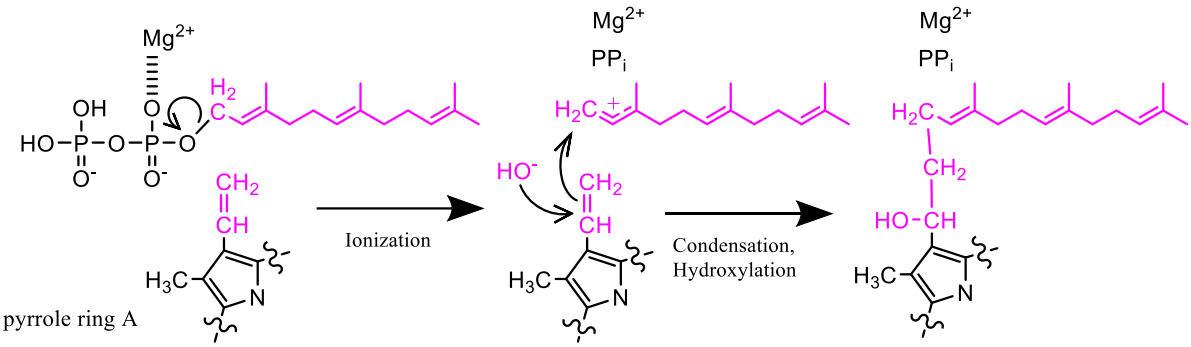

Figure 1.2 Proposed reaction mechanism for the conversion of heme *b* to heme *o*

HOS catalyzes the transfer of a farnesyl moiety (in pink) from farnesyl diphosphate to the vinyl group of heme *b* (in pink) at pyrrole ring A. For simplicity, only pyrrole ring A of the heme is shown. Ionization of farnesyl diphosphate yields a farnesyl cation intermediate stabilized by delocalization across C′1-C′3. Interactions with Mg^{2+} ions (only one shown here) make the pyrophosphate a better leaving group and allow ionization to proceed. The vinyl group then attacks the carbocation intermediate to form a new C-C bond (condensation), and C1 is hydroxylated to produce heme *o*, which has a hydroxyethylfarnesyl substituent at pyrrole ring A. Note that the timing of these steps has not been established for HOS.

Interestingly, archaea synthesize modified versions of heme *o* with the usual hydroxyethylfarnesyl moiety replaced by an ethylprenyl group (hemes o_T and o_{P1}) or a hydroxyethylgeranylgeranyl group (heme o_{P2}) (26). The lack of a hydroxyl group in hemes o_T and o_{P1} suggests that for these hemes, heme *o* synthesis proceeds via the more common ionization-condensation-elimination mechanism, although dehydration of the hydroxyprenyl group could also occur (15). Synthesis of hemes with longer (C20) prenyl groups (o_{P1}, o_{P2},

and a_S) is thought to be due to the higher availability of geranylgeranyl pyrophosphate in some archaea (26).

Only one *in vitro* activity assay has been reported for HOS. This assay was performed using cytoplasmic membrane vesicles prepared from *E. coli* overexpressing the native *E. coli* HOS (CyoE, referred to as *Ec*HOS) (14). Heme *o* synthesis was observed upon addition of hemin (heme *b*), farnesyl diphosphate (FPP), Mg^{2+} or Ca^{2+}, and a reducing agent to the membrane vesicles. Reduction of the heme is presumably required to increase the electron density of the heme's vinyl groups and thus enable the vinyl C2 to perform a nucleophilic attack (14). This part of the mechanism is similar to the proposed mechanism for the biosynthesis of cytochrome *c*, which also involves nucleophilic attack by the vinyl groups of the substrate heme (72). Although studying HOS via *in vitro* activity assays is complicated by the difficulties associated with overexpressing a membrane protein, *in vivo* activity assays have been used to study the importance of key residues in different domains of HOS (73). Combined with insight gained from the available structures of UbiA prenyltransferases and a new structural model of HOS (42,49,50,74), a picture of how HOS binds cofactors and substrates is beginning to emerge.

Overview of aromatic intramembrane prenyltransferase (UbiA) superfamily structures

To date, two intermembrane prenyltransferases from hyperthermophilic archaea have been crystallized: *Aeropyrum pernix* UbiA (*Ap*UbiA) and *Archaeoglobus fulgidus* UbiA (*Af*UbiA) (49,50). The native substrates have not been identified for either enzyme, but *Ap*UbiA appears to be most closely related to the *p*-hydroxybenzoate prenyltransferase (UbiA) sub-family, while *Af*UbiA is not closely related to any well-characterized sub-families (42). The overall architectures of *Ap*UbiA and *Af*UbiA are very similar. Both have nine transmembrane (TM) helices. TM1-4 and TM5-8 form four-helical bundles that are related to each other by pseudo-twofold symmetry, suggesting an ancient gene duplication and fusion (50). This pair

of four-helical bundles surrounds a central cavity on the cytoplasmic (negative) side of the membrane. A cytoplasmic domain composed of the helix-loop linker between TM2-3 (HL23) and a second helix-loop linker between TM 6-7 (HL67) is positioned over the central cavity. Each of these linkers contains an aspartate-rich motif. Conserved residues in this extramembrane domain (including the aspartate residues) are involved in coordinating two Mg^{2+} ions, either directly or indirectly. While the stoichiometric ratio of Mg^{2+} ions to UbiA monomer has not been determined, XPP-bound structures show two Mg^{2+} ions positioned on either side of the pyrophosphate group, and binding assays have confirmed that the Mg^{2+}-coordinating residues are required for XPP binding. Other conserved, polar residues that face the central cavity also participate in pyrophosphate coordination. While the overall structure does not change much between the apoprotein and substrate-bound forms, this cytoplasmic region becomes more ordered when both Mg^{2+} and the XPP substrate are bound, restricting solvent access to the central cavity; the ability to protect the active site from water would be critical for a reaction mechanism involving a polyprenyl carbocation intermediate (49,50). Additionally, a strictly conserved tyrosine residue positioned near the XPP binding site could potentially stabilize a carbocation intermediate via cation-π interactions in a manner similar to that of soluble aromatic prenyltransferases (50,67,69).

Deeper in the membrane, the central cavity becomes more hydrophobic, reflecting its role as the prenyl tail binding site. Of course, because many members of the UbiA superfamily use very long chain polyprenyl diphosphates (up to C60) as substrates, the entire prenyl tail cannot fit within the central cavity (42). Since *Ap*UbiA and *Af*UbiA have only been crystallized with short chain XPP substrates, the exact location of the longer-chain polyprenyl binding site is not known. However, in *Ap*UbiA, the hydrophobic region of the central cavity has an opening to the lipid bilayer between TM1 and TM9 that could accommodate longer chain polyprenoids (49). In *Af*UbiA, different placement of TM9 blocks

direct access to the central cavity but also creates a longer hydrophobic tunnel between TM8 and 9 that connects the central hydrophobic pocket to the bilayer and could serve as a binding site for long polyprenyl tails (50). In addition to these alternate sites for prenyl tail binding, there are differences in the site where the prenyl acceptor binds. In *Ap*UbiA, a small basic pocket within the first four-helix bundle and adjacent to the hydrophobic portion of the central cavity forms a binding site for *p*-hydroxybenzoate, with conserved residue R43 interacting with the substrate's carboxyl group (49). In *Af*UbiA, this pocket lacks any basic residues, and the prenyl tail from the XPP analog binds here in the crystal structure (50). Thus, some of the key differences between the *A. pernix* and *A. fulgidus* structures arise either from different placement of TM9 or the chemical environment of the prenyl acceptor binding site. These differences likely reflect differences in substrate specificity (42).

HOS structural model and HOS mutagenesis

We constructed a structural model for *Bacillus subtilis* HOS (*Bs*HOS) using trRosetta (75) and refined this model via molecular dynamics simulations (74). The initial model was generated by trRosetta, a new high-accuracy machine learning method that predicts interresidue distances and orientations for each pair of amino acid residues in a protein sequence based on evolutionary relationships inferred from multiple sequence alignments (75). The rationale for this approach is that residues that co-vary are likely to interact in three-dimensional space and are therefore positioned close to each other in the model (75). The initial model generated by trRosetta was refined by physics-based molecular dynamics simulations (74) to generate the final structural model of *Bs*HOS shown in Figure 1.3. Although earlier investigators had reported hydropathy plots for HOS and predicted anywhere from 7 to 9 TM helices, our new model indicates that HOS has nine transmembrane helices like the UbiA homologs that have been crystallized (38,73,76). The HOS model suggests that the overall fold of HOS is similar to the known structures of the

UbiA superfamily, with a central cavity on the cytoplasmic side of the membrane that is capped by the cytoplasmic linkers bearing the aspartate-rich motifs. This cytoplasmic N-terminus/periplasmic C-terminus orientation is in agreement with the experimentally predicted topology for *Ec*HOS (77). The majority of the conserved residues in HOS face the central cavity, including several residues that are likely to interact with farnesyl diphosphate. For illustrative purposes, the position of the uncleavable XPP analog geranyl thiolopyrophosphate (GSPP) in the *Ap*UbiA crystal structure was used to guide the positioning of GSPP in the HOS model (Figure 1.3A-C). (*Ap*UbiA was chosen as the guide because this enzyme is more closely related to the HOS sub-family than *Af*UbiA) (42).

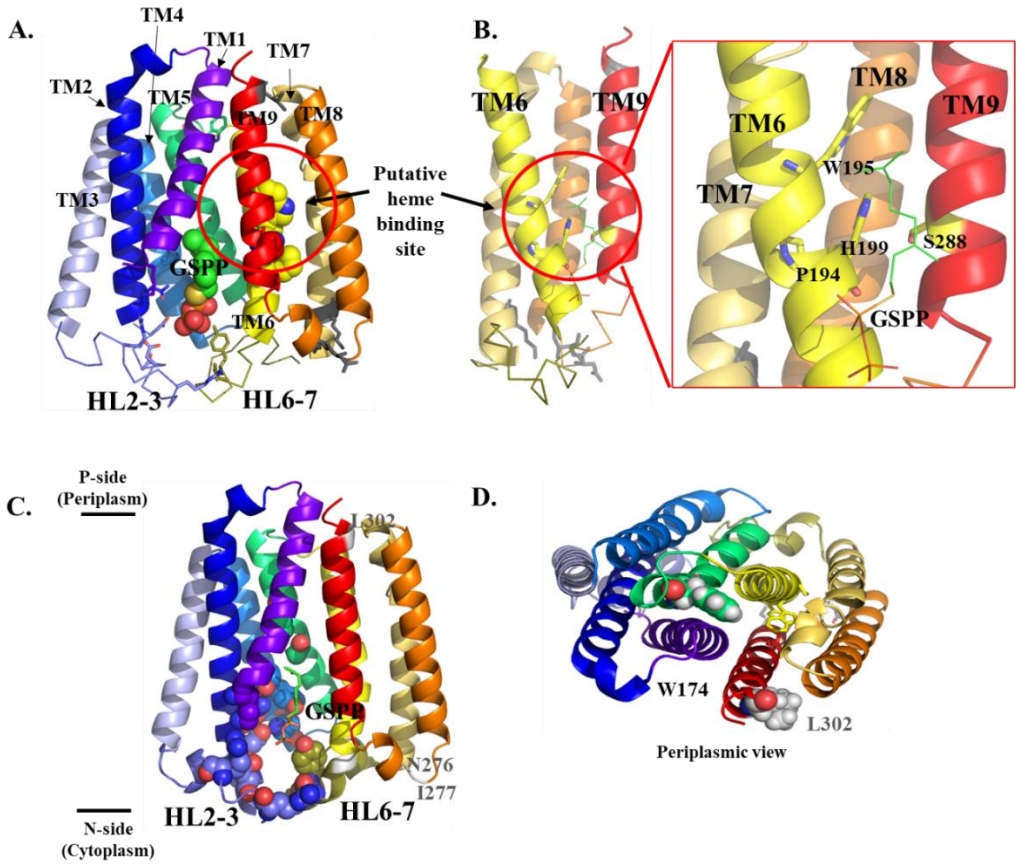

Figure 1.3 Structural model of *B. subtilis* HOS showing the cytoplasmic central cavity and predicted heme binding site

The N-terminus (aa 1-28) is not shown. GSPP placement in the central cavity was based on superimposition of the *Bs*HOS model with the substrate-bound structure of *Ap*UbiA (4od5) (49). Coloring: TM1 purple-blue, TM2 blue, HL2-3 slate (ribbon), TM3 light blue, TM4 marine, TM5 lime green, TM6 yellow, HL6-7 deep olive (ribbon), TM7 yellow-orange, TM8 orange, TM9 red. A. View from the plane of the membrane. GSPP is shown as spheres (red, orange, and green). The critical, central cavity-facing residues are shown as sticks (colors corresponding to secondary structure). The extramembrane residues (charged in *Ec*HOS, varying levels of conservation) are shown as gray sticks. The putative heme binding site between TM6 (yellow) and TM9 (red) is circled. Putative heme binding site residues are shown as spheres (yellow and red). B. The model is rotated 90º to show the putative heme binding site adjacent to the central cavity. For clarity, TM1-5 have been removed. Critical residues in the putative heme binding site are shown as yellow sticks, and GSPP is shown as lines. C. View from the TM plane highlighting critical residues that face the central cavity as well as charged, extramembrane residues that do not face the central cavity but are critical in *Ec*HOS. Key central cavity residues are shown as spheres. The backbone positions of three "charged" extramembrane key residues are shown in gray and labeled in gray. The substrate analog GSPP is shown as sticks (green, red, and yellow). D. Periplasmic view of W174, a critical residue that does not face the central cavity. W174 is shown in green spheres. L302 (analogous to the critical charged, extramembrane residue D282 in *Ec*HOS) is shown as gray spheres.

The most extensive mutagenesis study of a HOS gene was an alanine scanning mutagenesis experiment in which 40 residues from *Ec*HOS were substituted. Of these 40 residues, 23 were determined to be necessary for *in vivo* activity (Table 1.2) (73). These critical residues can be divided into three different categories based on their predicted position in our new HOS model: residues that face the central cavity, residues that are located in or near inter-helical loops but do not face the central cavity, and TM residues that do not face the central cavity. The majority of these critical residues (14 out of 23) fall into the first category, *i.e.*, residues that face the central cavity (7 in the cytoplasmic linkers HL2-3 and HL6-7, and 7 in various TM helices) (Figure 1.3C, Table 1.2). All 14 of these residues are conserved in HOS sequences, and the majority of them are conserved across sequences of the superfamily as well. Most residues in this category are charged or polar and are likely involved in coordinating Mg^{2+} or pyrophosphate. The number of critical, conserved residues in this region highlights the importance and the invariance of Mg^{2+} and pyrophosphate binding. Moreover, since our model was developed without taking into account the mutagenesis data, the positioning of these conserved residues at the central cavity active site indicates that the HOS model is in good agreement with the available experimental data.

Category	Location	*Bs*HOS residue[a]	*Ec*HOS residue[a]	Predicted function	References
Central-cavity facing					
	TM1	**K 30**[b]	**K 11**[b]		
	TM2	**N 81**	**N 57**	PP_i coordination	(49)
	HL23	**D 85**	**D 61**	Mg^{2+} coordination	(49)
	HL23	D 87	D 63		
	HL23	**D 89**	**D 65**	Mg^{2+} coordination	(49)
	HL23	**R 94**	**R 70**	PP_i coordination	(49)
	HL23	**R 98**	**R 74**	PP_i coordination	
	TM4	**Y 143**[b]	**Y 120**[b]		
	TM4	**Y 147**	**Y 124**	PP_i coordination; carbocation stabilization	(49,50)
	TM4	**K 152**	**K 129**	PP_i coordination	(49)
	TM5	**G 166**	**G 143**		
	TM5	**P 169**	**P 146**		
	HL67	**D 210**	**D 187**	Mg^{2+} coordination	(49)
	HL67	**Y 211**[b]	**Y 188**[b]		
Periplasmic TM5-TM6 interface					
	TM5	W 174[b]	Y 151[b]		
Heme binding site					
	TM6	**W 195**[b]	**W 172**[b]		
	TM6	**P 198**[b]	**P 175**[b]		
	TM6	**H 199**[b]	**H 176**[b]	Heme *b* (substrate) ligand	(38)
	TM9	**S 288**[b]	**S 268**[b]		
Charged, extramembrane					
	HL67	K 229[c]	K 206[c]		
	HL89	N 276	D 256		
	HL89	I 277	D 257		
	TM9	L 302	D 282		

Table 1.2: Key residues in HOS

Table 1.2 (cont'd)

The residues listed are critical for activity in *E. coli* HOS (*Ec*HOS), as demonstrated by loss of *in vivo* HOS function when substituted with alanine (73). The residues can be grouped into four topological categories on the basis of our new structural model of *B. subtilis* HOS (*Bs*HOS). The predicted functions of residues facing the central cavity were assigned based on the alignment of *Bs*HOS with *A. pernix* UbiA (*Ap*UbiA) (49). TM – transmembrane helix; HL23 – Helix-loop between TM2 and TM3; PP_i – pyrophosphate.

[a]Residues in **bold** are highly conserved in HOS.
[b]Residues at this position are only conserved in the HOS sub-family.
[c]There is a preference for a charged residue at this position in the UbiA superfamily.

In addition to the 14 conserved residues that face the central cavity, there are 4 critical residues in *Ec*HOS predicted to be in or near inter-helical loops in the C-terminal four-helical bundle (Figure 1.3C-D, Table 1.2). All four of these residues are charged in *Ec*HOS. K206 (K229 in *Bs*HOS) is predicted to be near the C-terminal end of HL6-7, at a position where there is a preference for positively charged residues in the superfamily. D256 and D257 (N276 and I277 in *Bs*HOS) are predicted to be in the cytoplasmic loop between TM8 and TM9. Neither position is strongly conserved, but nonpolar residues seem to be excluded from these positions. Finally, D282 (L302 in *Bs*HOS) is predicted to be at the periplasmic end of TM9, a site where there is a preference for negatively charged residues, with aspartate predominating. The specific functions of these four charged residues remain unclear, as they appear to be too far from the central cavity to be involved in pyrophosphate or Mg^{2+} binding. However, their extramembrane locations serves to confirm that the overall topology of the model is likely accurate.

The remaining residues that lead to abolished activity when substituted with alanine in *Ec*HOS are conserved residues in TM helices that do not face the central cavity. These residues are all located in the C-terminal four helical bundle (*B. subtilis* numbering listed first, followed by *E. coli* numbering in parentheses): W174 (Y151), W195 (W172), P198 (P175), H199 (H176), and S288 (S268). W174 is not very close to the other residues. It is located near the periplasmic end of TM5 (facing TM6) (Figure 1.3D, Table 1.2). Overall,

there is a preference for an aromatic residue at this position in the superfamily, but its role is unclear.

The other four residues are clustered together and are only conserved in the HOS sub-family. W195, P198, and H199 are all located on TM6 (Figure 1.3A-B, Table 1.2). P198 faces the center of the second four helical bundle, while W195 and H199 face TM9. H199 is directly across from S288 on TM9; both residues are adjacent to the central cavity. The position of H199 in the model (Figure 1.3B) is particularly intriguing since this residue is only strictly conserved in the HOS sub-family and is thought to be the ligand for heme *b* (the prenyl acceptor). Consistent with this hypothesis, isolated *Bs*HOS (overexpressed in *E. coli*) has a Soret peak that would be typical of histidine ligation (38). Furthermore, the H199A *Bs*HOS variant is inactive *in vivo* even though the expression level of the substituted protein is similar to that of the wild-type enzyme (38). Assuming H199 is the heme ligand, this would place the heme binding site partly within the second four helical bundle, likely between TM6 and TM9. In the current structural model, the N^{δ} of H199 is approximately 8 Å from the closest carbon atoms in the GSPP prenyl tail, indicating that a heme ligated by H199 would be reasonably close to the active site. It should be noted that the model does not possess enough space between TM6 and TM9 for heme to bind. This crowdedness is due to the fact that the method used for constructing the model places residues that coevolve in close proximity to each other but does not take into account the possibility that a substrate (such as heme) could be located between coevolving residues (74).

The most obvious difference between the structural model of HOS and the known crystal structures of related proteins is the location of the prenyl acceptor binding site. As mentioned above, *Ap*UbiA is most closely related to *p*-hydroxybenzoate prenyltransferases, and a substrate-bound form has been crystallized with electron density that matches *p*-hydroxybenzoate in a basic pocket within the N-terminal four-helical bundle (42,49). The

arginine (R43 in *Ap*UbiA) that makes the pocket basic appears to interact with the carboxylate of *p*-hydroxybenzoate. This arginine is only conserved within the *p*-hydroxybenzoate prenyltransferase sub-family. When substituted, it completely abolishes *p*-hydroxybenzoate binding, supporting the notion that the basic binding pocket is the true substrate binding site for this sub-family. On the other hand, in *Bs*HOS, the prenyl acceptor site (heme binding site) seems to be located within the C-terminal four-helical bundle, on the opposite side of the central cavity. Most of the highly conserved residues unique to the HOS sub-family are located on TM6, including H199 (Figure 1.3B). Because there are few sequence motifs that are indicative of a heme binding site, it can be hard to predict exactly which residues will form a heme binding pocket. However, heme binding pockets tend to be enriched in aromatic residues that can form stacking interactions with the heme (78). In our model, W195, which is strictly conserved in HOS sequences, is positioned at the interface between TM6 and TM9 just above H199. This observation, along with the presence of a strictly conserved histidine on TM6 (H199 in *Bs*HOS) that could serve as a heme ligand and a highly conserved serine (S288) facing H199, strongly suggests that heme *b* binds between TM6 and TM9, adjacent to the central cavity. As discussed above, the crystal structures of *Ap*UbiA and *Af*UbiA indicate that TM9 placement defines prenyl tail binding locations. In HOS, TM9 seems to serve an additional role, forming part of the prenyl acceptor binding pocket.

The effects of several mutations in genes encoding eukaryotic HOS have also been studied. HOS from the pathogenic yeast *Aspergillus fumigatus* has been substituted at three positions in HL2-3: E230A, D234A, and R243Q (79). The latter two HOS variants exhibit decreased *in vivo* activity, as would be expected since the analogous *Ec*HOS variants (D65A and R74A) are also inactive (73). The first conserved aspartate of the aspartate-rich motif is replaced by glutamate in *A. fumigatus*; interestingly, substituting E230 with alanine does not

affect *in vivo* HOS activity (79). In contrast, the aspartate at this position is required for activity not only for *Ec*HOS (D61A is inactive), but also for other *E. coli* octaprenyltransferases (UbiA and MenA) from the UbiA superfamily (49,50,73). Additionally, in *Af*UbiA, the corresponding aspartate ligates a Mg^{2+} ion, and in both of the archaeal homologs that have been crystallized, the analogous aspartate-to-alanine variants are essentially unable to bind XPP (49,50). The tolerance of the fungal HOS for the substitution of a conserved glutamate to alanine in HL2-3 could perhaps indicate a species-specific difference in HL2-3 arrangement or Mg^{2+} coordination.

In contrast to bacteria and yeast, which have alternate respiratory and/or fermentative pathways, respiration in humans depends on heme *o* biosynthesis since heme *o* is the precursor for the heme *a* cofactor of cytochrome *c* oxidase, the only available terminal oxidase. Therefore, mutations that completely abolish HOS activity are most likely embryonic lethal in humans and thus have not been observed. However, four single amino acid substitutions have been identified in human HOS that retain a residual level of activity, yet are still severe enough to cause diseases due to the loss of cytochrome *c* oxidase function (76,80). Two of these substitutions map to residues within the cytoplasmic loops that sit over the central cavity and are relatively (P225) and highly (D336) conserved, respectively. (The corresponding residues in *Bs*HOS are P99 and D210). The other two substitutions, T196 and N204, are located in TM2. T196 is predicted to be located on the IMS (intramembrane space) side of TM2 facing the center of the N-terminal four-helical bundle. The disease-causing mutation in humans yields a T196K variant; the introduction of a positively charged residue at this position may be destabilizing, as has been demonstrated for the analogous substitution in the *S. cerevisiae* HOS (T188K) (81). N204K, on the other hand, is predicted to be on the matrix side of TM2, facing the central cavity. Interestingly, the analogous substitution in *S. cerevisiae*, N196K, is active and can actually rescue the stability or activity of other point

mutations affecting HOS (81,82). Additional data are needed to understand the discrepancy between substituting this position in human HOS versus yeast HOS. However, the dramatic effects produced by mutations in both species highlight the importance of residues that face the central cavity.

Biochemical characterization of HOS has thus far been difficult, given the challenges associated with overexpressing and purifying membrane proteins. However, the crystallization of two archaeal homologs from the UbiA superfamily and the development of powerful new structural modeling techniques have allowed us to gain new insight into the structure and function of HOS. This model indicates that, like other members of the superfamily, HOS has a central cavity lined with conserved polar and charged residues at the cytoplasmic side that likely functions as the active site where farnesyl diphosphate binds. Heme *b* most likely binds adjacent to this central cavity. Although the exact positioning of the heme *b* substrate and structure of the heme binding pocket have yet to be determined, it is logical to assume that the heme binds in such a way that the vinyl group from pyrrole ring A protrudes into the active site. Future work will also be needed to elucidate the details of HOS's reaction mechanism, and the conformational changes that may need to occur for substrate binding or product release.

Heme a *synthase*

Heme a *properties and function*

After heme *b* is farnesylated to produce heme *o*, heme *a* synthase (HAS) catalyzes the oxidation of the C8 methyl group of heme *o* (pyrrole ring D) to a formyl group (Figures 1B, 4). This is the second and final step of the heme *a* biosynthetic pathway (15,19,25). The conversion of pyrrole ring D's methyl substituent to an electron-withdrawing formyl group increases the redox potential of heme *a* relative to hemes *b* and *o*. For example, the reduction potential of heme *a* bound to a heme protein maquette is 179 mV more positive than that of

heme *o* bound to the same maquette (54). This increase in redox potential is due to a decrease in the binding affinity of ferric (Fe^{3+}) heme *a* relative to ferrous (Fe^{2+}) heme *a*. The destabilization of ferric heme *a*'s binding affinity is, however, offset by the presence of the hydroxyethylfarnesyl substituent, which, as discussed above for heme *o*, substantially increases the binding affinity of hemes *o* and *a* for a heme protein maquette relative to heme *b*. Functionally, in an aa_3 terminal oxidase, the high midpoint reduction potential of heme *a* (+380 mV) allows it to accept electrons from relatively poor electron donors such as cytochrome *c* (midpoint redox potential = +260 mV) (1,83-85). Thus, the two modified porphyrin ring substituents of heme *a* appear to act in concert to provide a heme cofactor that has a relatively high reduction potential, yet can still bind tightly to a heme-copper oxidase.

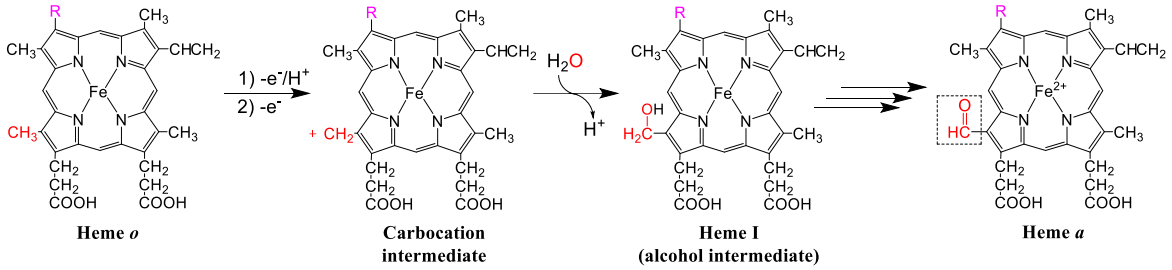

Figure 1.4: Overview of the proposed reaction mechanism for the conversion of heme *o* to heme *a*

The C-8 methyl group (shown in red) loses a proton and two electrons, generating a carbocation. An oxygen atom from water (shown in red) traps this carbocation, yielding heme I, an alcohol intermediate. A second oxidation step ultimately converts the alcohol into an aldehyde, generating heme *a*.

HAS mechanism

HAS oxidizes the methyl group of pyrrole ring D to an aldehyde (Figures 4 and 5) (15,18-25). Like HOS, HAS is an integral membrane protein located in the cytoplasmic membrane of prokaryotes or in the inner mitochondrial membrane of eukaryotes (16,21). A single-turnover *in vitro* activity assay with membranes isolated from *E. coli* overexpressing HAS was reported, which indicated that HAS could convert heme *o* to heme *a* in the presence of reductant (86); however, no successful activity assay has been described for purified HAS. Other activity assays published to date are *in vivo* studies in which HAS is expressed in a species that lacks a gene encoding HAS. For example, HAS was heterologously overexpressed in *E. coli*, which lacks a native gene for HAS, and the substrate, heme *o*, was provided either by *E. coli*'s native HOS, or by overexpressing HOS (22,23,38). Expression of *B. subtilis* HAS (*Bs*HAS) in *E. coli* demonstrated that HAS can catalyze the successive oxidation of the C8 methyl group of heme *o* to an alcohol, aldehyde, and carboxylate (22). The aldehyde product is heme *a*, and the alcohol and carboxylate products are presumed to be an intermediate (heme I) and an overoxidized product (heme II), respectively (Figure 1.4). Synthesis of heme *a* (and hemes I and II) was also shown to depend on the presence of

oxygen (22). Because HAS is a heme-binding, oxygen-dependent protein, it was speculated that the oxygen atom from heme *a*'s aldehyde group was initially derived from O_2 using a cytochrome P_{450}-like monooxygenase mechanism (20,22,25,86). A similar oxygen-activating mechanism has been reported for chlorophyll *a* oxygenase, a nonheme iron monooxygenase which also catalyzes the oxidation of a methyl group from a pyrrole ring (87-89). Isotope labeling studies, however, indicate that O_2 is not the source of the oxygen in the formyl group of heme *a* or in the hydroxyl group of heme I. Instead, the oxygen atom added at the C8 position is most likely derived from water. Therefore, although cytochrome P_{450} and HAS are both oxygen-activating enzymes, it seems most likely that HAS uses a peroxidase-like mechanism in which O_2 activation yields a high-valent iron-oxo species that serves as an oxidant but not as an oxygen donor (Figure 1.5) (23).

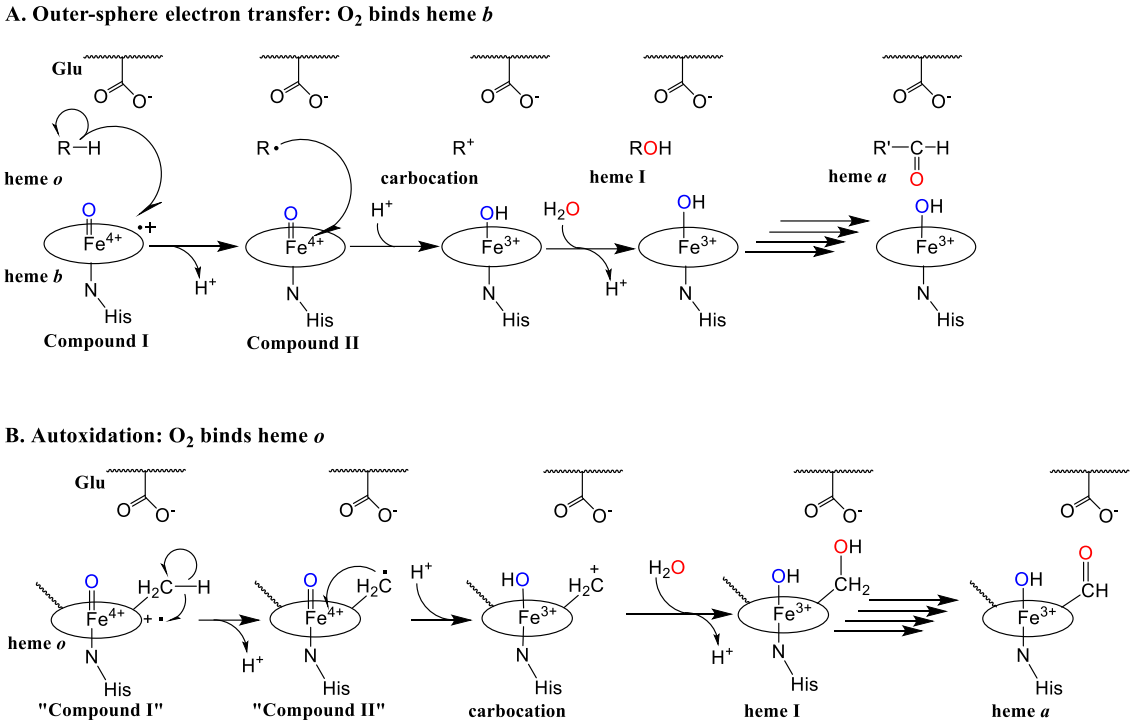

Figure 1.5: Possible mechanisms of oxygen activation by HAS

In HAS, O_2 activation may occur at heme *b* (A) or heme *o* (B). Either proposed mechanism would likely require the displacement of a histidine ligand to allow O_2 to bind. A. Outer-sphere electron transfer. O_2 activation leads to the formation of a high-valent iron-oxo species (compound I, far left) that removes an electron from the C8 methyl group of heme *o* (shown as R-H). This leads to the formation of a radical intermediate and compound II. Compound II then removes another electron from the substrate radical, forming a carbocation intermediate. Water traps the carbocation intermediate to form heme I. This process can then be repeated with heme I as the substrate to form a geminal diol (not shown), which readily dehydrates to form the aldehyde in heme *a*, the final product. A conserved glutamate positioned near the heme *o* binding site is proposed to stabilize the carbocation intermediate. B. Autoxidation mechanism. Heme *o* activates O_2 to form a compound I-like species. "Compound I" of heme *o* then oxidizes its own C8 methyl group using the general mechanism described in mechanism A.

In the well-established mechanism for plant heme peroxidases (such as horseradish peroxidase), peroxide binds end-on at the distal side of the active site heme (heme *b*). Cleavage of the O-O bond is catalyzed by the electron-donating "push" of the proximal heme histidine ligand and the "pull" of a distal histidine, which acts as a general acid/base catalyst to facilitate proton removal from the proximal oxygen and protonation of the distal oxygen (90-92). Heterolytic O-O bond cleavage produces a high-valent iron-oxo species known as

compound I, an Fe(IV)=O porphyrin cation radical. Subsequent stepwise electron donation from an external electron donor (often an aromatic substrate) reduces the porphyrin ring and then the heme iron, with protonation of the second oxygen atom leading to its release as water (90,91). In the case of HAS, two alternative modified versions of this mechanism can be envisioned (23), in which compound I formation is initiated by O_2 binding to the heme iron instead of peroxide binding (Figure 1.5). Reduction of the oxyferrous complex to the peroxo state requires the donation of two electrons from an external source. In yeast, these electrons seem to be provided by mitochondrial ferredoxin (Yah1) and ferredoxin dehydrogenase (Arh1) (25,93). Once the peroxo state is reached, the remaining two electrons needed to cleave the O-O bond and generate a compound I-like species could be provided by the heme iron and porphyrin ring as in the peroxidase mechanism. Compound I is a very potent oxidant that could remove an electron from the C8 methyl group of heme *o*, converting the methyl group into a carbon-centered radical and reducing compound I to compound II. Compound II, which is still a potent oxidant, could then remove a second electron from the radical to form a carbocation. Finally, water could trap the carbocation to produce heme I, the hydroxylated intermediate. This process could then be repeated to oxidize heme I to heme *a*. This proposed mechanism is consistent with the available isotope-labeling data on HAS, but the details have yet to be confirmed experimentally (22,23).

One of the unanswered questions about heme *a* synthase's reaction mechanism is whether O_2 binds to the heme *o* substrate or to heme *b*, which usually co-purifies with HAS and is thought to serve as a cofactor (Figure 1.5) (20,21,43,52,94,95). Since both hemes appear to be low-spin hexacoordinate in the resting state of the enzyme (20), it is not clear which heme is the site of O_2 binding and subsequent compound I formation. Arguments can be made for both scenarios. As discussed below, the two hemes are likely close enough to each other to allow for electron transfer between them. Thus, it is feasible that O_2 could bind

heme *b* and form a "true" compound I that could remove electrons from the target methyl on heme *o* via outer sphere electron transfer (23). This is the mechanism typically employed by peroxidases (Figure 1.5A) (91). Alternatively, O_2 could bind heme *o* and form a prenylated compound I-like Fe(IV)=O porphyrin cation radical that catalyzes the oxidation of its own methyl substituent. In this case, heme *b* would serve strictly in an electron transfer capacity (Figure 1.5B) (23). This autoxidation mechanism is similar to the proposed mechanism for the modification of the heme cofactor in mammalian peroxidases. In this family of peroxidases, the active site heme is proposed to generate compound I and autocatalytically modify its methyl substituent. This reaction step generates a carbocation at the methyl position that is normally trapped by a nearby glutamate side chain to form an ester crosslink in the isolated form of the enzyme. Substitution of the crosslinking glutamate with aspartate, however, prevents this crosslink from forming, presumably because the shorter residue is too far away from the heme. Instead, the carbocation intermediate is trapped by water, yielding a hydroxylated heme similar to the heme I intermediate generated by HAS (96,97). Thus, precedence in the literature exists for both compound I-catalyzed autoxidation as well as for outer sphere electron transfer. These two mechanisms cannot be distinguished based on the currently available data.

Overview of HAS topology and mutagenesis

HAS is a multipass integral membrane protein located in the prokaryotic cell membrane or the eukaryotic inner mitochondrial membrane. Genes encoding HAS from all three domains of life belong to the same family, termed the Cox15/CtaA family (15,18,24,25,43,44). There are a few phylogenetically diverse groups from archaea (*Sulfolobaceae*) (Table 1.1) and lower-order eukaryotes (rhodophyte and glaucophyte algae along with jakobids) where a sequence encoding HAS has not been identified in the genome despite the presence (or predicted presence) of an aa_3 terminal oxidase (26,44). However,

given the low sequence similarity between distantly related HAS proteins, this does not completely rule out the possibility that a gene encoding a member of the Cox15/CtaA family is present in these organisms.

Most identified HAS sequences possess eight transmembrane helices. Sequence homology between the N-terminal half of HAS (TM 1-4) and the C-terminal half (TM 5-8) suggests that the standard 8-TM topology resulted from duplication and fusion of an ancient 4-TM gene. The TM helices are connected with very short loops, with the exception of the N-terminal periplasmic loop between TM1-2 (L1-2), the corresponding C-terminal loop between TM5-6 (L5-6), and the loop that links the two halves of the protein (L4-5) (Figure 1.6A) (43,94,95,98). HAS sequences can be broadly divided into two types based on the presence (type 1) or absence (type 2) of a pair of conserved cysteine residues in L1-2. Type-1 HAS is found in archaea and several bacterial clades, while type-2 HAS is found in other bacterial clades and in all eukaryotes (with only one exception) (43,44). Type-1 HAS proteins can be further subdivided into three classes (A-C) (99). (Class D is equivalent to type 2.) Class A HAS representatives are found in certain archaea, and possess only one four-helical bundle that includes the pair of conserved cysteine residues in L1-2. These truncated HAS proteins appear to function as dimers (43,46). Classes B-D comprise the majority of known HAS sequences and have 8 TM helices. These classes have a cysteine pair in both L1-2 and L5-6 (class B), only in L1-2 (class C), or in neither elongated loop (class D/type 2) (44,99). The most well-characterized HAS, *Bs*HAS, belongs to class B. Mutagenesis of the gene encoding *Bs*HAS indicates that the less highly conserved C-terminal cysteine pair (C191, C197) is not required for activity, while the N-terminal cysteine pair (C35, C42) is important for activity in type-1 HAS (43,94,95). (*B. subtilis* numbering is used throughout this section.) Since the N-terminal pair of cysteinyl residues is replaced by nonpolar residues in type-2 HAS, it has been suggested that the cysteines do not directly participate in the catalytic

mechanism of HAS, but are perhaps important for structural reasons or for mediating species-specific protein-protein interactions (43,44). This loop is considerably longer in type-2 (eukaryotic) HAS than in type-1 HAS, which might facilitate additional protein-protein interactions not possible in type-1 HAS. One intriguing possibility is that this loop is responsible for mediating interactions with heme-copper oxidase assembly factors, although this hypothesis has yet to be explored experimentally.

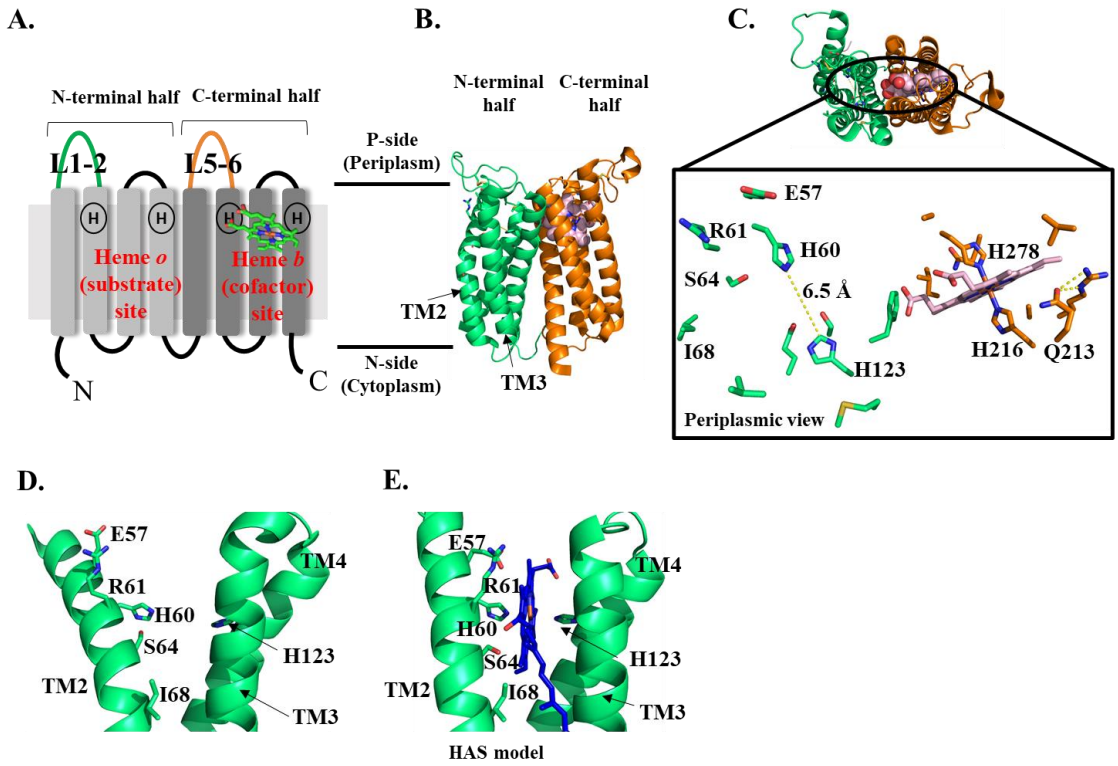

Figure 1.6: HAS topology (A), crystal structure (B-D), and substrate-bound model (E)

A. Diagram showing the 8 TM helices of HAS and the position of the two heme binding sites, each with two highly conserved His residues. The elongated loops connecting TM1 and 2 (L1-2) and TM5 and 6 (L5-6) are colored green and orange, respectively. B. Crystal structure of *B. subtilis* HAS showing heme *b* in the C-terminal heme binding site and the empty N-terminal heme binding site. The N-terminal four-helical bundle is shown in green; the C-terminal four-helical bundle is shown in orange and heme *b* is shown in light pink (spheres). C. This structure is rotated 90˚ to show the top-down view from the periplasm. Top: TM helices are shown as a cartoon; heme *b* is shown as spheres (light pink). Bottom: conserved residues in the N-terminal and C-terminal heme binding sites. Heme *b* is shown as light pink sticks. Residues discussed in the text are labeled, with the exception of G65. D-E. The N-terminal heme binding site of *Bs*HAS with (D) and without (E) heme *o*. D. The crystal structure shown in B is rotated 90° to show the empty heme binding site. E. A model based on the crystal structure of *Bs*HAS is shown with TM2 straightened and heme *o* placed into the N-terminal heme binding site. Figures 6B-D and 6E were prepared using a previously published crystal structure (PDB ID: 6IED and a previously published model (model PDB file: pnas.1813346115.sd01), respectively (51).

In addition to the cysteinyl pair that is conserved in type-1 HAS, there are only a few residues that are highly conserved across all HAS proteins (43,44). Most notably, there are four highly conserved histidine residues in HAS, two in the N-terminal half (H60 and H123, located on TM2 and TM4) and two at corresponding positions in the C-terminal half (H216 and H278, located on TM6 and TM8) (Figure 1.6A) (43,94,95). All four of these histidines are present in almost all known genes encoding HAS (Table 1.1) (43,44,95). Early work with *Bs*HAS isolated from *B. subtilis* showed the presence of two *bis*-histidine axially-ligated hemes, heme *a* (presumably unreleased product) and heme *b* (the putative cofactor) (20,21)[2]. HAS from different organisms also typically co-purifies with heme *b* and heme *o* or heme *a* when expressed in *E. coli*, although the heme type and heme/protein stoichiometry varies (46,52,86,95,100). Therefore, it was postulated that all four conserved histidine residues could act as heme ligands (20,86,94,95).

Each highly conserved histidine residue in *Bs*HAS has been individually substituted. These histidine variants were overexpressed and purified in either *E. coli* (95) or *B. subtilis* (94). As has been discussed in a previous review (43), these mutagenesis studies did not fully clarify which histidine ligated which type of heme because all of the stable mutants still co-purified both with prenylated heme(s) and heme *b* (94,95). However, the mutagenesis data did show that all four histidines are necessary for full HAS activity. Similarly, substitution of each of the analogous histidine residues in eukaryotic HAS resulted in a complete loss of *in vivo* activity (98,101,102). Careful analysis of the *Bs*HAS variant properties suggests that the

[2] HAS from different organisms also typically co-purifies with heme *b* and heme *o* or heme *a* when expressed in *E. coli*, although the heme type and heme/protein stoichiometry varies (Sakamoto et al. 1999; Lewin and Hederstedt 2006; Mogi 2009b; Hannappel et al. 2011; Zeng et al. 2020).

histidines have unique roles. For example, substitution of an N-terminal histidine did not produce the same result as altering its C-terminal counterpart. Substitution of either N-terminal histidine (H60 or H123) to a non-heme-ligating residue (A or L) completely abolishes activity, although this does not prevent heme *o* from binding to HAS. In contrast, alteration of the C-terminal histidines (H216 or H278) to non-ligating residues sometimes resulted in partially active HAS. However, changing the C-terminal histidines (and some other conserved C-terminal residues) also destabilized *Bs*HAS in most cases (43,94,95).

In addition to this discrepancy between the N-terminal and C-terminal substitutions, the data obtained from expressing *Bs*HAS in *B. subtilis* indicated that the two histidines belonging to the same half of HAS also seem to have distinct roles. For example, substituting the N-terminal histidine H123 with methionine, an alternate heme ligand, completely abolishes activity, but substituting the other N-terminal histidine for methionine (H60M) yields an enzyme that is partially active but co-purifies with a lower level of heme *a* than observed for the wild-type HAS (43,94). Overall, these data indicate that while all four histidine residues are important for proper HAS function, they seem to serve unique roles, supporting the hypothesis that HAS has two heme binding sites with different functions.

Besides the histidine variants mentioned above, the only point mutations associated with eukaryotic HAS that have been experimentally characterized are mimics of disease-causing mutations in humans. As discussed above for HOS, substitutions that completely abolish HAS activity are presumably embryonic lethal. However, three missense mutations have been identified in human HAS that significantly decrease HAS activity and result in very severe diseases associated with low levels of cytochrome *c* oxidase activity (98,103-107). One of these mutations results in the substitution of L139 with valine (human numbering) (107). L139 is predicted to map to L1-2, the elongated loop between TM1 and TM2 where several highly conserved residues are located. The second disease-causing

alteration, yielding the S344P variant, is located at the N-side (matrix) end of TM6 and destabilizes HAS, although the explanation for this instability is unclear (98). The position of the third known disease-causing point alteration is in the P-side (IMS) loop connecting TM3 and TM4. This loop is very short in *Bs*HAS (~4 amino acids), but longer in eukaryotic HAS (~10-14 amino acids), where the residue in question, R217, appears to be fairly well conserved (98). Expression of the variant human protein in human fibroblasts and of the analogous substitution in *S. cerevisiae* HAS indicates that this change inactivates HAS without affecting stability (98). In the absence of additional structural information about type-2 HAS, the role of this amino acid residue is unclear.

The remaining highly conserved residues in HAS are clustered on the periplasmic (IMS) side of the TM helices or in the elongated periplasmic loops, L1-2 and L5-6. As discussed above, the N- and C-terminal halves of HAS exhibit low sequence homology, and the pattern of highly conserved residues from the two halves of the protein are therefore fairly well correlated (21,43,94). For example, the conserved histidine from TM2 is preceded by a glutamate and followed by an arginine, forming the motif EXXHR, while the analogous C-terminal histidine from TM6 is part of a very similar motif, Q/HXXHR. However, both the number of conserved residues and the conservation level of most of these residues is higher in the N-terminal half of HAS than in the C-terminal half. This discrepancy is most evident for L1-2 versus L5-6, but also holds true for the transmembrane domain. However, prior to the determination of the HAS structure, it was not clear how these relatively minor differences in the sequence motifs of the N- and C-terminal halves of HAS resulted in a protein with two functionally distinct heme binding sites.

HAS structure

Recently, the structures of two different type-1 bacterial HASs have been solved. The structure of *Bs*HAS was determined by X-ray crystallography at 2.2 Å resolution (Figure

1.6B-C) (51), and the structure of HAS from the hyperthermophilic bacterium *Aquifex aeolicus* (*Aa*HAS) was solved by cryo-EM at 4.2 Å resolution (52). Both structures show the same overall fold, and a homology model for *Aa*HAS based on the *Bs*HAS crystal structure fit well within the cryo-EM density for the TM helices. *Aa*HAS forms a trimer, which will be discussed briefly. Here we focus primarily on the crystal structure of *Bs*HAS and on the accompanying substrate-bound model.

The structure of *Bs*HAS reveals that the N- and C-terminal halves of HAS each form a four-helical bundle (Figure 1.6B) (51). These bundles are pseudo-symmetrically related, as was predicted based on sequence homology between the two halves of HAS (43,94,98). Heme *b* is bound within the C-terminal bundle, near the periplasmic side of the membrane. Consistent with previous optical and electron paramagnetic resonance analysis, heme *b* is ligated by two of the conserved histidine residues with nearly perpendicular imidazole planes (H216 and H278) and with an Fe-His distance of ~2 Å for each (20,108) (Figure 1.6C). The cryo-EM structure of *Aa*HAS also shows density in the center of the C-terminal four-helical bundle that is likely a heme (52). The corresponding N-terminal heme binding site, where the other two conserved histidine residues (H60 and H123) are located, is empty in the crystal structure (Figure 1.6C-D) (51) and also appears to be empty in the cryo-EM structure (52). This empty heme binding site is likely where the substrate, heme *o*, binds. In the crystal structure, the two elongated periplasmic loops (L1-2 and L5-6) are positioned above the N- and C-terminal heme binding sites, respectively. All of the highly conserved residues in HAS are clustered around the two heme binding sites (Figure 1.6C).

Although the overall fold of the N-terminal heme binding site matches that of the C-terminal heme binding site, the conformation of TM2 deviates from its C-terminal counterpart, TM6. TM2 is bent at a semi-conserved glycine (G65), which places the N-terminal histidine ligands (H60 and H123) too far apart (6.5Å) to provide *bis*-histidine axial

heme ligation (Figure 1.6C-D) (51). Since *bis*-histidine axial ligation is expected for prenylated substrate/product hemes (hemes *o*/*a*), heme *o* binding was modeled by straightening TM2 using the conformation of TM6 as a guide (51). This modification allows heme *o* to be ligated by both H60 and H123 in the model (Figure 1.6E).

The determination of a crystal structure showing heme *b* tightly bound to the C-terminal four-helical bundle provides strong support for the hypothesis that HAS possesses both a cofactor heme binding site and a substrate heme binding site (51). Identification of the C-terminal four-helical bundle site as the binding site for heme *b* and the N-terminal bundle as the substrate binding site also seems to explain the discrepancy in stability between the N- and C- terminal *Bs*HAS mutants (43,94,95). Because the N-terminal four-helical bundle has to bind substrate and release product, it seems likely that this domain exhibits some conformational flexibility, especially at TM2, which is predicted to move toward the center of the four-helical bundle after substrate binding (51). This built-in flexibility may allow the N-terminal half of HAS to tolerate mutations that perturb its structure in the heme binding site. In contrast, the cofactor heme binding site is more likely to be rigid, as there is no need for the cofactor to be released. Thus, it seems logical that disruptions to the heme *b* binding site may compromise protein stability. Interestingly, the structure of *Aa*HAS supports this idea. *As*HAS forms heat-stable trimers with the C-terminal four-helical bundle of each monomer at the core of the trimer. This observation suggests that the C-terminal half of HAS is fairly rigid (52).

The predicted movement of TM2 upon heme *o* binding in *Bs*HAS may represent a generally applicable method for substrate binding in HAS. In both the crystal structure and the substrate-bound model, there is a fairly large lateral opening between TM2 and TM3 that connects the N-terminal heme binding site to the bilayer. In the model, the hydroxyethylfarnesyl tail of heme *o* protrudes through this opening (Figures 6E, 7). (In

contrast, the C-terminal four-helical bundle has a much smaller lateral opening.) On the basis of their model, Niwa et al. (2018) predicted that hydrogen bonding and hydrophobic interactions between residues on TM2 and TM3 are important for drawing heme *o* into the heme binding site. Three residues from TM2 seem to be the most important side chains for this mode of substrate binding in *Bs*HAS: S64 and I68 (Figure 1.6C-E), which presumably interact with the hydroxyl and the polyprenyl portions of the hydroxyethylfarnesyl moiety of heme *o*, and G65, the location of the kink in TM2 (51). Interestingly, although G65 is only conserved in approximately 30% of HAS sequences, glycine occurs frequently in HAS sequences at the positions corresponding to S64 and I68 in *Bs*HAS. These glycines may either substitute for G65 in providing the kink in TM2 or interact with the lipid portion of heme *o*'s hydroxyethylfarnesyl moiety. This sequence specificity suggests that all HAS proteins may share *Bs*HAS's strategy of moving TM2 to allow substrate entry.

The substrate-bound model of *Bs*HAS also has some interesting catalytic implications. First, the model indicates that the substrate and cofactor hemes are positioned close to each other, with their propionates facing each other (Figure 1.7). This orientation suggests that direct electron transfer between the two hemes is possible (51), which is necessary for either version of the proposed catalytic mechanism (Figure 1.5) (23). Straightening TM2 also positions E57 (Figure 1.6E), a highly conserved glutamate, near the C8 methyl group of heme *o*. Because this methyl group is oxidized during catalysis, the proximity strongly suggests that E57 plays a role in the oxidation of the C8 methyl (51). In light of the putative peroxidase-like mechanism for HAS, it seems plausible that the negatively charged glutamate could stabilize a carbocation intermediate that forms during the oxidation of the C8 methyl group, in a manner similar to the proposed mechanism for the glutamate-to-aspartate mammalian peroxidase variant discussed above (23,96,97). It should be noted, however, that both the outer sphere electron transfer mechanism and the

autoxidation mechanism include the formation of a carbocation intermediate, so the placement of E57 cannot be used to unambiguously distinguish between the two mechanisms. In the C-terminal heme-binding site, a glutamine (Q213) replaces E57 (51). This nonpolar residue likely cannot stabilize a carbocation intermediate as effectively as glutamate, providing another line of evidence that the N-terminal heme binding site is the substrate binding site.

Ever since it was first observed that HAS co-purifies with heme *b* and heme *a*, investigators have speculated that HAS possesses distinct substrate and cofactor heme binding sites, although experimental evidence in support of this hypothesis was tenuous prior to structural determination. TM1-4 and TM5-8 were also correctly predicted to form homologous four-helical bundles. The four-helical bundle structure of each half of HAS, and the characterization of both heme *b* and heme *a* as low-spin, hexacoordinate hemes is reminiscent of certain electron transfer heme proteins, such as cytochrome *b* from complex III, supporting the idea that one of these heme groups is involved in electron transfer from an external electron donor (20,25,51,108,109). The other heme is expected to bind and activate O_2 during catalysis, requiring displacement of one of the histidine ligands. However, it is not clear from the substrate-bound model which histidine is displaced, due to the nearly equivalent positioning of the histidine residues in both heme binding sites. This question will have to be addressed by future mechanistic studies. The structures of *Bs*HAS and *Aa*HAS also suggest a possible mechanism for substrate entry and product exit from the N-terminal heme binding site based on the apparent conformational flexibility of this domain (51,52). This observation raises intriguing questions about how prenylated hemes transfer to and from HAS, which will be discussed in the final section of this review.

Heme trafficking in the heme a *biosynthetic pathway*

Overview of prenylated heme trafficking

A successful heme *a* biosynthetic pathway depends not only on the synthesis of heme *o* and heme *a*, but also on proper heme trafficking throughout the course of this biosynthetic pathway. Specifically, heme must be transferred from the upstream proteins involved in heme *b* synthesis and/or trafficking to HOS, from HOS to HAS, and finally to the heme-copper oxidase recipient (Figure 1.7). In general, intracellular heme trafficking is mediated by proteins, such as heme chaperones or transporters, or by lipid vesicle transport. This delivery process allows the intracellular concentration of "free" heme to be kept very low, which protects the cell from oxidative damage that might otherwise be caused by non-protein-bound heme (48,110). Since heme *a* has a higher redox potential than heme *b* (and thus is a better oxidant), controlling heme *a* transport seems to be particularly important in terms of protecting the cell from oxidative damage (83,84,111). However, intracellular heme trafficking in general, and trafficking of prenylated hemes in particular, is still poorly understood (48,110,112). The recent structural advances that have been made for HOS and HAS have provided some missing pieces of the puzzle, but many questions remain. Here, we discuss the currently available information on heme transfer through the heme *a* biosynthetic pathway, with an emphasis on the new structural data.

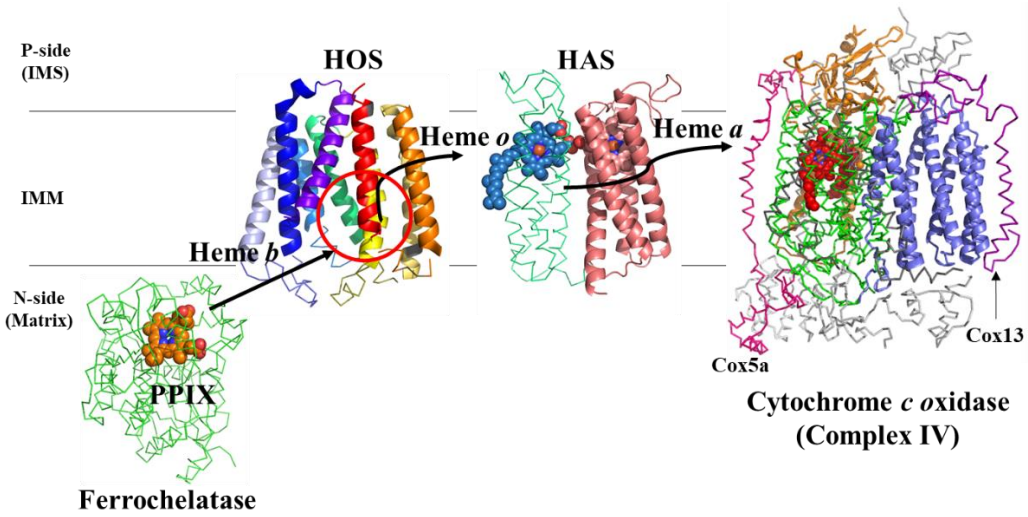

Figure 1.7 Proposed heme trafficking route in the eukaryotic heme *a* biosynthetic pathway

Heme must be transferred from ferrochelatase to HOS, from HOS to HAS, and finally from HAS to cytochrome *c* oxidase. Note that these transfer steps could involve an unknown heme chaperone (see text). Proteins shown: Membrane-associated (eukaryotic) ferrochelatase (green ribbon) is shown in complex with protoporphyrin IX (PPIX) (orange spheres). The porphyrin plane is roughly parallel to the membrane lipids, and pyrrole rings A and D are closest to the membrane. Note that while mammalian ferrochelatase can dimerize, only one monomer is shown here (113-115). (Ferrochelatase structure (human): PDB E343K) (115). HOS model (this study) is shown with the proposed heme binding site circled in red (*Bs*HOS). HAS model (51) showing heme *o* (blue spheres) bound in the N-terminal heme binding site on the P-side (periplasmic or IMS side) of the membrane. This model is based on the crystal structure of *Bs*HAS, which has an empty N-terminal heme binding site (model PDB file: pnas.1813346115.sd01). Cytochrome *c* oxidase is depicted as in Figure 1.1A, except that hemes *a* and a_3 are shown as red spheres. Subunit I (Cox1) is shown in green ribbon; the other core subunits are shown as orange and slate cartoons. The nuclear-encoded subunits are shown as gray ribbons, except for Cox5a (hot pink) and Cox13 (purple). IMS – intermembrane space; IMM – inner mitochondrial membrane; P-side – positive side; N-side – negative side.

Transfer of heme b *to HOS*

The heme *a* biosynthetic pathway is one of several competing routes for newly synthesized heme *b*. Heme *b*, the prototypical cellular heme, is used as a cofactor without further modification in a wide array of proteins with different sub-cellular locations, including cytochrome *b* from the cytochrome bc_1 complex (complex III in eukaryotes), the cytochromes P_{450}, and hemoglobin and myoglobin. In addition, heme *b* is also the precursor for biosynthetic pathways that modify the heme, such as for cytochrome *c* maturation and heme *a* synthesis. Thus, heme *b* must ultimately be distributed to many proteins and locations throughout the cell. In the case of heme *a* biosynthesis, heme *b* must be trafficked from the enzyme that catalyzes the final step of heme *b* biosynthesis to HOS.

The final step in heme *b* biosynthesis is catalyzed by ferrochelatase, which inserts iron into the porphyrin ring of its substrate, protoporphyrin IX (PPIX). Prokaryotic ferrochelatases are soluble proteins located in the cytoplasm, whereas eukaryotic ferrochelatases are localized to the mitochondrial matrix and contain a hydrophobic domain that allows them to interact with the matrix side of the inner mitochondrial membrane (Figure 1.7) (47). The heme binding site in HOS almost certainly faces the matrix in eukaryotes; therefore, direct transfer of heme *b* from ferrochelatase to HOS may be possible. Because product release is the rate-limiting step in the ferrochelatase reaction, it has been suggested that ferrochelatase's interactions with the apoprotein form of hemoproteins could cause a conformational change in ferrochelatase, thereby leading to heme transfer (110). Ferrochelatase could interact with HOS in a similar manner to deliver heme *b*. Although there is currently no experimental evidence to substantiate this particular interaction, many potential interaction partners for ferrochelatase have been identified by affinity purification of murine ferrochelatase and mass spectrometry analysis of its interactome (116). Because ferrochelatase also interacts with putative heme chaperones (PGRMC1 and PGRMC2), it is

also possible that one of these chaperones (or a currently unidentified chaperone) transfers heme *b* to HOS (116).

Transfer of heme b *to HAS*

Because HAS utilizes heme *b* as a cofactor, delivery of heme *b* to HAS is also required. Both of the heme binding sites in HAS are on the P-side (IMS side or periplasmic side) of the membrane, which would suggest that heme *b* must traverse the membrane to be inserted into HAS. In terms of membrane solubility, hemes are amphipathic molecules with a fairly nonpolar porphyrin ring and two negatively charged propionates. In theory, heme could cross the membrane unaided if the propionates are protonated or their negative charge is shielded by cations. Due to the oxidizing capacity of heme, however, it is generally assumed that heme transfer across membranes is mediated by proteins to protect the cells from oxidative damage (117). In light of these considerations, it seems likely that heme *b* is delivered to HAS either from the N-side (matrix or cytosolic side) of the membrane via interactions with ferrochelatase or a heme chaperone, or heme *b* could be transported across the membrane and delivered by a chaperone from the P-side. Both of these heme delivery routes have also been proposed for the hemylation of cytochrome *b*, another inner mitochondrial membrane hemoprotein (118). Understanding the hemylation of HAS and other membrane proteins will require further investigation.

Transfer of heme o *to from HOS to HAS*

After HOS converts heme *b* to heme *o*, heme *o* must be transferred to HAS (Figure 1.7). (Delivery of heme *o* to prokaryotic terminal oxidases will be discussed briefly below.) The fact that HOS precedes HAS in the heme *a* biosynthetic pathway seems to be an important strategy in heme trafficking. Conversion of the vinyl group on pyrrole ring A to a hydroxyethylfarnesyl moiety makes heme *o* much more hydrophobic than heme *b*, effectively sequestering heme *o* in the membrane. Adding the lipid tail first and then oxidizing the

methyl group on pyrrole ring D to synthesize heme *a* prevents misincorporation of a high-potential heme (*i.e.*, heme with a formyl substituent) into water-soluble proteins (54).

Although heme *o* is lipid-soluble, the location of the heme bindings sites of HOS and HAS on opposite sides of the membrane seems to require the movement of the negatively charged propionates from heme *o* through the lipid bilayer, an energetically unfavorable process (Figure 1.7) (118). There are at least three different scenarios one can envision to overcome this problem and transfer heme *o* from HOS to HAS. First, HOS could release heme *o* into the membrane, and heme *o* could diffuse into the active site of HAS. As discussed above, this process would require shielding the negatively charged propionates from the hydrophobic environment of the lipid bilayer via protonation or interaction with metal cations (117). Alternatively, HOS and HAS could interact to transfer substrate. This interaction would also shield heme *o*'s propionates from the lipid environment, and it has the added benefit of protecting the lipids in the bilayer from oxidative damage mediated by heme *o*. Finally, heme *o* delivery to HAS could be mediated by a chaperone or transporter. However, a heme *o* chaperone/transporter has never been identified despite decades of research on prokaryotic and eukaryotic heme-copper oxidases and the genes required for their assembly (109). Therefore, it seems more likely that heme *o* transfer from HOS to HAS is accomplished without the aid of additional proteins.

Prokaryotic HOS and HAS have been shown to interact when heterologously overexpressed in *E. coli*. Specifically, these experiments demonstrated that both type-1 (*B. subtilis*) HAS and type-2 (*R. sphaeroides*) HAS coimmunoprecipitate with *Bs*HOS and *R. sphaeroides* HOS, respectively (109). This result suggests that in prokaryotes, HOS and HAS may interact directly to transfer heme *o*. An interaction between eukaryotic HOS and eukaryotic HAS (also type-2), however, has never been demonstrated experimentally, despite several investigations into the protein-protein interactions of both HOS and HAS in *S.*

cerevisiae (81,93,98,101,119,120). Therefore, if HOS and HAS interact in eukaryotes, this interaction is likely transient.

Although difficult to detect experimentally, the physiologically relevant interaction of HOS and HAS is an intriguing possibility. As discussed above, heme *o* entry into HAS likely requires conformational changes in HAS that widen a lateral opening into the N-terminal heme binding site of HAS. While it seems clear that the heme binding site in HOS is located between two TM helices adjacent to the central cavity, it is less clear how heme *o* is released from HOS. It has been predicted that in closely related HOS homologs (*p*-hydroxybenzoate prenyltransferases), the polyprenyl tail protrudes into the lipid bilayer through an opening between TM1 and TM9 (analogous to the purple-blue and red helices shown in Figures 3 and 7) (49). Thus, heme *o* could exit "tail-first" by traveling through the central cavity. This substrate release process would require a conformational change to allow the porphyrin ring access to the lipid bilayer. Alternatively, heme *o* might be able to exit "propionate-first" through the C-terminal four-helical bundle if the appropriate conformational change were made to release heme *o* from the heme binding site. In either case, it could be imagined that interactions with HAS facilitate this conformational change. Elucidating the details of a potentially transient HOS-HAS interaction (or lack thereof) will probably require a combination of *in vivo* imaging techniques and structural and computational approaches.

Transfer of prenylated hemes (hemes o *and* a*) to subunit I of terminal heme-copper oxidases*

Heme *a*'s ultimate fate is insertion into either aa_3 or ba_3 heme-copper terminal oxidases. Specifically, one or two heme *a* molecules must be inserted into the largest oxidase subunit, termed subunit I in mitochondrial-like aa_3 oxidases (from class A) (Figure 1.7). Subunit I is one of the core oxidase subunits and also binds a copper cofactor (Cu_B) in addition to the two heme cofactors. Insertion of these metal cofactors into subunit I is part of the larger process

of heme-copper oxidase biogenesis, a complex process that involves the sequential assembly of the multiple protein subunits of the oxidase.

Heme-copper oxidase assembly has thus far been studied most extensively for family-A heme-copper oxidases from model organisms, such as the bo_3 quinol oxidase from *E. coli* (121-123), the cytochrome *c* oxidase from *P. denitrificans* (112,124), and the mitochondrial aa_3 oxidase from *S. cerevisiae* (118,125). Assembly of prokaryotic oxidases involves a minimal set of assembly factors (112,122), while the assembly of eukaryotic cytochrome *c* oxidase, also known as complex IV, is much more complicated (118,125). This added layer of complexity is due to the fact that eukaryotes have to coordinate the assembly of three core mitochondrial-encoded subunits and multiple nuclear-encoded subunits that are unique to eukaryotes (10,125-127). Correct assembly of eukaryotic cytochrome *c* oxidase involves up to 30 additional assembly factors that typically interact with one or more structural subunits to form subassembly complexes at specific stages of oxidase assembly (118,125). The steps of oxidase assembly, the sequence of these steps, and the number of assembly factors involved varies among eukaryotes and especially between eukaryotes and prokaryotes. Despite these differences, insertion of the heme and copper cofactors into subunit I usually occurs fairly early in the assembly of both prokaryotic and eukaryotic heme-copper terminal oxidases (112,118,125).

Whereas copper chaperones are necessary for copper insertion in both prokaryotic and eukaryotic heme-copper oxidases, only two potential heme *a* chaperones have been identified, and they are not universally conserved among organisms with aa_3 or ba_3 oxidases. One of these chaperones, CbaX, is only found in the bacterial *Thermaceae* group. CbaX has been implicated in heme *a* insertion into the ba_3 oxidase (family B) from *T. thermophilus*, but this protein has not yet been fully characterized (128). The putative heme *a* chaperone Surf1 (Shy1 in yeast) has been studied more extensively. Genes encoding Surf1/Shy1 have been

identified in eukaryotes, proteobacteria, and, more recently, in actinobacteria. The importance of Surf1/Shy1 in cytochrome *c* oxidase assembly has been confirmed in several model organisms with family A oxidases, including *Paracoccus denitrificans*, *S. cerevisiae*, and *Corynebacterium glutamicum*, as well as in humans (7,125,129,130). The specific function of Surf1/Shy1, however, is still debated, and it may play slightly different roles in prokaryotes and eukaryotes. In almost all Surf1-containing species studied thus far, residual levels of cytochrome *c* oxidase activity remain even when Surf1/Shy1 is truncated or deleted, indicating that a small amount of subunit I is still hemylated correctly in the absence of this putative chaperone (100,112,125,131). Heterologous coexpression of *P. denitrificans* Surf1, HOS, and HAS in *E. coli* indicated that Surf1 could bind heme *a*, and incubation of *P. denitrificans* HAS with Surf1 demonstrated that HAS can transfer heme *a* to Surf1 *in vitro* (112,132). However, mutation of the histidine predicted to ligate heme in Shy1 from *S. cerevisiae* indicated that heme *a* binding was not required for the assembly factor's function (101,112). Instead, Shy1 seems to be important for stabilizing a subunit I-containing subassembly complex that forms at the time of heme *a* insertion in yeast (81,101,111,133). Surf1c also seems to associate with subunit I-containing subassembly complexes in *P. denitrificans* (124). Therefore, although Surf1/Shy1 is required for efficient maturation of subunit I in eukaryotes and some prokaryotes, it may not be a true heme *a* chaperone that shuttles heme *a* between HAS and subunit I.

The apparent lack of a heme *a* chaperone in many prokaryotic species suggests that in these species, heme *a* transfer to subunit I may occur via a direct interaction between HAS and subunit I. Because the heme binding sites in HAS and subunit I are both located closer to the P-side (periplasmic/IMS side) of the membrane, a transporter is probably not required to translocate the propionate groups of heme *a* through the membrane (118). Therefore, heme *a* could, in theory be released directly into the lipid bilayer. Heme *a* can also spontaneously

bind synthetic four-helical bundles that mimic the structure of heme-copper oxidases, suggesting that from a thermodynamic standpoint, a chaperone is not necessarily required to facilitate the binding of heme *a* to subunit I (83). The most common argument against unassisted heme *a* diffusion in the lipid bilayer is that heme *a* transfer must be controlled to protect the lipid bilayer from heme *a*, a prooxidant (54,110,111).

An attractive alternative hypothesis is that HAS delivers heme *a* directly to subunit I. This hypothesis is supported by the observation that overexpression of HAS often results in copurification of HAS and its unreleased product, heme *a*. This phenomenon has been reported not only for heterologous overexpression of HAS in *E. coli*, but also for lower-level, more physiologically relevant expression conditions in *B. subtilis* (20,43,46,86,100). These results have led to the suggestion that in addition to synthesizing heme *a*, HAS functions as a heme *a* reservoir/chaperone, remaining bound to heme *a* until interactions with subunit I (or a subunit-I containing subassembly complex) trigger its release (43). At present, the most obvious conformational change in HAS that would lead to heme *a* release would be movement of TM2 away from the center of the four-helical bundle where heme *a* binds, which would effectively remove one of the histidine ligands from the heme binding site (51). Of course, the existence of novel, uncharacterized prokaryotic heme *a* chaperones that trigger heme *a* release from HAS cannot be ruled out.

Heme-copper oxidases with heme *o* in the active site require proper heme *o* insertion into subunit I. However, there is generally less information available about the assembly of these oxidases. Studies of quinol bo_3 assembly in *E. coli* indicate that both heme *b* and heme *o* are inserted into subunit I post-translationally (121,122). Efficient hemylation only seems to occur after subunit I has formed a complex with two other subunits (III and IV), possibly because interactions with these subunits induce a conformational change in subunit I that allows for the formation of the heme binding pockets (123). No heme *o* chaperone has been

identified, and the precise process governing the insertion of heme *b* into the low-spin heme binding pocket and heme *o* into the high-spin heme binding pocket is unknown. However, it seems likely that the structural difference between heme *b* and heme *o* (*i.e.*, the presence of a hydroxyethylfarnesyl tail on heme *o*) helps guide the insertion of each heme into the correct site.

Incorporation (or misincorporation) of alternate heme types into the same oxidase can occur in some prokaryotes, indicating that the assembly process for these oxidases is more flexible than that of their highly-regulated eukaryotic counterparts. For example, heme *o* can be misincorporated into the low-spin site of the *bo*$_3$ quinol oxidase in *E. coli* strains overexpressing their native HOS, resulting in a functional *oo*$_3$ oxidase (4,53). For a handful of prokaryotic species, functional switching between heme *o* and heme *a* as cofactors for the same oxidase has also been reported (4,30-37). Interestingly, the switch from heme *a* to heme *o* occurs under microaerobic conditions, although it is not clear if this switch is regulated transcriptionally or if low O_2 availability prevents heme *a* synthesis.

Taken together, these results suggest that either HOS or HAS may interact with subunit I or subunit I-containing assembly intermediates in these organisms to deliver heme, although the existence of an unidentified heme *o* chaperone or heme *a* chaperone in these organisms cannot be ruled out. A bifunctional chaperone is also possible, as exemplified by a mutant version of *P. denitrificans* Surf1 that can bind both heme *o* and heme *a*, although this variant does not seem to support insertion of either heme into its cognate oxidase (100). In summary, the process of heme *a* transfer from HAS and insertion into heme-copper terminal oxidases seems to vary across species. While heme *a* insertion into subunit I may not require a heme *a* chaperone in all organisms, this process does seem to be tightly regulated, especially in eukaryotes. Future work will be needed to clarify the role of potential heme *a* chaperones (or lack thereof) and the details of heme *a* transfer and insertion into subunit I.

Summary and thesis outline

Heme *a* is essential for aerobic respiration in eukaryotes and many prokaryotes due to its role as a cofactor for the majority of known heme-copper terminal oxidases. The heme *a* biosynthetic pathway is a two-step process in which the prenylation and oxidation of specific sites on the porphyrin ring of heme *b* are catalyzed by HOS and HAS, respectively. The genes necessary for these modifications appear to be conserved in almost all species known to synthesize heme *a*, while some other prokaryotic species, such as *E. coli*, only possess the gene for HOS and utilize a heme *o*-containing terminal oxidase. For both heme *o* synthase and heme *a* synthase, only a relatively small set of residues are strictly conserved. Structural and biochemical data indicate that some of these conserved residues are either metal ligands or participate in the catalytic mechanism. While investigations of protein families related to HOS have provided a reasonable proposed catalytic mechanism for HOS (Figure 1.2), studies probing the proposed catalytic mechanism for HAS (Figures 4, 5) are lacking. Additionally, although recent structural data has confirmed that the heme binding sites of HOS and HAS are most likely on opposite sides of the membrane, it remains unclear how heme is transferred from HOS to HAS and from HAS to the terminal oxidase. To address these questions, we have investigated the protein-protein interactions of eukaryotic (*S. cerevisiae*) HAS (Chapter 2), and we have used prokaryotic (*S. oneidensis*) HAS to study the role of highly conserved residues in substrate binding and catalysis (Chapter 3). Overall, these studies have broadened our understanding of the intriguing mechanism of heme *a* synthase and its potential role in prenylated heme transfer.

REFERENCES

REFERENCES

1. Ferguson-Miller, S., and Babcock, G. T. (1996) Heme/copper terminal oxidases. *Chem Rev* **96**, 2889-2908

2. Borisov, V. B., Gennis, R. B., Hemp, J., and Verkhovsky, M. I. (2011) The cytochrome *bd* respiratory oxygen reductases. *Biochim Biophys Acta* **1807**, 1398-1413

3. Borisov, V. B., and Siletsky, S. A. (2019) Features of organization and mechanism of catalysis of two families of terminal oxidases: heme-copper and *bd*-type. *Biochemistry (Mosc)* **84**, 1390-1402

4. Garcia-Horsman, J. A., Barquera, B., Rumbley, J., Ma, J., and Gennis, R. B. (1994) The superfamily of heme-copper respiratory oxidases. *J Bacteriol* **176**, 5587-5600

5. Schafer, G., Engelhard, M., and Muller, V. (1999) Bioenergetics of the Archaea. *Microbiol Mol Biol Rev* **63**, 570-620

6. Refojo, P. N., Sena, F. V., Calisto, F., Sousa, F. M., and Pereira, M. M. (2019) Chapter six: the plethora of membrane respiratory chains in the phyla of life. in *Advances in Microbial Physiology* (Poole, R. K. ed.), Academic Press. pp 331-414

7. Pereira, M. M., Sousa, F. L., Veríssimo, A. F., and Teixeira, M. (2008) Looking for the minimum common denominator in haem-copper oxygen reductases: towards a unified catalytic mechanism. *Biochim Biophys Acta* **1777**, 929-934

8. Maréchal, A., Meunier, B., Lee, D., Orengo, C., and Rich, P. R. (2012) Yeast cytochrome *c* oxidase: a model system to study mitochondrial forms of the haem-copper oxidase superfamily. *Biochim Biophys Acta* **1817**, 620-628

9. Wikstrom, M., Krab, K., and Sharma, V. (2018) Oxygen activation and energy conservation by cytochrome *c* oxidase. *Chem Rev* **118**, 2469-2490

10. Pereira, M. M., Santana, M., and Teixeira, M. (2001) A novel scenario for the evolution of haem-copper oxygen reductases. *Biochim Biophys Acta* **1505**, 185-208

11. Hemp, J. G., Robert, B. (2008) Bioenergetics: energy conservation and conversion. in *Bioenergetics: Energy Conservation and Conversion* (Schäfer, G. n. P., Harvey S. ed., 2008 Ed., Springer, Berlin

12. Puustinen, A., and Wikstrom, M. (1991) The heme groups of cytochrome *o* from *Escherichia coli*. *Proceedings of the National Academy of Sciences* **88**, 6122-6126

13. Saiki, K., Mogi, T., and Anraku, Y. (1992) Heme O biosynthesis in *Escherichia coli*: the *cyoE* gene in the cytochrome *bo* operon encodes a protoheme IX farnesyltransferase. *Biochemical and biophysical research communications* **189**, 1491-1497

14. Saiki, K., Mogi, T., Ogura, K., and Anraku, Y. (1993) *In vitro* heme O synthesis by the *cyoE* gene product from *Escherichia coli*. *The Journal of biological chemistry* **268**, 26041-26044

15. Mogi, T., Saiki, K., and Anraku, Y. (1994) Biosynthesis and functional role of haem O and haem A. *Molecular microbiology* **14**, 391-398

16. Glerum, D. M., and Tzagoloff, A. (1994) Isolation of a human cDNA for heme A:farnesyltransferase by functional complementation of a yeast *cox10* mutant. *Proceedings of the National Academy of Sciences* **91**, 8452-8456

17. Hill, J., Goswitz, V. C., Calhoun, M., Garcia-Horsman, J. A., Lemieux, L., Alben, J. O., and Gennis, R. B. (1992) Demonstration by FTIR that the *bo*-type ubiquinol oxidase of *Escherichia coli* contains a heme-copper binuclear center similar to that in cytochrome *c* oxidase and that proper assembly of the binuclear center requires the *cyoE* gene product. *Biochemistry* **31**, 11435-11440

18. van der Oost, J., von Wachenfeld, C., Hederstedt, L., and Saraste, M. (1991) *Bacillus subtilis* cytochrome oxidase mutants: biochemical analysis and genetic evidence for two aa_3-type oxidases. *Molecular microbiology* **5**, 2063-2072

19. Svensson, B., Lübben, M., and Hederstedt, L. (1993) *Bacillus subtilis* CtaA and CtaB function in haem A biosynthesis. *Molecular microbiology* **10**, 193-201

20. Svensson, B., Andersson, K. K., and Hederstedt, L. (1996) Low-spin heme A in the heme A biosynthetic protein CtaA from *Bacillus subtilis*. *European journal of biochemistry* **238**, 287-295

21. Svensson, B., and Hederstedt, L. (1994) *Bacillus subtilis* CtaA is a heme-containing membrane protein involved in heme A biosynthesis. *J Bacteriol* **176**, 6663-6671

22. Brown, K. R., Allan, B. M., Do, P., and Hegg, E. L. (2002) Identification of novel hemes generated by heme A synthase: evidence for two successive monooxygenase reactions. *Biochemistry* **41**, 10906-10913

23. Brown, K. R., Brown, B. M., Hoagland, E., Mayne, C. L., and Hegg, E. L. (2004) Heme A synthase does not incorporate molecular oxygen into the formyl group of heme A. *Biochemistry* **43**, 8616-8624

24. Mueller, J. P., and Taber, H. W. (1989) Structure and expression of the cytochrome aa_3 regulatory gene *ctaA* of *Bacillus subtilis*. *Journal of Bacteriology* **171**, 4979-4986

25. Barros, M. H., Carlson, C. G., Glerum, D. M., and Tzagoloff, A. (2001) Involvement of mitochondrial ferredoxin and Cox15p in hydroxylation of heme O. *FEBS letters* **492**, 133-138

26. Lübben, M., and Morand, K. (1994) Novel prenylated hemes as cofactors of cytochrome oxidases: archaea have modified hemes A and O. *The Journal of biological chemistry* **269**, 21473-21479

27. Lübben, M., Warne, A., Albracht, S. P., and Saraste, M. (1994) The purified SoxABCD quinol oxidase complex of *Sulfolobus acidocaldarius* contains a novel haem. *Molecular microbiology* **13**, 327-335

28. Castelle, C. J., Roger, M., Bauzan, M., Brugna, M., Lignon, S., Nimtz, M., Golyshina, O. V., Giudici-Orticoni, M. T., and Guiral, M. (2015) The aerobic respiratory chain of the acidophilic archaeon *Ferroplasma acidiphilum*: a membrane-bound complex oxidizing ferrous iron. *Biochim Biophys Acta* **1847**, 717-728

29. Bandeiras, T. M., Refojo, P. N., Todorovic, S., Murgida, D. H., Hildebrandt, P., Bauer, C., Pereira, M. M., Kletzin, A., and Teixeira, M. (2009) The cytochrome *ba* complex from the thermoacidophilic crenarchaeote *Acidianus ambivalens* is an analog of bc_1 complexes. *Biochimica et Biophysica Acta (BBA) - Bioenergetics* **1787**, 37-45

30. Matsushita, K., Ebisuya, H., and Adachi, O. (1992) Homology in the structure and the prosthetic groups between two different terminal ubiquinol oxidases, cytochrome a_1 and cytochrome *o*, of *Acetobacter aceti*. *The Journal of biological chemistry* **267**, 24748-24753

31. Matsushita, K., Ebisuya, H., Ameyama, M., and Adachi, O. (1992) Change of the terminal oxidase from cytochrome a_1 in shaking cultures to cytochrome *o* in static cultures of *Acetobacter aceti*. *J Bacteriol* **174**, 122-129

32. Sone, N., and Fujiwara, Y. (1991) Haem O can replace haem A in the active site of cytochrome *c* oxidase from thermophilic bacterium PS3. *FEBS letters* **288**, 154-158

33. Sone, N., Ogura, T., Noguchi, S., and Kitagawa, T. (1994) Proton pumping activity and visible absorption and resonance Raman spectra of a *cao*-type cytochrome *c* oxidase isolated from the thermophilic bacterium *Bacillus* PS3. *Biochemistry* **33**, 849-855

34. Auer, G., Mayer, B., Wastyn, M., Fromwald, S., Eghbalzad, K., Alge, D., and Peschek, G. A. (1995) Promiscuity of heme groups in the cyanobacterial cytochrome-C oxidase. *Biochemistry and molecular biology international* **37**, 1173-1185

35. Peschek, G. A., Alge, D., Fromwald, S., and Mayer, B. (1995) Transient accumulation of heme O (cytochrome *o*) in the cytoplasmic membrane of semi-anaerobic *Anacystis nidulans*: evidence for oxygenase-catalyzed heme O/A transformation. *The Journal of biological chemistry* **270**, 27937-27941

36. Contreras-Zentella, M., Mendoza, G., Membrillo-Hernández, J., and Escamilla, J. E. (2003) A novel double heme substitution produces a functional bo_3 variant of the quinol oxidase aa_3 of *Bacillus cereus*: purification and paratial characterization. *The Journal of biological chemistry* **278**, 31473-31478

37. Schröter, T., Winterstein, C., Ludwig, B., and Richter, O.-M. H. (1998) Expression of the *Escherichia coli cyo* operon in *Paracoccus denitrificans* results in a fully active quinol oxidase of unexpected heme composition. *FEBS letters* **432**, 109-112

38. Mogi, T. (2009) Over-expression and characterization of *Bacillus subtilis* heme O synthase. *Journal of biochemistry* **145**, 669-675

39. Throne-Holst, M., and Hederstedt, L. (2000) The *Bacillus subtilis ctaB* paralogue, *yjdK*, can complement the heme A synthesis deficiency of a CtaB-deficient mutant. *FEMS microbiology letters* **183**, 247-251

40. Lyons, J. A., Aragão, D., Slattery, O., Pisliakov, A. V., Soulimane, T., and Caffrey, M. (2012) Structural insights into electron transfer in caa_3-type cytochrome oxidase. *Nature* **487**, 514-518

41. Scharf, B., Wittenberg, R., and Engelhard, M. (1997) Electron transfer proteins from the haloalkaliphilic archaeon *Natronobacterium pharaonis*: possible components of the respiratory chain include cytochrome *bc* and a terminal oxidase cytochrome ba_3. *Biochemistry* **36**, 4471-4479

42. Li, W. (2016) Bringing bioactive compounds into membranes: the UbiA superfamily of intramembrane aromatic prenyltransferases. *Trends in biochemical sciences* **41**, 356-370

43. Hederstedt, L. (2012) Heme A biosynthesis. *Biochim Biophys Acta* **1817**, 920-927

44. He, D., Fu, C. J., and Baldauf, S. L. (2016) Multiple origins of eukaryotic *cox15* suggest horizontal gene transfer from bacteria to jakobid mitochondrial DNA. *Molecular biology and evolution* **33**, 122-133

45. Lübben, M. (1995) Cytochromes of archaeal electron transfer chains. *Biochim Biophys Acta* **1229**, 1-22

46. Lewin, A., and Hederstedt, L. (2006) Compact archaeal variant of heme A synthase. *FEBS letters* **580**, 5351-5356

47. Heinemann, I. U., Jahn, M., and Jahn, D. (2008) The biochemistry of heme biosynthesis. *Archives of biochemistry and biophysics* **474**, 238-251

48. Swenson, S. A., Moore, C. M., Marcero, J. R., Medlock, A. E., Reddi, A. R., and Khalimonchuk, O. (2020) From synthesis to utilization: the ins and outs of mitochondrial heme. *Cells* **9**

49. Cheng, W., and Li, W. (2014) Structural insights into ubiquinone biosynthesis in membranes. *Science (New York, N.Y.)* **343**, 878-881

50. Huang, H., Levin, E. J., Liu, S., Bai, Y., Lockless, S. W., and Zhou, M. (2014) Structure of a membrane-embedded prenyltransferase homologous to UBIAD1. *PLoS biology* **12**, e1001911

51. Niwa, S., Takeda, K., Kosugi, M., Tsutsumi, E., Mogi, T., and Miki, K. (2018) Crystal structure of heme A synthase from *Bacillus subtilis*. *Proceedings of the National Academy of Sciences of the United States of America* **115**, 11953-11957

52. Zeng, H., Zhu, G., Zhang, S., Li, X., Martin, J., Morgner, N., Sun, F., Peng, G., Xie, H., and Michel, H. (2020) Isolated heme A synthase from *Aquifex aeolicus* is a trimer. *mBio* **11**

53. Puustinen, A. (1992) A novel type haem group of cytochrome *o* from *Escherichia coli*. *Acta physiologica Scandinavica. Supplementum* **607**, 265-268

54. Zhuang, J., Reddi, A. R., Wang, Z., Khodaverdian, B., Hegg, E. L., and Gibney, B. R. (2006) Evaluating the roles of the heme *a* side chains in cytochrome *c* oxidase using designed heme proteins. *Biochemistry* **45**, 12530-12538

55. Abramson, J., Riistama, S., Larsson, G., Jasaitis, A., Svensson-Ek, M., Laakkonen, L., Puustinen, A., Iwata, S., and Wikström, M. (2000) The structure of the ubiquinol oxidase from *Escherichia coli* and its ubiquinone binding site. *Nature structural biology* **7**, 910-917

56. Iwata, S., Ostermeier, C., Ludwig, B., and Michel, H. (1995) Structure at 2.8 A resolution of cytochrome *c* oxidase from *Paracoccus denitrificans*. *Nature* **376**, 660-669

57. Wang, N., Zhao, X., and Lu, Y. (2005) Role of heme types in heme-copper oxidases: effects of replacing a heme *b* with a heme *o* mimic in an engineered heme-copper center in myoglobin. *Journal of the American Chemical Society* **127**, 16541-16547

58. Buschmann, S., Warkentin, E., Xie, H., Langer, J. D., Ermler, U., and Michel, H. (2010) The structure of cbb_3 cytochrome oxidase provides insights into proton pumping. *Science (New York, N.Y.)* **329**, 327-330

59. Sharma, V., Wikström, M., and Kaila, V. R. (2011) Stabilization of the peroxy intermediate in the oxygen splitting reaction of cytochrome cbb_3. *Biochim Biophys Acta* **1807**, 813-818

60. Nobrega, M. P., Nobrega, F. G., and Tzagoloff, A. (1990) *COX10* codes for a protein homologous to the ORF1 product of *Paracoccus denitrificans* and is required for the synthesis of yeast cytochrome oxidase. *The Journal of biological chemistry* **265**, 14220-14226

61. Melzer, M., and Heide, L. (1994) Characterization of polyprenyldiphosphate: 4-hydroxybenzoate polyprenyltransferase from *Escherichia coli*. *Biochim Biophys Acta* **1212**, 93-102

62. Bräuer, L., Brandt, W., Schulze, D., Zakharova, S., and Wessjohann, L. (2008) A structural model of the membrane-bound aromatic prenyltransferase UbiA from *E. coli*. *Chembiochem : a European journal of chemical biology* **9**, 982-992

63. Wessjohann, L., and Sontag, B. (1996) Prenylation of benzoic acid derivatives catalyzed by a transferase from *Escherichia coli* overproduction: method development and substrate specificity. *Angewandte Chemie International Edition in English* **35**, 1697-1699

64. Poulter, C. D., and Rilling, H. C. (1978) The prenyl transfer reaction: enzymatic and mechanistic studies of the 1'-4 coupling reaction in the terpene biosynthetic pathway. *Accounts of Chemical Research* **11**, 307-313

65. Hosfield, D. J., Zhang, Y., Dougan, D. R., Broun, A., Tari, L. W., Swanson, R. V., and Finn, J. (2004) Structural basis for bisphosphonate-mediated inhibition of isoprenoid biosynthesis. *The Journal of biological chemistry* **279**, 8526-8529

66. Kavanagh, K. L., Dunford, J. E., Bunkoczi, G., Russell, R. G., and Oppermann, U. (2006) The crystal structure of human geranylgeranyl pyrophosphate synthase reveals a novel hexameric arrangement and inhibitory product binding. *The Journal of biological chemistry* **281**, 22004-22012

67. Bayse, C. A., and Merz, K. M. (2014) Mechanistic insights into Mg^{2+}-independent prenylation by CloQ from classical molecular mechanics and hybrid quantum mechanics/molecular mechanics molecular dynamics simulations. *Biochemistry* **53**, 5034-5041

68. Luk, L. Y., and Tanner, M. E. (2009) Mechanism of dimethylallyltryptophan synthase: evidence for a dimethylallyl cation intermediate in an aromatic prenyltransferase reaction. *Journal of the American Chemical Society* **131**, 13932-13933

69. Yang, Y., Miao, Y., Wang, B., Cui, G., and Merz, K. M., Jr. (2012) Catalytic mechanism of aromatic prenylation by NphB. *Biochemistry* **51**, 2606-2618

70. Rudolf, J. D., and Poulter, C. D. (2013) Tyrosine O-prenyltransferase SirD catalyzes S-, C-, and N-prenylations on tyrosine and tryptophan derivatives. *ACS chemical biology* **8**, 2707-2714

71. Rudolf, J. D., Wang, H., and Poulter, C. D. (2013) Multisite prenylation of 4-substituted tryptophans by dimethylallyltryptophan synthase. *Journal of the American Chemical Society* **135**, 1895-1902

72. Kranz, R. G., Richard-Fogal, C., Taylor, J. S., and Frawley, E. R. (2009) Cytochrome *c* biogenesis: mechanisms for covalent modifications and trafficking of heme and for heme-iron redox control. *Microbiol Mol Biol Rev* **73**, 510-528, Table of Contents

73. Saiki, K., Mogi, T., Hori, H., Tsubaki, M., and Anraku, Y. (1993) Identification of the functional domains in heme O synthase: site-directed mutagenesis studies on the *cyoE* gene of the cytochrome *bo* operon in *Escherichia coli*. *The Journal of biological chemistry* **268**, 26927-26934

74. Heo, L., and Feig, M. (2020) High-accuracy protein structures by combining machine-learning with physics-based refinement. *Proteins* **88**, 637-642

75. Yang, J., Anishchenko, I., Park, H., Peng, Z., Ovchinnikov, S., and Baker, D. (2020) Improved protein structure prediction using predicted interresidue orientations. *Proceedings of the National Academy of Sciences of the United States of America* **117**, 1496-1503

76. Antonicka, H., Leary, S. C., Guercin, G. H., Agar, J. N., Horvath, R., Kennaway, N. G., Harding, C. O., Jaksch, M., and Shoubridge, E. A. (2003) Mutations in *COX10* result in a defect in mitochondrial heme A biosynthesis and account for multiple,

early-onset clinical phenotypes associated with isolated COX deficiency. *Human molecular genetics* **12**, 2693-2702

77. Chepuri, V., and Gennis, R. B. (1990) The use of gene fusions to determine the topology of all of the subunits of the cytochrome *o* terminal oxidase complex of *Escherichia coli*. *The Journal of biological chemistry* **265**, 12978-12986

78. Li, T., Bonkovsky, H. L., and Guo, J. T. (2011) Structural analysis of heme proteins: implications for design and prediction. *BMC structural biology* **11**, 13

79. Li, Y., Zhang, Y., Zhang, C., Wang, H., Wei, X., Chen, P., and Lu, L. (2020) Mitochondrial dysfunctions trigger the calcium signaling-dependent fungal multidrug resistance. *Proceedings of the National Academy of Sciences of the United States of America* **117**, 1711-1721

80. Valnot, I., von Kleist-Retzow, J. C., Barrientos, A., Gorbatyuk, M., Taanman, J. W., Mehaye, B., Rustin, P., Tzagoloff, A., Munnich, A., and Rötig, A. (2000) A mutation in the human heme A:farnesyltransferase gene (*COX10*) causes cytochrome *c* oxidase deficiency. *Human molecular genetics* **9**, 1245-1249

81. Khalimonchuk, O., Kim, H., Watts, T., Perez-Martinez, X., and Winge, D. R. (2012) Oligomerization of heme *o* synthase in cytochrome oxidase biogenesis is mediated by cytochrome oxidase assembly factor Coa2. *The Journal of biological chemistry* **287**, 26715-26726

82. Bestwick, M., Khalimonchuk, O., Pierrel, F., and Winge, D. R. (2010) The role of Coa2 in hemylation of yeast Cox1 revealed by its genetic interaction with Cox10. *Molecular and cellular biology* **30**, 172-185

83. Zhuang, J., Amoroso, J. H., Kinloch, R., Dawson, J. H., Baldwin, M. J., and Gibney, B. R. (2006) Evaluation of electron-withdrawing group effects on heme binding in designed proteins: implications for heme *a* in cytochrome *c* oxidase. *Inorganic chemistry* **45**, 4685-4694

84. Myer, Y. P., Saturno, A. F., Verma, B. C., and Pande, A. (1979) Horse heart cytochrome *c*: the oxidation-reduction potential and protein structures. *The Journal of biological chemistry* **254**, 11202-11207

85. Tsudzuki, T., and Wilson, D. F. (1971) The oxidation-reduction potentials of the hemes and copper of cytochrome oxidase from beef heart. *Archives of biochemistry and biophysics* **145**, 149-154

86. Sakamoto, J., Hayakawa, A., Uehara, T., Noguchi, S., and Sone, N. (1999) Cloning of *Bacillus stearothermophilus ctaA* and heme A synthesis with the CtaA protein produced in *Escherichia coli*. *Bioscience, biotechnology, and biochemistry* **63**, 96-103

87. Schneegurt, M. A., and Beale, S. I. (1992) Origin of the chlorophyll *b* formyl oxygen in *Chlorella vulgaris*. *Biochemistry* **31**, 11677-11683

88. Oster, U., Tanaka, R., Tanaka, A., and Rüdiger, W. (2000) Cloning and functional expression of the gene encoding the key enzyme for chlorophyll *b* biosynthesis

(CAO) from *Arabidopsis thaliana*. *The Plant journal : for cell and molecular biology* **21**, 305-310

89. Porra, R. J., Schäfer, W., Cmiel, E., Katheder, I., and Scheer, H. (1993) Derivation of the formyl-group oxygen of chlorophyll *b* from molecular oxygen in greening leaves of a higher plant (*Zea mays*). *FEBS letters* **323**, 31-34

90. Hiner, A. N., Raven, E. L., Thorneley, R. N., García-Cánovas, F., and Rodríguez-López, J. N. (2002) Mechanisms of compound I formation in heme peroxidases. *Journal of inorganic biochemistry* **91**, 27-34

91. Poulos, T. L. (2010) Thirty years of heme peroxidase structural biology. *Archives of biochemistry and biophysics* **500**, 3-12

92. Sono, M., Roach, M. P., Coulter, E. D., and Dawson, J. H. (1996) Heme-containing oxygenases. *Chem Rev* **96**, 2841-2888

93. Barros, M. H., and Tzagoloff, A. (2002) Regulation of the heme A biosynthetic pathway in *Saccharomyces cerevisiae*. *FEBS letters* **516**, 119-123

94. Hederstedt, L., Lewin, A., and Throne-Holst, M. (2005) Heme A synthase enzyme functions dissected by mutagenesis of *Bacillus subtilis* CtaA. *J Bacteriol* **187**, 8361-8369

95. Mogi, T. (2009) Probing structure of heme A synthase from *Bacillus subtilis* by site-directed mutagenesis. *Journal of biochemistry* **145**, 625-633

96. Ortiz de Montellano, P. R. (2008) Mechanism and role of covalent heme binding in the CYP4 family of P_{450} enzymes and the mammalian peroxidases. *Drug metabolism reviews* **40**, 405-426

97. Colas, C., Kuo, J. M., and Ortiz de Montellano, P. R. (2002) Asp-225 and glu-375 in autocatalytic attachment of the prosthetic heme group of lactoperoxidase. *The Journal of biological chemistry* **277**, 7191-7200

98. Swenson, S., Cannon, A., Harris, N. J., Taylor, N. G., Fox, J. L., and Khalimonchuk, O. (2016) Analysis of oligomerization properties of heme *a* synthase provides insights into its function in eukaryotes. *The Journal of biological chemistry* **291**, 10411-10425

99. Lewin, A., and Hederstedt, L. (2016) Heme A synthase in bacteria depends on one pair of cysteinyls for activity. *Biochim Biophys Acta* **1857**, 160-168

100. Hannappel, A., Bundschuh, F. A., and Ludwig, B. (2011) Characterization of heme-binding properties of *Paracoccus denitrificans* Surf1 proteins. *The FEBS journal* **278**, 1769-1778

101. Bareth, B., Dennerlein, S., Mick, D. U., Nikolov, M., Urlaub, H., and Rehling, P. (2013) The heme *a* synthase Cox15 associates with cytochrome *c* oxidase assembly intermediates during Cox1 maturation. *Molecular and cellular biology* **33**, 4128-4137

102. Merli, M. L., Cirulli, B. A., Menéndez-Bravo, S. M., and Cricco, J. A. (2017) Heme A synthesis and C*c*O activity are essential for *Trypanosoma cruzi* infectivity and replication. *The Biochemical journal* **474**, 2315-2332

103. Antonicka, H., Mattman, A., Carlson, C. G., Glerum, D. M., Hoffbuhr, K. C., Leary, S. C., Kennaway, N. G., and Shoubridge, E. A. (2003) Mutations in *COX15* produce a defect in the mitochondrial heme biosynthetic pathway, causing early-onset fatal hypertrophic cardiomyopathy. *American journal of human genetics* **72**, 101-114

104. Alfadhel, M., Lillquist, Y. P., Waters, P. J., Sinclair, G., Struys, E., McFadden, D., Hendson, G., Hyams, L., Shoffner, J., and Vallance, H. D. (2011) Infantile cardioencephalopathy due to a *COX15* gene defect: report and review. *American journal of medical genetics. Part A* **155a**, 840-844

105. Bugiani, M., Tiranti, V., Farina, L., Uziel, G., and Zeviani, M. (2005) Novel mutations in *COX15* in a long surviving Leigh syndrome patient with cytochrome *c* oxidase deficiency. *Journal of medical genetics* **42**, e28

106. Oquendo, C. E., Antonicka, H., Shoubridge, E. A., Reardon, W., and Brown, G. K. (2004) Functional and genetic studies demonstrate that mutation in the *COX15* gene can cause Leigh syndrome. *Journal of medical genetics* **41**, 540-544

107. Miryounesi, M., Fardaei, M., Tabei, S. M., and Ghafouri-Fard, S. (2016) Leigh syndrome associated with a novel mutation in the *COX15* gene. *Journal of pediatric endocrinology & metabolism : JPEM* **29**, 741-744

108. Zoppellaro, G., Bren, K. L., Ensign, A. A., Harbitz, E., Kaur, R., Hersleth, H.-P., Ryde, U., Hederstedt, L., and Andersson, K. K. (2009) Review: studies of ferric heme proteins with highly anisotropic/highly axial low spin (S = 1/2) electron paramagnetic resonance signals with *bis*-histidine and histidine-methionine axial iron coordination. *Biopolymers* **91**, 1064-1082

109. Brown, B. M., Wang, Z., Brown, K. R., Cricco, J. A., and Hegg, E. L. (2004) Heme O synthase and heme A synthase from *Bacillus subtilis* and *Rhodobacter sphaeroides* interact in *Escherichia coli*. *Biochemistry* **43**, 13541-13548

110. Donegan, R. K., Moore, C. M., Hanna, D. A., and Reddi, A. R. (2019) Handling heme: the mechanisms underlying the movement of heme within and between cells. *Free radical biology & medicine* **133**, 88-100

111. Khalimonchuk, O., Bird, A., and Winge, D. R. (2007) Evidence for a pro-oxidant intermediate in the assembly of cytochrome oxidase. *The Journal of biological chemistry* **282**, 17442-17449

112. Hannappel, A., Bundschuh, F. A., and Ludwig, B. (2012) Role of Surf1 in heme recruitment for bacterial COX biogenesis. *Biochim Biophys Acta* **1817**, 928-937

113. Burden, A. E., Wu, C., Dailey, T. A., Busch, J. L., Dhawan, I. K., Rose, J. P., Wang, B., and Dailey, H. A. (1999) Human ferrochelatase: crystallization, characterization of the [2Fe-2S] cluster and determination that the enzyme is a homodimer. *Biochim Biophys Acta* **1435**, 191-197

114. Wu, C. K., Dailey, H. A., Rose, J. P., Burden, A., Sellers, V. M., and Wang, B. C. (2001) The 2.0 A structure of human ferrochelatase, the terminal enzyme of heme biosynthesis. *Nature structural biology* **8**, 156-160

115. Medlock, A. E., Dailey, T. A., Ross, T. A., Dailey, H. A., and Lanzilotta, W. N. (2007) A pi-helix switch selective for porphyrin deprotonation and product release in human ferrochelatase. *Journal of molecular biology* **373**, 1006-1016

116. Piel, R. B., 3rd, Dailey, H. A., Jr., and Medlock, A. E. (2019) The mitochondrial heme metabolon: insights into the complex(ity) of heme synthesis and distribution. *Molecular genetics and metabolism* **128**, 198-203

117. Reddi, A. R., and Hamza, I. (2016) Heme mobilization in animals: a metallolipid's journey. *Acc Chem Res* **49**, 1104-1110

118. Kim, H. J., Khalimonchuk, O., Smith, P. M., and Winge, D. R. (2012) Structure, function, and assembly of heme centers in mitochondrial respiratory complexes. *Biochim Biophys Acta* **1823**, 1604-1616

119. Taylor, N. G., Swenson, S., Harris, N. J., Germany, E. M., Fox, J. L., and Khalimonchuk, O. (2017) The assembly factor Pet117 couples heme *a* synthase activity to cytochrome oxidase assembly. *The Journal of biological chemistry* **292**, 1815-1825

120. Herwaldt, E. J., Rivett, E. D., White, A. J., and Hegg, E. L. (2018) Cox15 interacts with the cytochrome bc_1 dimer within respiratory supercomplexes as well as in the absence of cytochrome *c* oxidase. *The Journal of biological chemistry* **293**, 16426-16439

121. Stenberg, F., von Heijne, G., and Daley, D. O. (2007) Assembly of the cytochrome bo_3 complex. *Journal of molecular biology* **371**, 765-773

122. Price, C. E., and Driessen, A. J. (2010) Biogenesis of membrane bound respiratory complexes in *Escherichia coli*. *Biochim Biophys Acta* **1803**, 748-766

123. Palombo, I., and Daley, D. O. (2012) Heme incorporation into the cytochrome bo_3 occurs at a late stage of assembly. *FEBS letters* **586**, 4197-4202

124. Schimo, S., Wittig, I., Pos, K. M., and Ludwig, B. (2017) Cytochrome *c* oxidase biogenesis and metallochaperone interactions: steps in the assembly pathway of a bacterial complex. *PloS one* **12**, e0170037

125. Timón-Gómez, A., Nývltová, E., Abriata, L. A., Vila, A. J., Hosler, J., and Barrientos, A. (2018) Mitochondrial cytochrome *c* oxidase biogenesis: recent developments. *Seminars in cell & developmental biology* **76**, 163-178

126. Capaldi, R. A. (1990) Structure and assembly of cytochrome *c* oxidase. *Archives of biochemistry and biophysics* **280**, 252-262

127. Tsukihara, T., Aoyama, H., Yamashita, E., Tomizaki, T., Yamaguchi, H., Shinzawa-Itoh, K., Nakashima, R., Yaono, R., and Yoshikawa, S. (1996) The whole structure of

the 13-subunit oxidized cytochrome *c* oxidase at 2.8 A. *Science (New York, N.Y.)* **272**, 1136-1144

128. Werner, C., Richter, O. M., and Ludwig, B. (2010) A novel heme *a* insertion factor gene cotranscribes with the *Thermus thermophilus* cytochrome ba_3 oxidase locus. *J Bacteriol* **192**, 4712-4719

129. Davoudi, C. F., Ramp, P., Baumgart, M., and Bott, M. (2019) Identification of Surf1 as an assembly factor of the cytochrome bc_1-aa_3 supercomplex of *Actinobacteria*. *Biochimica et biophysica acta. Bioenergetics* **1860**, 148033

130. Niebisch, A., and Bott, M. (2001) Molecular analysis of the cytochrome bc_1-aa_3 branch of the *Corynebacterium glutamicum* respiratory chain containing an unusual diheme cytochrome c_1. *Archives of microbiology* **175**, 282-294

131. Smith, D., Gray, J., Mitchell, L., Antholine, W. E., and Hosler, J. P. (2005) Assembly of cytochrome-*c* oxidase in the absence of assembly protein Surf1p leads to loss of the active site heme. *The Journal of biological chemistry* **280**, 17652-17656

132. Bundschuh, F. A., Hannappel, A., Anderka, O., and Ludwig, B. (2009) Surf1, associated with Leigh syndrome in humans, is a heme-binding protein in bacterial oxidase biogenesis. *The Journal of biological chemistry* **284**, 25735-25741

133. Pierrel, F., Khalimonchuk, O., Cobine, P. A., Bestwick, M., and Winge, D. R. (2008) Coa2 is an assembly factor for yeast cytochrome *c* oxidase biogenesis that facilitates the maturation of Cox1. *Molecular and cellular biology* **28**, 4927-4939

Chapter 2: Cox15 protein interactions reveal its interaction with the cytochrome bc_1 complex both within and apart from the respiratory supercomplexes[1]

[1] This chapter was adapted from Herwaldt, E. J., Rivett, E. D., White, A. J., and Hegg, E. L. (2018) Cox15 interacts with the cytochrome bc_1 dimer within respiratory supercomplexes as well as in the absence of cytochrome *c* oxidase. *The Journal of biological chemistry* **293**, 16426-16439. DOI: https://doi.org/10.1074/jbc.RA118.002496. Permission to adapt the original article is granted under the Creative Commons Attribution License (CC BY). E.J. Herwaldt designed the study and wrote the initial draft of the paper. E.D. Rivett prepared Figure 2.2, performed replicate experiments for data presented in Figure 2.3 and Figure 2.5B, performed control experiments for the Cor1 antibody and prepared Figure 2.6, and performed the studies on mutant Cox15 presented in Figures 2.6 and 2.10. A.J. White performed and prepared Figures 1A and 1C and also performed many background experiments leading up to this work. E.J. Herwaldt performed all other experiments and prepared the rest of the figures.

Abstract

Heme *a* is an obligatory cofactor in the terminal enzyme complex of the electron transport chain, cytochrome *c* oxidase. The heme *a* molecule is synthesized from heme *o* by a multi-spanning inner membrane protein, heme *a* synthase (Cox15 in yeast). The insertion of heme *a* is critical for cytochrome *c* oxidase function and assembly, but this process has not been fully elucidated. To increase our understanding of heme *a* insertion into cytochrome *c* oxidase, we investigated the protein-protein interactions that occur with Cox15 in *Saccharomyces cerevisiae*. In addition to observing Cox15 in homo-oligomeric complexes, we observed that a portion of Cox15 associated with the mitochondrial respiratory supercomplexes. When supercomplex formation was abolished, as in the case of stalled cytochrome bc_1 or cytochrome *c* oxidase assembly, Cox15 maintained an interaction with select proteins from both of the respiratory complexes. In the case of stalled cytochrome bc_1 assembly, Cox15 was found to interact with the late-assembling cytochrome *c* oxidase subunit, Cox13. When cytochrome *c* oxidase assembly was stalled, Cox15 maintained its interaction with the cytochrome bc_1 protein, Cor1. Our data indicate that Cox15 and Cor1 interact in the cytochrome bc_1 dimer in the absence of supercomplexes or when the supercomplexes are destabilized due to the loss of Rcf1. These findings reveal that Cox15 not only associates with respiratory supercomplexes but, unexpectedly, also interacts with the cytochrome bc_1 dimer even in the absence of cytochrome *c* oxidase.

Introduction

Cytochrome *c* oxidase, a large multi-subunit enzyme in the inner membrane of the mitochondria, plays a vital role in aerobic respiration in eukaryotic organisms. Serving as the terminal electron acceptor in the electron transport chain, cytochrome *c* oxidase catalyzes the reduction of O_2 to two water molecules while four protons are pumped across the inner mitochondrial membrane (1-3). For this chemistry to occur, two heme *a* molecules must be properly inserted into Cox1, the catalytic heme-containing subunit of cytochrome *c* oxidase (2-7).

Heme *a* is synthesized via two reactions catalyzed by two integral membrane proteins, heme *o* synthase (Cox10) and heme *a* synthase (Cox15), which are located in the mitochondrial inner membrane. Cox10 catalyzes the conversion of a heme *b* molecule into a heme *o* molecule. Then, in a process that has not been fully elucidated, heme *o* is further modified into heme *a* by Cox15 (7-12). The only known destination for the resulting heme *a* is cytochrome *c* oxidase (11). While much progress has been made in understanding the assembly of cytochrome *c* oxidase, very little is known about how heme *a* is inserted into Cox1. Because of the reactive nature of heme *a*, due in part to its increased reduction potential relative to the other types of heme (13), it is thought that heme insertion into Cox1 either occurs co-translationally or that a protein chaperone delivers heme from Cox15 to cytochrome *c* oxidase (14).

It has been debated whether the inner membrane protein, Shy1 (Surf1 in humans and bacteria), acts as the metallochaperone that delivers heme *a* to cytochrome *c* oxidase or whether it strictly mediates the protein environment around the heme *a* site during heme insertion into Cox1. Studies in the bacterium *Paracoccus denitrificans* indicate that Surf1 is capable of binding heme, suggesting a role in heme *a* delivery to Cox1 (15,16). In contrast, work in *Saccharomyces cerevisiae* has not been able to demonstrate that Shy1 is capable of binding heme, but it has revealed that Shy1 is present in the early assembly intermediate complexes that exist with Cox1 near the time of heme insertion (7,17,18). Additionally, Shy1 must be present for Cox1 to be fully hemylated (17). This work in yeast suggests that Shy1 acts as a scaffold during heme insertion into Cox1 rather than a heme binding and delivery protein. Unraveling the protein-protein interactions that occur with Cox15 may better inform us of the protein interactions that occur following heme *a* synthesis and delivery to cytochrome *c* oxidase.

It has been established that Cox15 exists in high molecular weight protein complexes as observed via blue native polyacrylamide gel electrophoresis (BN-PAGE) (8,10,19). Recently, it has been shown that these complexes largely represent oligomers of Cox15 that are stabilized by strong hydrophobic interactions (8), and some evidence may suggest that Cox15 is able to interact sub-stoichiometrically with assembling Cox1 (10). Additionally, Bareth et al. suggest Cox15 may interact with Shy1 within some of the lower Cox15-containing complexes (10), an interesting observation given the suggestion that Shy1 may be a heme chaperone. Both determining the identity of the proteins that interact with Cox15 in the Cox15 high molecular weight complexes and understanding how the complexes are regulated have been equally perplexing. Cox15 high molecular weight complexes still form in cytochrome *c* oxidase mutants, when Cox15 is catalytically inactive, and when there is an impairment in heme *o* biosynthesis (8,10,20). Two recent findings have begun to shed light on some of the factors that are important in Cox15 oligomerization. First, the unstructured linker region that connects the N- and C-terminal halves of Cox15 has been shown to be important for Cox15 function and its oligomerization, although it does not seem to significantly impact the steady-state levels of Cox15 (8). Second, the previously uncharacterized Pet117, known to be important for cytochrome *c* oxidase assembly, was shown to interact with Cox15 and is the first protein identified that when knocked out abolishes the Cox15 complexes observed on BN-PAGE (9). Interestingly, however, Cox15 was still found to interact with itself in the absence of Pet117, indicating that Pet117 is important for the stabilization but not the formation of the Cox15 oligomers (9).

In this report, we analyzed the Cox15 complexes to further elucidate heme *a* delivery to cytochrome *c* oxidase. We have found, like others (8), that much of the Cox15 complexes reflect oligomeric states of Cox15, but that in addition to oligomeric Cox15, two of the Cox15 complexes reflect the presence of Cox15 within respiratory supercomplexes. Our

results indicate that a relatively small amount of Cox15 is present within the supercomplexes, suggesting that Cox15 only exists within a subset of respiratory supercomplexes. We probed for interactions that occur between Cox15 and proteins of the cytochrome bc_1 complex as well as cytochrome *c* oxidase. We found that Cox15 is capable of interacting with Cor1 from the cytochrome bc_1 complex as well as Cox5a and Cox13 from cytochrome *c* oxidase, presumably within the supercomplexes. Interactions with Cox13 appear to be maintained in the absence of supercomplexes. Of particular interest was the finding that Cox15 and Cor1 interact in the absence of supercomplexes, likely within the dimer of cytochrome bc_1. Thus, it appears that not only is a portion of Cox15 present in the supercomplexes, but also that its presence within the supercomplexes may be mediated by the cytochrome bc_1 protein, Cor1.

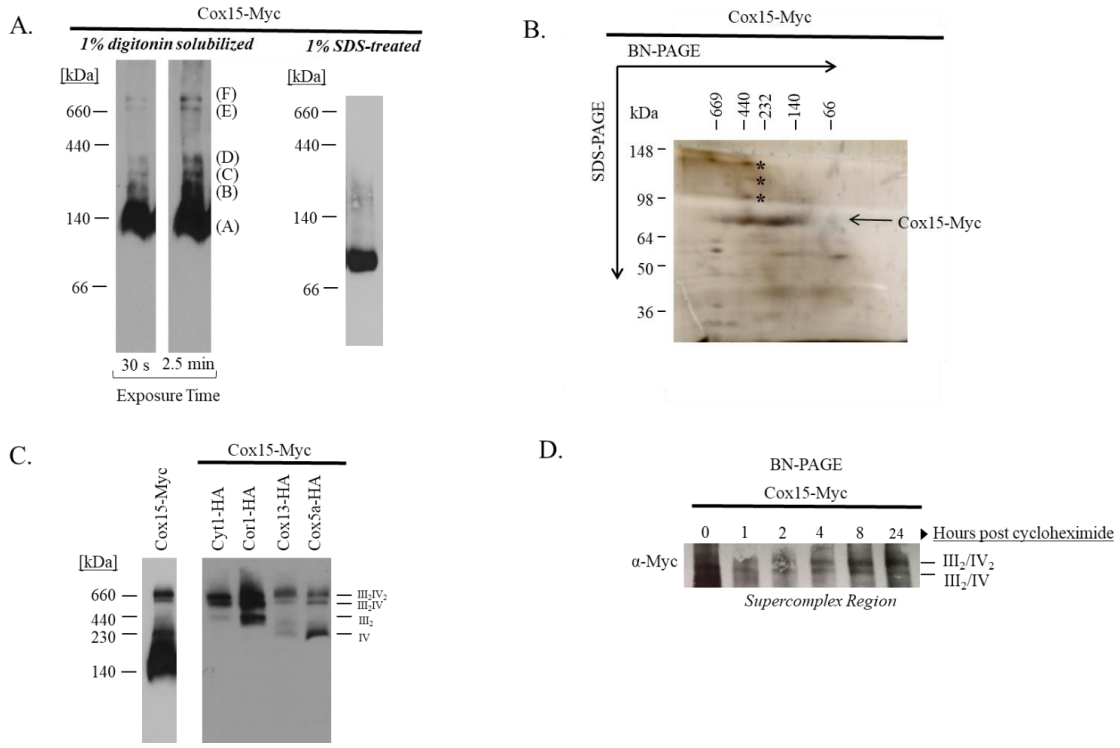

Figure 2.1: BN-PAGE of Cox15-Myc$_{(13x)}$ reveals the presence of Cox15 in oligomeric complexes and within respiratory supercomplexes

A. Western blot of BN-PAGE using mitochondria containing a 13x C-terminal myc tag on Cox15 (Cox15-Myc) solubilized in either 1% digitonin (repeated with numerous biological replicates) or 1% SDS (repeated in three independent experiments (biological replicates)). Both blots represent 10 µg of mitochondria and are probed with an anti Myc antibody. B. Silver stain of a two-dimensional BN/SDS-PAGE of purified Cox15-Myc using non-denaturing anti c-Myc purification (repeated in two independent experiments (biological replicates).

Results

Cox15-Myc exists in both oligomeric high molecular weight protein complexes and protein complexes that reveal the presence of Cox15 within respiratory supercomplexes

In an effort to understand the protein-protein interactions that occur with Cox15, we observed the distribution of Cox15 with a 13x (13-fold repeated) C-terminal Myc tag (Cox15-Myc) via BN-PAGE. The Cox15-Myc complexes that we observed range in size from about 140 kDa to larger than 660 kDa (Figure 2.1A). Consistently, Cox15-Myc distributes primarily in the lowest complex which migrates at ~140 kDa, and its distribution in the upper complexes is less abundant. We were able to break apart the high molecular weight Cox15-Myc

complexes with sodium dodecyl sulfate (SDS) and observed a single band migrating between the 66 and 140 kDa molecular weight markers (Figure 2.1A), likely reflecting monomeric Cox15-Myc which is 75 kDa with the 13x Myc tag. The upper complexes we observe ranging from ~232 kDa to larger than 660 kDa on BN-PAGE clearly represent Cox15 high molecular weight protein complexes as these complexes are about three to thirteen times greater in size than monomeric Cox15.

Recently, it was reported that Cox15 in yeast forms stable, oligomeric complexes (8). Our work concurs with the assessment that many of the Cox15 complexes represent Cox15 multimers. One of the strategies we undertook to identify other proteins that may be part of the Cox15 complex was 2D BN/SDS-PAGE. Cox15-Myc was purified from *S. cerevisiae* using non-denaturing anti-Myc chromatography and run on BN-PAGE. A lane from the blue native gel was excised and mounted to the top of an SDS-PAGE gel. Following SDS-PAGE, the gel was silver stained (Figure 2.1B). This allowed us to observe the distribution of purified Cox15 in the high molecular weight complexes as well as any other proteins that are part of the complex. Other proteins will appear either above or below Cox15 on the SDS-PAGE gel. In our 2D gels, Cox15 can be observed in high molecular weight complexes ranging from ~140-600 kDa. In particular, the 2D gel showed Cox15 associating in two distinct areas. Cox15 is most enriched around 440 kDa and in a broader range between ~140-250 kDa. Both the higher molecular weight band at 440 kDa and the broad band from 140-250 kDa were excised and analyzed by mass spectrometry to determine if any other proteins with the same molecular weight as Cox15-Myc were also present in these bands. Cox15 was the only protein identified by mass spectrometry in both of the bands analyzed.

In addition, we compared the BN/SDS-PAGE gels of purified Cox15-Myc and purified, untagged mitochondrial extract, and we detected very few obvious differences in the protein bands above and below Cox15 between the two gels (Figure 2.1B and data not

shown). The bands we excised and analyzed by mass spectrometry are indicated with an asterisk. The protein concentration of these bands was not high enough to positively identify these proteins, indicating that no other protein can be detected forming a stoichiometric complex with Cox15 within the purified high molecular weight complexes. Based on these data and the findings of others (8), it seems likely that the Cox15-Myc complexes A-D in Figure 2.1A represent mostly homo-oligomeric complexes.

Interestingly, the two Cox15 complexes observed via BN-PAGE higher than 660 kDa in Figure 2.1A resemble the complex III-containing and complex IV-containing supercomplexes reported by Cruciat et al. and Schagger and Pfeiffer (21,22). These complexes are represented by bands E and F in Figure 2.1A and match the distribution of hemagglutinin-tagged (HA-tagged) cytochrome bc_1 and cytochrome *c* oxidase proteins within the respiratory supercomplexes (Figure 2.1C). While only a small proportion of Cox15-Myc appears to be present within these putative respiratory supercomplex bands, we noted that Cox15-Myc is stably present within them. Cox15-Myc levels remain largely unchanged, including within the high molecular weight bands of the supercomplexes (Figure 2.1D), for at least 24 hours following the addition of the translation inhibitor, cycloheximide.

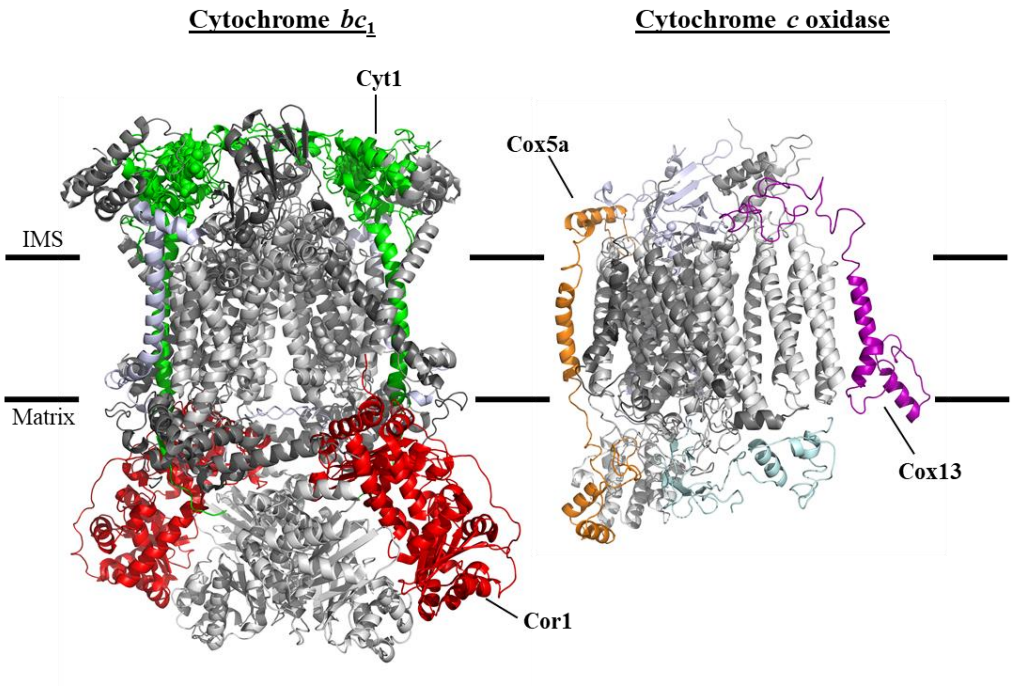

Figure 2.2: Proteins from cytochrome *c* oxidase and cytochrome bc_1 used to assess co-immunoprecipitation with Cox15-Myc(13x)

A C-terminal HA tag was appended to Cox5a (shown in orange) and Cox13 (purple) of cytochrome *c* oxidase as well as the Cyt1 (green) protein of cytochrome bc_1. An antibody recognizing Cor1 (red) of cytochrome bc_1 was also used. This figure was prepared using a crystal structure of *S. cerevisiae* cytochrome bc_1 (23) (PDB 3CX5) and a homology model of *S. cerevisiae* cytochrome *c* oxidase based on the bovine crystal structure (24).

Cox15-Myc interacts with Cor1 of the cytochrome bc$_1$ *complex and subunits from cytochrome* c *oxidase*

To test if the two Cox15 complexes larger than 660 kDa represent Cox15 in association with respiratory supercomplexes, we probed for an interaction of Cox15 with selected proteins from both cytochrome *c* oxidase and the cytochrome bc_1 complex. An HA tag was appended to the C-terminus of Cox5a and Cox13, two cytochrome *c* oxidase subunits (Figure 2.2). Additionally, an HA tag was appended to the C-terminus of the Cyt1 protein, and an antibody recognizing Cor1 was used to assess the presence of cytochrome bc_1 (Figure 2.2). Co-immunoprecipitation experiments pulling down Cox15-Myc revealed that Cox13-HA from cytochrome *c* oxidase as well as Cor1 from cytochrome bc_1 could be detected with Cox15-Myc (Figure 2.3A). In addition, a weak band representing Cox5a-HA from cytochrome *c*

oxidase was also found to co-immunoprecipitate with Cox15-Myc (Figure 2.3A). Curiously, we were not able to detect a significant interaction between Cox15-Myc and Cyt1-HA. Control co-immunoprecipitation experiments in which Cox15 did not contain a Myc tag were performed to ensure that Cox5a-HA, Cox13-HA, and Cor1 did not bind adventitiously to the anti Myc resin (Figure 2.4). Two additional controls were performed which utilized the proteins Oxa1, a five-transmembrane inner membrane protein which served as a hydrophobic control, and Cbp4, a cytochrome bc_1 assembly factor that is not itself part of fully assembled cytochrome bc_1. Neither protein co-immunoprecipitated with Cox15-Myc (Figure 2.3A), suggesting that the positive interactions we observed are not artifacts occurring during the solubilization and co-immunoprecipitation procedures (Table 2.1).

It should be noted that the co-immunoprecipitation of Cox15-Myc with Cox5a-HA, Cox13-HA, and Cor1 may represent either direct or indirect interactions. In other words, Cox15-Myc might physically interact with one or more of these proteins, or co-immunoprecipitation could be mediated through other proteins or complexes. Our data do not allow us to distinguish between these two types of interactions.

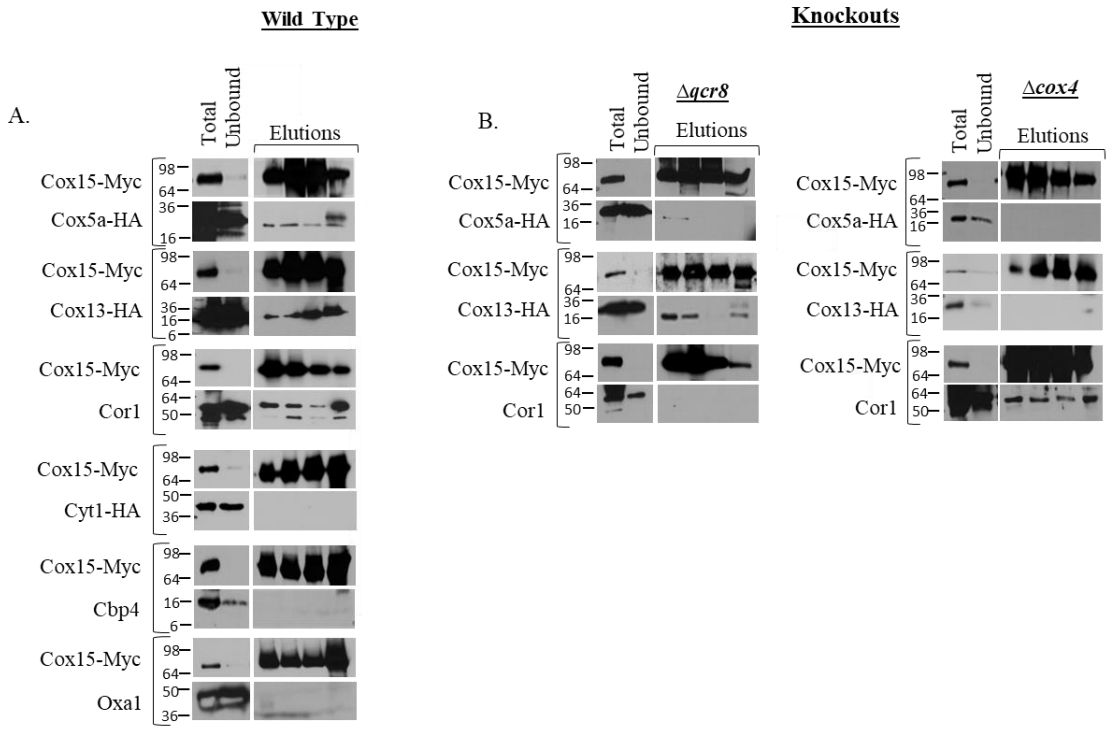

Figure 2.3: Co-immunoprecipitation experiments using anti Myc resin to pull down Cox15-Myc$_{(13x)}$ reveal the cytochrome *c* oxidase proteins Cox13-HA and Cox5a-HA and the cytochrome *bc*$_1$ protein, Cor1, interact with Cox15

A. Blots of SDS-PAGE gels following co-immunoprecipitation of Cox15-Myc from mitochondria isolated from wild-type strains (containing the indicated tags). For the blots probing native proteins, a strain containing only *COX15::MYC* was used. For blots probed for Cox15-Myc: (Total: <0.1 µg mitochondria loaded on gel; Unbound: 0.05% of the unbound fraction loaded on gel; Elutions: 33% of total elution). Blots probed for HA-tagged proteins: (Total: 40-100 µg mitochondria; Unbound: 2.5%-5% of unbound fraction; Elutions: 33% of total elution). Blots probed for native Cor1: (Total: 5 µg of mitochondria; 0.5% of unbound fraction; Elutions: 33% of elution). Blots probed for native Cbp4 and Oxa1: (Total: 85 µg (Cbp4) and 20 µg (Oxa1) of mitochondria; Unbound: 5% of the unbound fraction; Elutions: 33% of total elution). All co-IP experiments were performed 2 times (biological replicates); Cor1 experiments repeated in 3 biological replicates. B. Co-IP experiments performed in either Δ*qcr8* or Δ*cox4* mitochondria containing the indicated tags. Co-IPs between Cox15-Myc and native Cor1 in both Δ*qcr8* and Δ*cox4* utilized a *COX5A::HA* strain. Gel loading as in panel A. All experiments performed in at least two biological replicates.

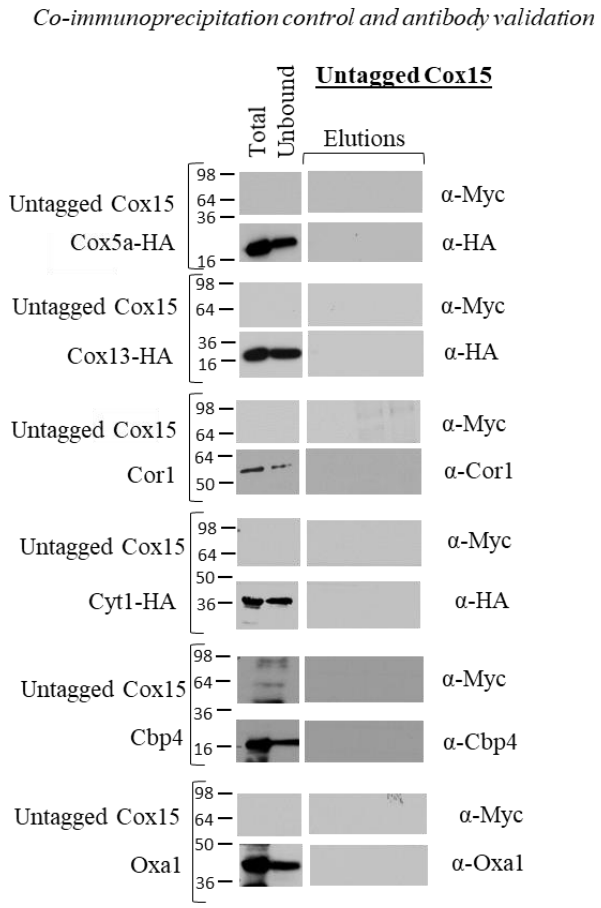

Figure 2.4: Control co-immunoprecipitation experiments confirm proteins used for co-immunoprecipitation studies do not adventitiously bind to anti Myc resin and serve as validation for the anti Myc, anti HA, anti Cor1, anti Cbp4, and anti Oxa1 primary antibodies.

Mitochondria containing untagged Cox15 was incubated with anti Myc resin using the same conditions as in Figure 2.2. Following immunoprecipitation, blots were probed with the respective antibodies. Because none of the proteins pulled down with the anti Myc resin, these experiments also served to validate the antibodies since no signal from any of the antibodies was detected in the elution portion of the blots. Strains used: *COX5A::HA (DY5113)*, *COX13::HA (DY5113)*, *CYT1::HA (DY5113)* and *DY5113 (WT)*. For blots probed for Cox15-Myc: (Total: <0.1 µg mitochondria loaded on gel; Unbound: 0.05% of the unbound fraction loaded on gel; Elutions: 33% of total elution). Blots probed for HA-tagged proteins: (Total: 40 µg mitochondria; Unbound: 2.5% of unbound fraction; Elutions: 33% of total elution). Blots probed for native Cor1: (Total: 5 µg of mitochondria; 0.5% of unbound fraction; Elutions: 33% of elution).

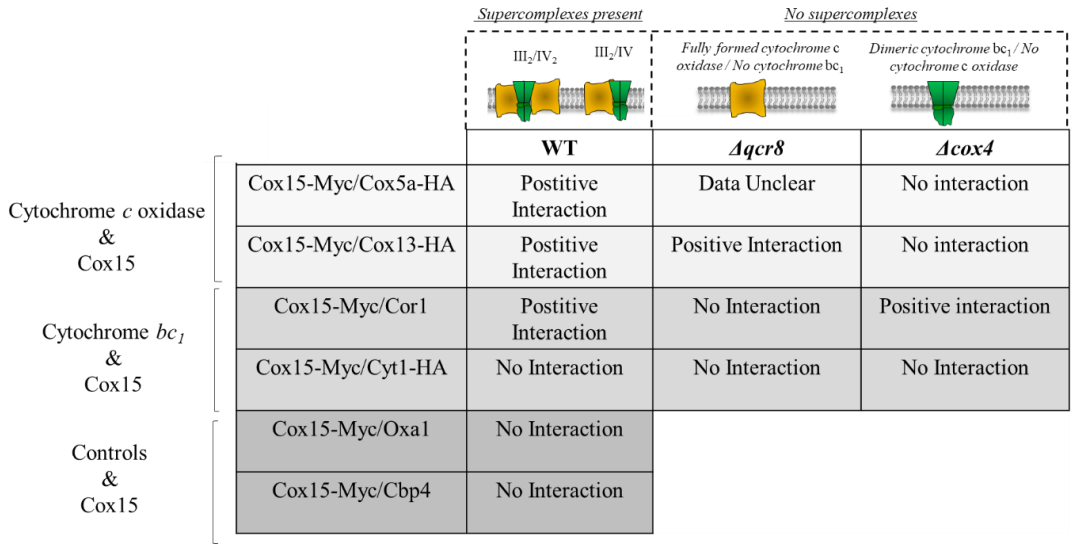

		WT	*Δqcr8*	*Δcox4*
Cytochrome *c* oxidase & Cox15	Cox15-Myc/Cox5a-HA	Postitive Interaction	Data Unclear	No interaction
	Cox15-Myc/Cox13-HA	Postitive Interaction	Positive Interaction	No interaction
Cytochrome bc_1 & Cox15	Cox15-Myc/Cor1	Postitive Interaction	No Interaction	Positive interaction
	Cox15-Myc/Cyt1-HA	No Interaction	No Interaction	No Interaction
Controls & Cox15	Cox15-Myc/Oxa1	No Interaction		
	Cox15-Myc/Cbp4	No Interaction		

Table 2.1: Summary of co-immunoprecipitation experiments

Cox15-Myc interacts with Cox13-HA from cytochrome c *oxidase and Cor1 from the cytochrome* bc_1 *complex in the absence of supercomplexes*

Presumably the interactions between Cox15-Myc and Cox5a-HA, Cox13-HA, and Cor1 occur within respiratory supercomplexes. We next tested whether these interactions persist in the absence of supercomplexes. Our first approach was to follow the interaction of Cox15-Myc with the cytochrome *c* oxidase proteins, Cox5a-HA and Cox13-HA, using a Δ*qcr8* strain in which mature cytochrome bc_1 fails to form yet cytochrome *c* oxidase is still present. This created a scenario in which cytochrome *c* oxidase exists in the absence of supercomplexes (Table 2.1). We found Cox15-Myc still co-immunoprecipitates with Cox13-HA (Figure 2.3B). Conversely, the interaction with Cox5a-HA is nearly abolished, although it is important to note that the total amount of Cox5a-HA present in *Δqcr8* mitochondria appears to be reduced compared to wild-type mitochondria. Because only weak Cox5a-HA bands could be detected in the co-immunoprecipitation experiments using wild-type mitochondria (Figure 2.3A), it is possible that weak bands observed in Figure 2.3B are simply the result of a decrease in the total amount of Cox5a-HA in *Δqcr8* mitochondria. Finally, in the absence

of fully formed cytochrome *c* oxidase *(Δcox4* strain), Cox15-Myc and Cox5a-HA do not interact, and the interaction between Cox15-Myc and Cox13-HA is also eliminated (Figure 2.3B), indicating that intact cytochrome *c* oxidase is needed to maintain the Cox15-Cox13 interaction when supercomplexes are absent.

To probe further the relationship between Cox15 and Cor1, we tested whether Cox15-Myc interacts with Cor1 in the absence of fully assembled cytochrome *c* oxidase using a Δ*cox4* strain. Cox4, a nuclear encoded subunit of cytochrome *c* oxidase, assembles in an early intermediate complex with the Cox1 and Cox5a subunits (25-29). In its absence, this core complex does not form and cytochrome *c* oxidase fails to assemble, yet cytochrome bc_1 remains intact (Table 2.1). Surprisingly, Cox15 co-immunoprecipitates with Cor1 to the same extent in both wild-type and *Δcox4* strains (Figure 2.3B). Cox15-Myc and Cor1 do not interact in a Δ*qcr8* strain, however, indicating that intact cytochrome bc_1 is required to maintain the Cox15-Cor1 interaction (Figure 2.3B).

Where does Cox15-Myc interact with cytochrome c *oxidase in the absence of supercomplexes?*

Based on the robust interaction observed between Cox15-Myc and Cox13-HA, we hypothesized that some of the lower molecular weight Cox15 complexes (bands A-D on BN-PAGE) may represent interactions with Cox13 in sub-assembly intermediates. Cox13 is one of the last subunits to be incorporated into cytochrome *c* oxidase while Cox5a forms an early intermediate with Cox1 to which the rest of the subunits are added (26,30-32). Perhaps Cox15 interacts with Cox13 and some other late assembling intermediates away from the assembling core of cytochrome *c* oxidase. To address if Cox15 forms specific interactions with Cox13, we probed the BN-PAGE distribution of Cox15-Myc complexes in a Δ*cox13* strain. While Cox13 is necessary to maintain full cytochrome *c* oxidase function, it is not necessary for the stability of the rest of the enzyme complex, and its absence does not abolish

supercomplex formation as marked by the presence of Cor1 within both supercomplexes (Figure 2.5A) (29,33). As shown in Figure 2.5A, all Cox15-Myc complexes, including Cox15 within supercomplexes, are maintained in the absence of Cox13. This indicates that none of the lower Cox15-Myc complexes are solely represented by Cox13-Cox15 interactions and that Cox13 is not required to draw Cox15 into supercomplexes.

Next, to better understand the differences we observed between the Cox15-Cox13 versus the Cox15-Cox5a interactions (Figure 2.3B), we tested whether Cox13-HA and Cox5a-HA form distinct complexes from each other when Qcr8 is absent. In mitochondria from wild-type cells, Cox5a-HA is found mainly within both supercomplexes (III_2/IV_2 and III_2/IV) and also in what appears to be the cytochrome *c* oxidase monomer (Figure 2.5B). Depending on the resolution of the gel, the band representing the cytochrome *c* oxidase monomer can be observed as two distinct bands or one large band. This is consistent with previous reports which have identified two distinct forms of cytochrome *c* oxidase via BN-PAGE as marked by a slower migrating complex (termed IV*) that is positioned directly above where monomeric cytochrome *c* oxidase would be expected (33,34). As predicted, in the absence of Qcr8, Cox5a-HA appears to associate exclusively into what appears to be the two bands reflecting monomeric cytochrome *c* oxidase (Figure 2.5B). In contrast, while Cox13-HA is only found within the two supercomplexes in wild-type mitochondria, when Qcr8 is absent, the predominate amount of Cox13 is in a complex that migrates in what appears to be the slower migrating form of monomeric cytochrome *c* oxidase on BN-PAGE (IV*) as well as two less-abundant, higher molecular weight complexes. Taking all of our data together, we conjecture that Cox15 interacts with Cox13-HA in these low-abundant intermediates that are independent of Cox5a, although we cannot rule out the possibility that Cox15 may also interact weakly with both Cox13 and Cox5a in the IV* form of monomeric cytochrome *c* oxidase.

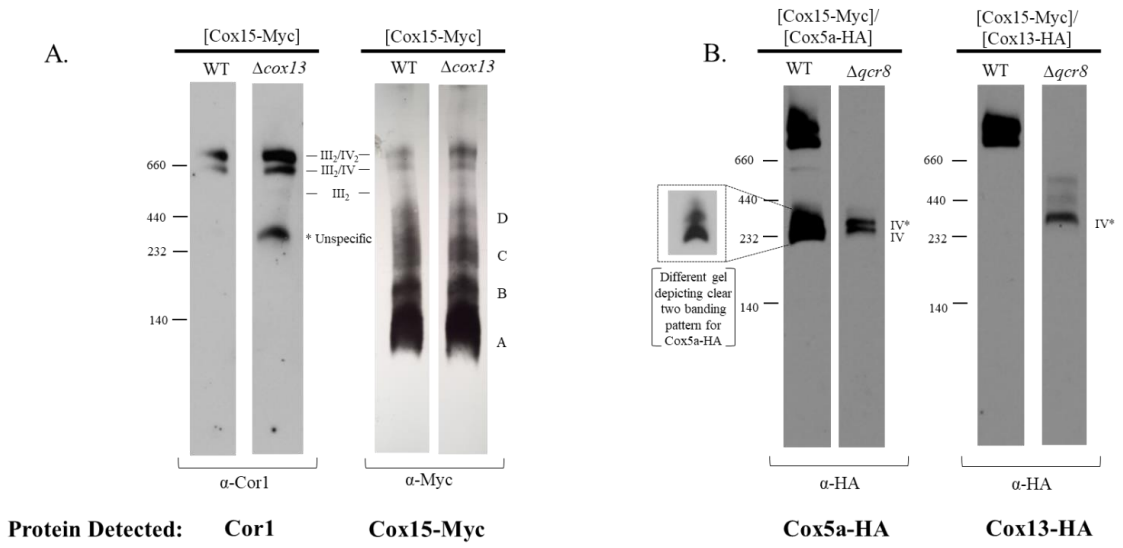

Figure 2.5: Cox15 likely does not form significant interactions with Cox13 within assembly intermediates and in the absence of supercomplexes likely interacts with Cox13 either in IV* or the two complexes above IV*

A. BN-PAGE of Cor1 (10 µg of mitochondria loaded) and Cox15-Myc$_{(13X)}$ (20 µg of mitochondria loaded) within WT (*COX15::MYC*) or Δ*cox13/COX15::MYC* strains probed with either anti Cor1 or anti Myc antibodies. The band on the Cor1 blot at ~440 kDa represents non-specific binding of the anti Cor1 antibody (See Figure 2.6). B. BN-PAGE probing for Cox5a-HA complexes (40 µg mitochondria) or Cox13-HA complexes (50 µg mitochondria) in wild-type or Δ*qcr8* backgrounds. Cells used for experiments in figures A and B were grown in 2% galactose and 0.5% lactate YP media. All experiments were performed two times (biological replicates).

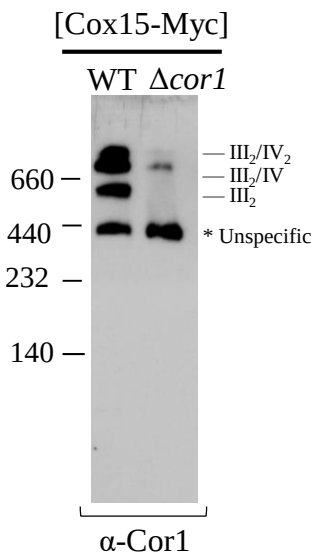

Protein Detected: Cor1

Figure 2.6: BN-PAGE using mitochondria prepared from WT and *Δcor1* cells probed with anti Cor1 antibody reveals band detected at 440 kDa is unspecific

Gels reflect 50 µg mitochondria. Strains used: *COX15::MYC* and *Δcor1/COX15::MYC.* All strains were grown in 2% galactose/0.5% lactate YP media.

Cox15-Myc interacts with Cor1 within the cytochrome bc*1 dimer in the absence of supercomplexes*

As previously discussed, Cox15-Myc interacts with Cor1 in the absence of supercomplexes only if cytochrome bc_1 is fully formed (Figure 2.3B), prompting us to investigate if Cox15-Myc and Cor1 interact within the dimer of cytochrome bc_1 when supercomplexes are absent. We observed the distribution of Cor1 and Cox15-Myc on BN-PAGE in a Δ*cox4* strain. As expected, BN-PAGE revealed that Cor1 was only present in the dimer of cytochrome bc_1 (Figure 2.7A), indicating that this is the only location in which Cox15-Myc could interact with Cor1 when Cox4 is absent. Indeed, when Cox15-Myc complexes are observed on BN-PAGE in a Δ*cox4* strain, a marked accumulation of Cox15 within an intermediate at the same molecular weight as the cytochrome bc_1 dimer is observed (Figure 2.7A). As expected, when Qcr8 is absent, Cor1 is no longer observed in the dimer of cytochrome bc_1 because the

cytochrome *bc*$_1$ complex no longer forms. Likewise, Cox15 is no longer observed in the supercomplex region when Qcr8 is absent (Figure 2.7A). Together, these data suggest that when the III_2/IV_2 and the III_2/IV supercomplexes are absent, Cox15-Myc and Cor1 interact within the cytochrome *bc*$_1$ dimer.

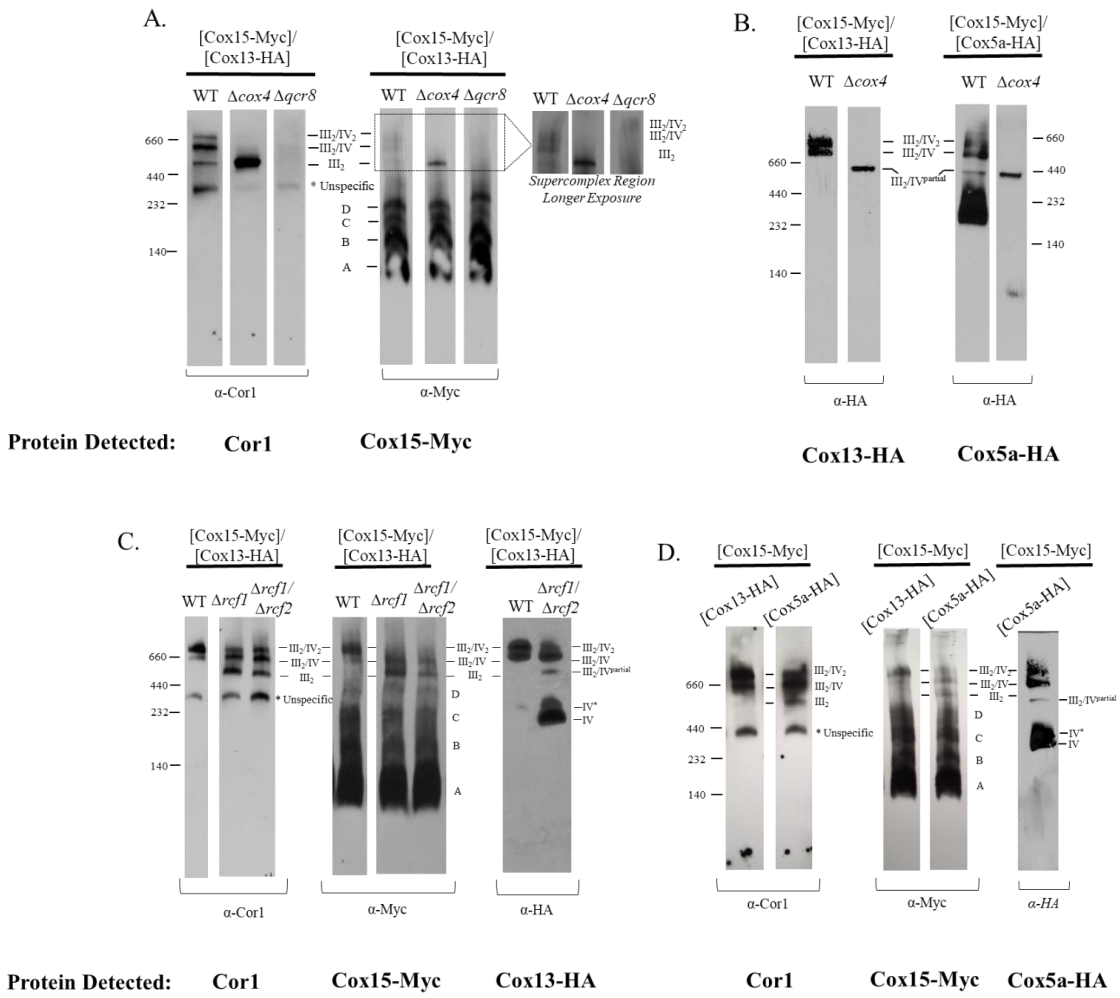

Figure 2.7: BN-PAGE experiments reveal that Cox15-Myc$_{(13x)}$ is present in the cytochrome *bc*$_1$ dimer when supercomplexes are destabilized

A. BN-PAGE of Cor1 (50 µg mitochondria) and Cox15-Myc (10 µg mitochondria). Strains used: *COX15::MYC/COX13-HA, Δcox4/COX15::MYC/COX13HA, Δqcr8/COX15::MYC/COX13HA.* B. BN-PAGE of Cox13-HA (50 µg mitochondria) and Cox5a-HA (40 µg mitochondria). Stains used: *COX15::MYC/COX13::HA* and *COX15::MYC/COX5a::*HA (in both wild-type and *Δcox4* backgrounds). C. BN-PAGE of Cor1 (50 µg mitochondria), Cox15-Myc (10 µg mitochondria), and Cox13-HA (50 µg mitochondria) using a *COX15::MYC /COX13::HA* strain in wild-type, Δ*rcf1*, or Δ*rcf1*/Δ*rcf2* backgrounds. D. BN-PAGE probing for Cor1 (20 µg mitochondria) or Cox15-Myc (10 µg mitochondria) in either *COX5A::HA/COX15::MYC* or *COX13::HA/COX15::*MYC strains. The blot probing for Cox5a-HA (50 µg mitochondria) utilizes the *COX5A::HA/COX15::MYC* strain. All strains represented in the entire figure were grown in 2% galactose/0.5% lactate YP media, and every BN-PAGE was performed 2-3 times (biological replicates). The bands at 440 kDa on the anti Cor1 blots in A, C, and D represent non-specific binding of the anti Cor1 antibody (See Figure 2.6).

Interestingly, we also noted that when Cox4 is absent under our experimental conditions, both Cox13-HA and Cox5a-HA were observed exclusively within an intermediate that also appeared to be the same molecular weight as the cytochrome bc_1 dimer (Figure 2.7B). This observation is consistent with the findings of others who report that subunits from cytochrome *c* oxidase can associate with the cytochrome bc_1 dimer when cytochrome *c* oxidase assembly is stalled (26,35). This intermediate was termed III_2/IV* by Mick et al. (26) and is referred to as $III_2/IV^{partial}$ in this work, to avoid confusion with the IV^* nomenclature used elsewhere. Therefore, it is possible that Cox15-Myc and Cor1 interact within a cytochrome bc_1 dimer that has already associated with some cytochrome *c* oxidase subunits.

We tracked the presence of Cox15-Myc, Cor1, and Cox13-HA within the supercomplexes in Δ*rcf1* and Δ*rcf1*/Δ*rcf2* strains. It is known that in the absence of respiratory supercomplex factor 1 (Rcf1), the distribution of the supercomplexes is altered such that the III_2/IV_2 supercomplex is diminished and a buildup of III_2 is observed (33,36,37). In both Δ*rcf1* and Δ*rcf1*/Δ*rcf2* strains, BN-PAGE probing for Cor1-containing complexes confirmed that the III_2/IV_2 supercomplex is diminished and that the cytochrome bc_1 dimer accumulates (Figure 2.7C). Cox15-Myc reflected the trend observed for Cor1 in that Cox15-Myc was nearly absent in the III_2/IV_2 supercomplex but accumulated in a complex that appeared to be the dimer of cytochrome bc_1 (Figure 2.7C). When we probed for the distribution of Cox13-HA in a wild-type strain, we observed that Cox13-HA is only present in the III_2/IV_2 and III_2/IV supercomplexes. In Δ*rcf1* and Δ*rcf1*/Δ*rcf2* strains, however, the predominant amount of Cox13-HA is found not only within the two supercomplexes, but also as two bands migrating around 232 kDa. As discussed above, these two bands at 232 kDa likely reflect Cox13 within the two monomeric forms of cytochrome *c* oxidase. Finally, we do note a minor amount of Cox13 that appears to migrate at the same molecular weight as the

likely $III_2/IV^{partial}$ complex, again suggesting that Cox15 and Cor1 may interact within a cytochrome bc_1 dimer that is in association with some cytochrome *c* oxidase subunits. In sum, under conditions in which the cytochrome bc_1 dimer is favored, as in the case of supercomplex destabilization from the loss of Rcf1 and Rcf1/Rcf2, we detect Cox15-Myc shifting its distribution from the III_2/IV_2 and III_2/IV supercomplexes into what appears to be either the cytochrome bc_1 dimer or the $III_2/IV^{partial}$ complex, while Cox13 shifts its distribution towards complexes IV and IV*.

In the course of our studies, we observed that in contrast to a Cox13-HA strain, a C-terminal HA tag on Cox5a causes a slight build-up of Cor1 within the cytochrome bc_1 dimer without significant change to the abundance of Cor1 within the III_2/IV_2 or III_2/IV supercomplexes (Figure 2.7D). Intriguingly, Cox15-Myc again models the arrangement of Cor1 within supercomplexes. As observed with Cor1, Cox15-Myc is only present in the III_2/IV_2 or III_2/IV supercomplexes in a Cox13-HA strain but displays a build-up within the cytochrome bc_1 dimer when Cox5a has a C-terminal HA tag (Figure 2.7D). When observing the distribution of Cox5a-HA from wild-type mitochondria, Cox5a-HA was predominately found either within the supercomplexes or the two forms of monomeric cytochrome *c* oxidase, with a trace amount also detected within the probable $III_2/IV^{partial}$ complex. As observed with the loss of Rcf1, when supercomplexes are destabilized due to a C-terminal HA tag on Cox5a, the distribution of Cox15-Myc is again shifted into the cytochrome bc_1 dimer or the $III_2/IV^{partial}$ complex.

Cox15 maintains its interaction with Cor1 even when catalytically inactive and when unable to oligomerize

Finally, we wanted to ascertain if the Cox15-Cor1 interaction required fully functioning Cox15. In the first experiment, we probed whether the interaction was maintained in a H431A amino acid variant of Cox15. H431, one of the four strictly

conserved His residues, is assumed to be located at one of the two heme binding sites and has been shown previously to be required for activity (11). Both wild-type (WT) Cox15-Myc and mutant H431A Cox15-Myc were expressed individually from the pRS415 plasmid in *Δcox15 S. cerevisiae* (Table 2.2) at comparable steady-state levels (Figure 2.8). Only WT Cox15-Myc was able to rescue respiratory competence (Figure 2.8). The ability of native Cor1 to co-immunoprecipitate with the plasmid-borne enzymes was assessed. Both the plasmid-borne WT Cox15-Myc and H431A Cox15-Myc consistently co-immunoprecipitated with native Cor1 in the fourth elution, indicating that heme *a* is not required for the Cox15-Cor1 interaction (Figure 2.9).

Next, we investigated if the Cox15-Cor1 interaction is maintained when Cox15 is unable to form homooligomers. Recently Swenson et al. identified a 20 amino acid deletion mutant of Cox15 (L-20 variant) that maintained close to normal steady-state levels but was unable to oligomerize (8). We expressed the L-20 Cox15-Myc deletion mutant from the pRS415 plasmid (Table 2.2) in a *Δcox15* strain, and we assessed whether plasmid-borne L-20 Cox15-Myc was able to interact with native Cor1. The plasmid-borne L-20 Cox15-Myc exhibited lower steady state levels than observed for plasmid-borne WT Cox15-Myc or H431A Cox15-Myc (Figure 2.8). Interestingly, however, the Cox15-Cor1 interaction was maintained in the L-20 Cox15-Myc mutant, despite the reduction in steady state levels for L-20 Cox15-Myc (Figure 2.9). Together, these data indicate that the ability of Cox15 to interact either directly or indirectly with Cor1 and the cytochrome bc_1 dimer does not depend on either the presence of heme *a* or the oligomeric state of Cox15.

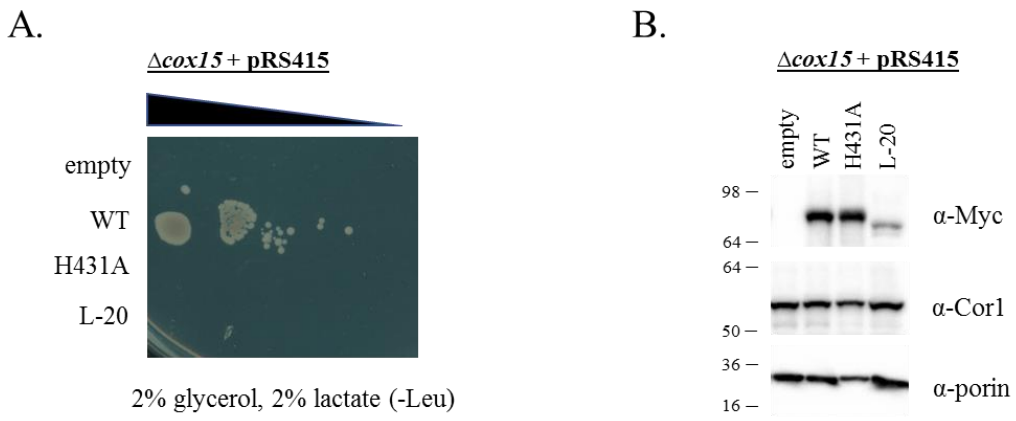

Figure 2.8: Respiratory competency test and steady-state SDS-PAGE reveal that plasmid-borne WT Cox15-Myc$_{(13x)}$ is active while H431A Cox15-Myc$_{(13x)}$ and L-20 Cox15-Myc$_{(13x)}$ are not

Each Cox15-Myc variant was expressed from pRS415 under the control of its own promoter in a Δ*cox15* background. A Δ*cox15* strain with empty pRS415 is also shown as a negative control. A. Growth test on nonfermentable carbon source. Each strain was grown in liquid synthetic medium (2% galactose, 0.1% glucose), normalized, serially diluted, and spotted onto a synthetic 2% glycerol, 2% lactate plate. B. Steady-state SDS-PAGE of Cox15-Myc, Cor1, and porin in the Δ*cox15* strains used in this study. All three gels (anti Myc, anti Cor1, and anti porin) were loaded with 5 µg of mitochondria from each strain. All strains were grown in synthetic dextrose (2% glucose) minimal media.

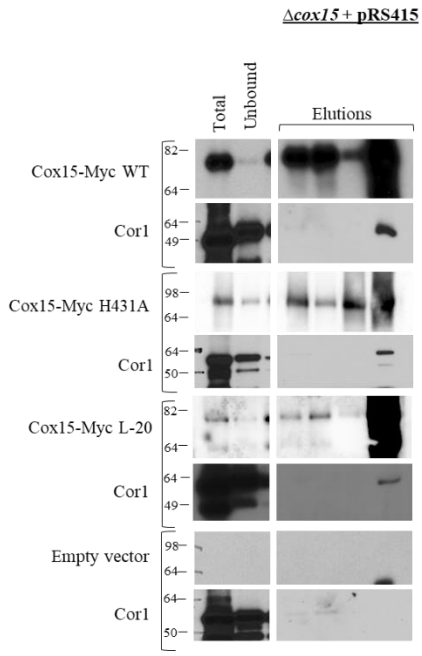

Figure 2.9: Blots of SDS-PAGE gels following co-immunoprecipitation of WT Cox15-Myc$_{(13x)}$, H431A Cox15-Myc$_{(13x)}$, and L-20 Cox15-Myc$_{(13x)}$ with native Cor1

Each Cox15-Myc variant was expressed from pRS415 under the control of the native COX15 promoter in a Δ*cox15* strain. A control co-immunoprecipitation experiment using mitochondria from a Δ*cox15* strain carrying empty pRS415 is also shown. Due to the lower steady-state level of Cox15-Myc L-20, 1.5 mg of mitochondria from this strain was used for co-immunoprecipitation experiments instead of 1 mg. For blots probed for Cox15-Myc: (Total: <0.5 µg mitochondria loaded on gel; Unbound: 0.05% of the unbound fraction loaded on gel; Elutions: 33% of total elution). Blots probed for native Cor1: (Total: 5 µg of mitochondria; 0.5% of unbound fraction; Elutions: 33% of elution). All experiments were performed 2-4 times (biological replicates).

Strain	Genetic background	Source or reference
DY5113	*MATa, ade2-, can1-, leu2-, ura3-, trp1-, his3-*	*W303a, WT*
COX5A::HA, DY5113	*MATa, ade2-, can1-, leu2-, ura3-, TRP1+, his3-, COX5A::3HA*	This study
COX13A::HA, DY5113	*MATa, ade2-, can1-, leu2-, ura3-, TRP1+, his3-, COX13::3HA*	This study
COX15::MYC	*MATa, ade2-, can1-, leu2-, ura3-, trp1-, HIS3+, COX15::13MYC*	(38)
COR1::HA, COX15::MYC	*MATa, ade2-, can1-, leu2-, ura3-, TRP1+, HIS3+, COR1::3HA, COX15::13MYC*	This study
CYT1::HA, COX15::MYC	*MATa, ade2-, can1-, leu2-, ura3-, TRP1+, HIS3+, CYT1::3HA, COX15::13MYC*	This study
COX5A::HA, COX15::MYC	*MATa, ade2-, can1-, leu2-, ura3-, TRP1+, HIS3+, COX5A::3HA, COX15::13MYC*	This study
COX13::HA, COX15::MYC	*MATa, ade2-, can1-, leu2-, ura3-, TRP1+, HIS3+, COX13::3HA, COX15::13MYC*	This study
SSA1::HA, COX15::MYC	*MATa, ade2-, can1-, leu2-, ura3-, TRP+, HIS+, SSA1::3HA, COX15::13MYC*	This study
Δqcr8, COX5A::HA, COX15::MYC	*MATa, ade2-, can1-, leu2-, URA3+, TRP1+, HIS3+, qcr8::URA3, COX5A::3HA, COX15::13MYC*	This study
Δqcr8, COX13::HA, COX15::MYC	*MATa, ade2-, can1-, leu2-, URA3+, TRP1+, HIS3+, qcr8::URA3, COX13::3HA, COX15::13MYC*	This study
Δcox4, COX5A::HA, COX15::MYC	*MATa, ade2-, can1-, leu2-, URA3+, TRP1+, HIS3+, cox4::URA3, COX5A::3HA, COX15::13MYC*	This study
Δcox4, COX13::HA, COX15::MYC	*MATa, ade2-, can1-, leu2-, URA3+, TRP1+, HIS3+, cox4::URA3, COX13::3HA, COX15::13MYC*	This study
Δcox13, COX15::MYC	*MATa, ade2-, can1-, leu2-, URA3+, trp1-, HIS3+, cox13::URA3, COX15::13MYC*	This study
Δrcf1, COX13::HA, COX15::MYC	*MATa, ade2-, can1-, leu2-, URA3+, TRP1+, HIS3+, rcf1::URA3, COX13::3HA, COX15::13MYC*	This study
Δrcf1, Δrcf2, COX13::HA, COX15::MYC	*MATa, ade2-, can1-, leu2-, URA3+, TRP1+, HIS3+, rcf1::URA3, rcf2::kanMX6, COX13::3HA, COX15::13MYC*	This study
Δcor1, COX15::MYC	*MATa, ade2-, can1-, leu2-, URA3+, trp1-, HIS+, cor1::URA3, COX15::13MYC*	This study
Δcox15	*MATa, ade2-, can1-, leu2-, ura3-, trp1-, his3-, cox15::KanMX*	This study
Plasmid	**Description**	**Source or reference**
pRS415 empty	Empty pRS415 vector	(8)
pRS415 *COX15-MYC*	*COX15-13MYC* with *COX15* promoter and *ADH1* terminator in pRS415	(8)
pRS415 *COX15-MYC H431A*	*cox15-13MYC H431A* with *COX15* promoter and *ADH1* terminator in pRS415	(8)
pRS415 *COX15-MYC L - 20*	*cox15-13MYC L – 20 (cox15-MYC* with 20 amino acids deleted from the linker between transmembrane helices IV and V) with *COX15* promoter and *ADH1* terminator	(8)

Table 2.2: Yeast strains and plasmids used in this study

Discussion

With the discovery of respiratory supercomplexes in *Saccharomyces cerevisiae* by Cruciat et al. and Schagger and Pfeiffer in 2000, our knowledge of the electron transport chain expanded (21,22). Since then, our understanding has continued to evolve as we learn that these supercomplexes likely do not solely represent the cytochrome bc_1 and cytochrome *c* oxidase complexes, but potentially contain other regulators, assembly proteins, and

transporter proteins. Among the proteins identified within respiratory supercomplexes in *S. cerevisiae* are the ADP/ATP carrier protein, AAC2 (39), the Tim23 inner membrane translocase complex (40-42), the mitochondrial cardiolipin transacylase, Taz1 (43), and the cytochrome *c* oxidase assembly factors Coa3, Shy1, and Cox14 (26,44). In this report, we add an additional cytochrome *c* oxidase assembly factor to this list, heme *a* synthase (Cox15). Although only a small percentage of Cox15 is present in respiratory supercomplexes, this is consistent with the distribution of many other non-respiratory complex proteins found to associate with supercomplexes (39-42). It has been speculated that different pools of respiratory supercomplexes may exist that vary with respect to the other interaction partners that associate with them. (45,46). It is possible that Cox15 also exists in a particular subset of respiratory supercomplexes, but more work is needed to address this question and, if so, determine if Cox15 serves a particular purpose within that subset. Interestingly, while many of the non-respiratory complex proteins reported to associate within supercomplexes are detected only under very mild solubilization conditions (0.5% digitonin) (39-42), the presence of Cox15 within respiratory supercomplexes is resistant to the harsher solubilization conditions used in this study (1% digitonin). This reflects a stable, albeit modest association with respiratory supercomplexes.

Given that Cox15 is present within respiratory supercomplexes, it is reasonable to expect Cox15 to co-purify with cytochrome *c* oxidase under non-denaturing conditions. Indeed, we detected an interaction between Cox15-Myc and both the Cox5a and Cox13 subunits of cytochrome *c* oxidase from wild-type mitochondria. Given that the only known function of Cox15 is to synthesize the heme *a* molecules that are utilized by cytochrome *c* oxidase, it is further reasonable to hypothesize that Cox15 should interact directly with monomeric forms of cytochrome *c* oxidase. To date, however, no significant interaction has been reported. Although Bareth et al. reported that a sub-stoichiometric amount of Cox15

may associate with the early assembly intermediates that form with Cox1 and its assembly factors (10), there was no evidence that Cox15 formed stable interactions with fully assembled cytochrome *c* oxidase. Likewise, in this work, we were not able to detect strong evidence suggesting that Cox15 interacts with monomeric cytochrome *c* oxidase. We discovered that Cox15 interacts directly or indirectly with Cox13 and that these interactions persist when supercomplexes are unable to form (*Δqcr8* mitochondria). Furthermore, we were unable to detect co-immunoprecipitation between Cox15 and Cox5a outside of supercomplexes, although the co-immunoprecipitating bands between Cox15 and Cox5a are weak even in the presence of supercomplexes. Therefore, while we cannot rule out the possibility that Cox15 interacts with Cox13 within the IV^* form of monomeric cytochrome *c* oxidase which contains Cox5a, we favor the conclusion that, in the absence of supercomplexes, Cox15 interacts with Cox13 in complexes lacking Cox5a that appear to be a higher molecular weight than the IV^* monomeric cytochrome *c* oxidase (Figure 2.10A).

In contrast, we detected a clear interaction between Cox15 and the cytochrome bc_1 protein, Cor1. Not only does Cox15 interact either directly or indirectly with Cor1 in wild-type mitochondria (presumably within supercomplexes), but Cox15 also interacts with Cor1 in the absence of supercomplexes in Δ*cox4* mitochondria, presumably within the cytochrome bc_1 dimer (Figure 2.10B). Cox15 does not co-immunoprecipitate with Cor1 when cytochrome bc_1 assembly is blocked *(*Δ*qcr8* mitochondria), implying that the two do not interact within Cor1 sub-assemblies of the bc_1 complex. Co-immunoprecipitation between Cox15-Myc and Cor1 is also maintained in mutants of Cox15 that are unable to produce heme *a* or are unable to oligomerize. Interestingly, Rcf1 was also found to interact with Cor1 and other cytochrome bc_1 proteins when cytochrome *c* oxidase assembly was stalled (36,37). The significance of the interaction between Rcf1 and Cor1 is less resolved, however, as Rcf1 was not found to migrate within any high molecular weight complexes in Δ*cox4*

mitochondria (33). It has been hypothesized that perhaps Rcf1 acts as a bridge or a stabilizer between the cytochrome bc_1 and cytochrome *c* oxidase complexes (36,37), although this remains to be confirmed. The observation that some Cox15 migrates with the III_2IV_2 and III_2IV supercomplexes in wild-type mitochondria as well as with the cytochrome bc_1 dimer in Δ*cox4* mitochondria suggests a more stable direct or indirect interaction between Cox15 and Cor1.

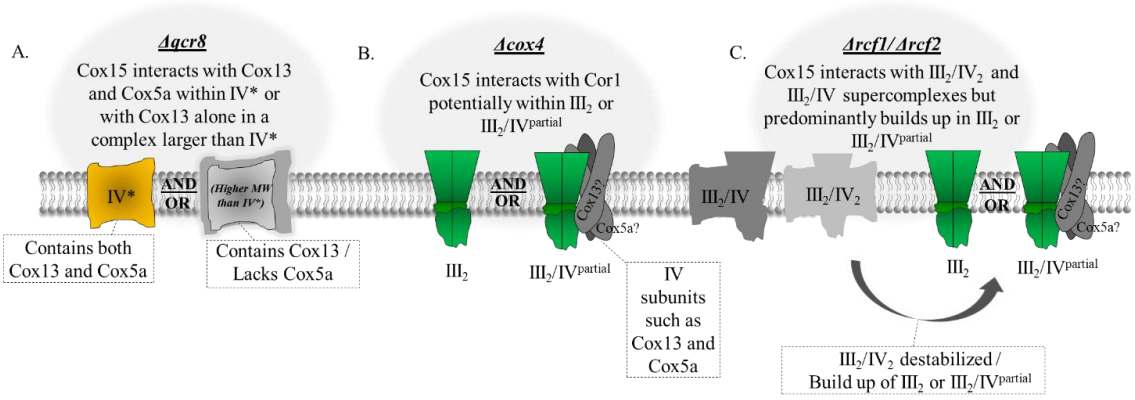

Figure 2.10: The protein complexes observed within the supercomplex region on BN-PAGE that Cox15 is likely a part of in *Δqcr8, Δcox4,* and *Δrcf1/ Δrcf2* mitochondria

In WT mitochondria, Cox15-Myc was found to associate within the III_2/IV_2 and III_2/IV supercomplexes. A. In *Δqcr8* mitochondria (cytochrome bc_1 fails to assemble but cytochrome *c* oxidase is present), Cox15 was found to interact with Cox13 from cytochrome *c* oxidase. Because we cannot exclude the possibility that Cox15 is capable of interacting with Cox5a in *Δqcr8* mitochondria, the interaction with Cox13 in *Δqcr8* mitochondria may occur either in the IV* form of monomeric cytochrome *c* oxidase or in complexes that are larger than monomeric cytochrome *c* oxidase which contain Cox13 but lack Cox5a. B. In *Δcox4* mitochondria, cytochrome *c* oxidase no longer assembles but dimeric cytochrome bc_1 still forms. Cox15 was found to maintain its interaction with Cor1 within the cytochrome bc_1 dimer. The cytochrome bc_1 dimer may be in association with cytochrome *c* oxidase subunits such as Cox13 and Cox5a. C. In *Δrcf1/ Δrcf2* mitochondria, the III_2/IV_2 supercomplex is somewhat destabilized and a buildup of the cytochrome bc_1 dimer occurs. The association of Cox15 with the III_2/IV_2 supercomplex was also somewhat destabilized and, like Cor1, Cox15 was found to associate with the cytochrome bc_1 dimer which may also be in association with some cytochrome *c* oxidase subunits.

We observed in this study that the cytochrome *c* oxidase proteins, Cox5a and Cox13, accumulate into what also appears to be the cytochrome bc_1 dimer in Δ*cox4* mitochondria. While there is some debate as to when assembling cytochrome *c* oxidase interacts with the cytochrome bc_1 complex, it has been either shown or postulated that partially assembled complex IV is capable of interacting with complex III (26,35). Likewise, it has also been demonstrated that partially assembled complex III can associate with complex IV (16,35,47). So, it is possible that what appears to be Cox5a and Cox13 within the cytochrome bc_1 dimer in Δ*cox4* mitochondria may reflect partially assembled pools of cytochrome *c* oxidase subunits associating with already dimerized cytochrome bc_1 (Figure 2.10B). Mick et al.

reported the presence of a complex found in Δ*cox2* mitochondria they termed III_2/IV^* (and we refer to as $III_2/IV^{partial}$) that migrates just above the cytochrome bc_1 dimer on their blue native gels (26). This $III_2/IV^{partial}$ complex could be detected under steady state conditions, and Shy1, Cyt1, and Cox4 were all found to be within this complex of partially assembled cytochrome *c* oxidase and dimerized cytochrome bc_1. It is possible that the Cox15-Cor1 interaction we detected in Δ*cox4* mitochondria occurs within the cytochrome bc_1 dimer that reflects this $III_2/IV^{partial}$ complex (Figure 2.10B). While it could be argued that Cox15 may be drawn into the $III_2/IV^{partial}$ by Cox5a or Cox13, our co-immunoprecipitation experiments did not detect any interaction between Cox15 and either Cox5a or Cox13 in Δ*cox4* strains, while a strong interaction with Cor1 was identified (Figure 2.3B). Additionally, our BN-PAGE data suggests that the Cox15 distribution within the supercomplexes more closely models Cor1 than either Cox5a or Cox13. This is most clearly observed in both Δ*rcf1* and Δ*rcf1/rcf2* mitochondria, where Cox15 was no longer observed in the upper III_2/IV_2 supercomplex but was shifted entirely into the III_2/IV complex or cytochrome bc_1 dimer (Figure 2.7C). Therefore, based on the data presented in this study, it appears more likely that an interaction with Cor1 is mediating the association of Cox15 with either the cytochrome bc_1 dimer or the $III_2/IV^{partial}$ complex.

Why would a protein whose only known function is to synthesize heme *a* for cytochrome *c* oxidase associate with Cor1 outside of supercomplexes? In fact, our data suggest that a portion of Cox15 is specifically conserved in the cytochrome bc_1 dimer when supercomplex formation is compromised. In Δ*rcf1* and Cox5a-HA mitochondria, Cox15 associates within the cytochrome bc_1 dimer even though the III_2/IV_2 and III_2/IV supercomplexes are still present. Additionally, in Δ*cox4* mitochondria it appears as if all the supercomplex-bound Cox15 shifts to the dimer of bc_1 rather than being absorbed back into the other lower molecular weight Cox15 complexes. Perhaps when supercomplex formation

is hindered, a pool of Cox15 is allocated to the bc_1 dimer to remain positioned for hemylation of Cox1 within supercomplexes. To support this hypothesis, various studies have obtained results suggesting that cytochrome *c* oxidase is capable of being assembled within the supercomplexes (26,27,48,49). If this is so, then perhaps Cox15 is needed for the hemylation of Cox1 as it is being incorporated into supercomplexes. Alternatively, recent reports have speculated that Cox15 may have an additional role within the cell in addition to the production of heme *a* for Cox1 due to the observations that Cox15 forms separate protein complexes from Cox10, the protein that functions immediately upstream in the heme *a* biosynthetic pathway, and that the Cox15 complexes form even in the absence of Cox1 or heme *o* (8,10,20,50). Additionally, it has been demonstrated that Cox15 protein levels are 8-10 times higher than that of Cox10 (38). Further elucidating the reason why Cox15 remains associated with Cor1 in the cytochrome bc_1 dimer, even in the absence of supercomplexes, may shed more light on a potential alternative function of Cox15 and may reveal the role Cox15 serves within the respiratory supercomplexes.

In summary, we have found that not only does Cox15 associate within respiratory supercomplexes, it also is capable of interacting with Cor1 within the cytochrome bc_1 dimer when supercomplex formation is compromised. Furthermore, while Cox15 and Cox13 also interact when supercomplex formation is compromised, the location of these interactions was not as readily discernable as those between Cox15 and Cor1, thus highlighting a unique and unexpected relationship between Cox15 and the cytochrome bc_1 complex.

Experimental procedures

Yeast strains and cloning

The *S. cerevisiae* strains described in this paper are derivatives of DY5113 (*MATa, ade2-, can1-, leu2-, ura3-, trp1-, his-*) and were generated within this strain or in a DY5113 strain containing *COX15* with a genomic C-terminal Myc_{13} epitope (Table 2.2). All cloning was

performed genomically by homologous recombination of gene-targeted PCR amplified cassettes via the lithium acetate method of yeast transformation (51,52). *RCF2* and *COX15* were deleted by replacement with the *kanMX6* cassette from the pFA6a vector (53), and all other gene deletions were made by replacement with the *URA3* cassette obtained from pBS1539 (Min-Hao Kuo, Michigan State University). C-terminal tagging of *COR1, CYT1*, *COX5A*, and *COX13* utilized the 3X hemagglutinin (HA)-*TRP1* cassette from pFA6a (53).

All plasmids used in the Cox15 mutant studies were a kind gift from Dr. Oleh Khalimonchuk (University of Nebraska-Lincoln). The plasmids were expressed in a *Δcox15* DY5113 background (Table 2.2).

Cell growth and mitochondrial isolation

Unless otherwise specified, yeast cultures were grown at 30 °C while shaking for 20 h in liquid YPD medium (1% yeast extract, 2% peptone (tryptone), and 2% glucose). To enhance formation of III_2/IV and III_2/IV_2 supercomplexes for better visualization in BN-PAGE experiments, yeast cultures were occasionally grown to mid log phase in liquid media containing 1% yeast extract, 2% peptone, 2% galactose, and 0.5% lactate (19,21) as noted in the appropriate figure captions. For both WT and mutant Cox15-Myc expressed from the pRS415 plasmid, yeast cultures were grown in synthetic media lacking leucine. Crude mitochondria were isolated as previously described (54,55).

Respiratory competence

The respiration competency of the *Δcox15* pRS415 strains was tested as previously described (8). Briefly, cells were grown in liquid synthetic medium (2% galactose, 0.1% glucose), normalized to an OD_{600} of 0.3, and then serially diluted and spotted onto plates containing 2% glycerol and 2% lactate.

Blue native PAGE

BN-PAGE was performed as described previously (56). Briefly, mitochondria were solubilized for 15 min on ice in 10 µL digitonin-containing buffer (20 mM Tris (pH 7.4), 0.1 mM EDTA, 50 mM NaCl, 10% v/v glycerol, 4 mM PMSF, and 1% wt/vol digitonin) per 10 µg starting mitochondria. Solubilized mitochondrial proteins were clarified via centrifugation at 12,000 x *g* for 15 min. Following centrifugation, 0.1 µL of sample buffer (5% Coomassie Brilliant Blue G-250, 500 mM 6-aminohexanoic acid, 0.1 mM Bis-Tris (pH 7.0)) per 1 µg of starting mitochondria was added to the clarified supernatant. Samples were loaded on a 4-15% gradient polyacrylamide gel (Biorad mini-PROTEAN-TGX system). Electrophoresis was conducted at 130 V for 6 h in cathode buffer containing 50 mM tricine, 7.5 mM imidazole, 0.02 g Coomassie Brilliant Blue G-250 (pH 7.0), and anode buffer containing 25 mM imidazole (pH 7.0). The gel was then electroblotted for 3 h at 60 V in buffer containing 50 mM tricine and 7.5 mM imidazole (pH 7.0). Before immunodecoration, the membrane was washed in 100% methanol for 5 min to remove Coomassie dye and rinsed with Tris buffer saline (25 mM Tris-HCl (pH=7.5), 150 mM NaCl, and 27 mM KCl). For molecular weight estimation, the gel lane containing the ladder (GE Healthcare, #17-0445-01) was excised, stained (2.5% Coomassie Brilliant Blue, 10% acetic acid, 25% methanol), and de-stained (10% acetic acid, 25% methanol). Swelling and shrinking of the gel slice during the staining and de-staining procedure was accounted for when aligning with electroblotted protein complexes.

When analyzing the distribution of SDS-treated Cox15 on BN-PAGE, mitochondria were first solubilized with 1% SDS at 4 ^{o}C in buffer containing 50 mM NaCl, 50 mM imidazole, 5 mM 6-aminohexanoic acid, and Roche protease inhibitor. Following SDS-solubilization, BN-PAGE was performed as described above.

Two-dimensional blue native/SDS-PAGE of purified Cox15-Myc followed by mass spectrometry

Mitochondria were prepared from 1.8 liters of *S. cerevisiae* containing C-terminal genomic Myc tagged Cox15 (Cox15-Myc) grown in YPD (using tryptone as mentioned above). Mitochondria were solubilized for 2 h in 600 mM sorbitol, 20 mM HEPES, 4.1% digitonin, 150 mM NaCl, and Roche protease inhibitor in 5 mL total volume. Solubilized mitochondrial proteins were clarified via centrifugation at 12,000 x *g* for 30 min and added to 300 µL of anti c-Myc resin (Sigma A7470). Lysate and resin were incubated overnight at 4 ^{o}C, washed 8 times with 1 mL phosphate buffer (137 mM NaCl, 27 mM KCl, 100 mM Na_2HPO_4, 18 mM KH_2PO_4), and eluted in 10 1-mL fractions of PBS (phosphate-buffered saline) containing 0.1 mg/mL c-Myc peptide and 0.1% digitonin. Each elution fraction was incubated with resin for 5 min before collecting. Elution fractions containing Cox15-Myc were pooled and concentrated using an Amicon 10 MWCO membrane until the total volume was reduced to 80 µl. The buffer was exchanged by adding 500 mM 6-aminohexanoic acid and 200 mM NaCl to a final volume of 200 µL, centrifuging at 14,000 x *g* (4 °C) to a final volume of about 80 µL, and repeating. Following buffer exchange, the sample was adjusted to 150 µL followed by the addition of 0.02% Ponceau and 10% glycerol (final concentrations). BN-PAGE was run as described previously. After BN-PAGE, a lane was excised and mounted to the top of an SDS-PAGE gel. Following electrophoresis, the gel was silver stained using the Proteosilver kit (Sigma). Protein bands of interest were excised, hydrolyzed by in-gel tryptic digest, and analyzed by mass spectrometry (LC-MS/MS) as described previously (57).

BN-PAGE of Cox15-Myc complexes in the presence of cycloheximide

To analyze the presence of Cox15-Myc within supercomplexes following stalled nuclear translation, 250 mL cultures of *SSA1::HA/COX15::MYC* in YPD were started from 5 mL

overnight cultures. The 250 mL cultures were allowed to grow for 20 h post inoculation. Cycloheximide was then added to each culture (150 µg/mL) and cultures were harvested at various time points up to 24 h post cycloheximide addition. In previous unpublished work, we noted that the cytosolic heat shock protein, Ssa1, could be co-purified with our isolated crude mitochondria, so mitochondria were prepared as described above and BN-PAGE was used to monitor the presence of Cox15-Myc within respiratory supercomplexes. SDS-PAGE of both Cox15-Myc and Ssa1-HA was used to monitor steady-state protein levels following cycloheximide addition.

Co-immunoprecipitation

For the anti-Myc co-immunoprecipitation experiments pulling down Cox15-Myc and probing for associated HA-tagged proteins, 1 mg of mitochondria was solubilized in 200 µL buffer (4.1% digitonin (Sigma D141), 150 mM NaCl, Roche Protease Inhibitor) for 2 h at 4 °C on a rocking platform. Samples were centrifuged for 30 min at 9,600 x *g* to pellet unsolubilized material. Solubilized mitochondria were added to 25 µL anti-Myc agarose (Sigma A7470) and allowed to incubate overnight at 4 °C on a rocking platform. After collecting the unbound fraction, the anti-Myc resin was washed 8 times with 1 mL of PBS. Protein was eluted by adding 30 µL of 2X SDS loading dye to the resin and rocking at 4 ° C for 10 min, 3 times. A final elution was performed by boiling the resin for 5 min at 100 °C in 30 µL of 2X SDS loading dye.

Anti-myc co-immunoprecipitation experiments pulling down Cox15-Myc that required the use of antibodies recognizing native Cor1 were performed as described above except an alternative anti-Myc agarose was used (Thermo, #20168) due to cross reactivity of the original agarose with the secondary antibodies at the same molecular weight as Cor1. Briefly, solubilized lysate was added to 25 µL resin volume and incubated overnight at 4 °C on a rocking platform. The resin was washed 6 times with 500 µL TBST (Tris-buffered

saline, 0.05% Tween-20), and the protein was eluted by adding 3 additions of 30 µL 50 mM NaOH while rocking at room temperature. A final elution was collected by boiling the resin 5 min with 30 µL 2X SDS-PAGE buffer.

Co-immunoprecipitation experiments using WT and mutant Cox15-Myc expressed from the pRS415 plasmid were performed as described above for experiments using native Cor1. Due to a decrease in L-20 Cox15-Myc steady-state levels, however, 1.5 mg of mitochondria was used for co-immunoprecipitation.

For all co-immunoprecipitation experiments, samples were separated by SDS-PAGE followed by transfer to polyvinylidene difluoride (PVDF) membranes. Control co-immunoprecipitation experiments were conducted in strains in which Cox15 was untagged to ensure the positive interactions observed were not artifacts.

Immunodetection

The commercially available primary antibodies utilized in these studies were anti Myc (Thermo #R950-25; lot 1827713), anti HA (Thermo #26183), and anti porin (Thermo 459500). Primary antibodies that recognized native proteins were a kind gift from Dr. Martin Ott (Stockholm University). All primary antibodies were validated as described in Figure 2.4. The secondary antibody utilized following the anti Myc, anti HA, and anti porin antibodies was goat anti mouse (Pierce #31430; lot PF202430). For the blots probing native proteins, the goat anti rabbit (Abcam #6721; lot GR169100-2) antibody was used. Supersignal West Pico (Thermo #34080) was used following SDS-PAGE to visualize blotted proteins on PVDF membranes. Following BN-PAGE of Cox15-Myc, a homemade chemiluminescent solution (*Solution A:* 100 mM Tris-Cl (pH=8.5), 2.5 mM luminol, 0.4 mM *p*-coumeric acid / *Solution B:* 100 mM Tris (pH=8.5), 0.06% of 30% H_2O_2) was used for visualizing protein bands on PVDF membranes. All blots were exposed to HyBlot autoradiography film or imaged with a Chemi-Doc MP imager (Bio-Rad).

REFERENCES

REFERENCES

1. Gennis, R., and Ferguson-Miller, S. (1995) Structure of cytochrome *c* oxidase, energy generator of aerobic life. *Science* **269**, 1063-1064

2. Zee, J. M., and Glerum, D. M. (2006) Defects in cytochrome oxidase assembly in humans: lessons from yeast. *Biochem. Cell Biol.* **84**, 859-869

3. Timón-Gómez, A., Nývltová, E., Abriata, L. A., Vila, A. J., Hosler, J., and Barrientos, A. (2018) Mitochondrial cytochrome *c* oxidase biogenesis: recent developments. *Semin. Cell Dev. Biol.* **76**, 163-178

4. Fontanesi, F., Soto, I. C., Horn, D., and Barrientos, A. (2006) Assembly of mitochondrial cytochrome *c*-oxidase, a complicated and highly regulated cellular process. *Am. J. Cell Physiol.* **291**, C1129-1147

5. Kim, H. J., Khalimonchuk, O., Smith, P. M., and Winge, D. R. (2012) Structure, function, and assembly of heme centers in mitochondrial respiratory complexes. *Biochim. Biophys. Acta* **1823**, 1604-1616

6. Shoubridge, E. A. (2001) Cytochrome *c* oxidase deficiency. *Am. J. Med. Genet.* **106**, 46-52

7. Khalimonchuk, O., Bestwick, M., Meunier, B., Watts, T. C., and Winge, D. R. (2010) Formation of the redox cofactor centers during Cox1 maturation in yeast cytochrome oxidase. *Mol. Cell Biol.* **30**, 1004-1017

8. Swenson, S., Cannon, A., Harris, N. J., Taylor, N. G., Fox, J. L., and Khalimonchuk, O. (2016) Analysis of oligomerization properties of heme *a* synthase provides insights into its function in eukaryotes. *J. Biol. Chem.* **291**, 10411-10425

9. Taylor, N. G., Swenson, S, Harris, N.J., Germany, E.M., Fox, J.L., Khalimonchuk, O. (2017) The assembly factor Pet117 couples heme *a* synthase activity to cytochrome oxidase sssembly. *J Biol Chem* **292**, 1815-1825

10. Bareth, B., Dennerlein, S., Mick, D. U., Nikolov, M., Urlaub, H., and Rehling, P. (2013) The heme *a* synthase Cox15 associates with cytochrome *c* oxidase assembly intermediates during Cox1 maturation. *Mol. Cell. Biol.* **33**, 4128-4137

11. Hederstedt, L. (2012) Heme A biosynthesis. *Biochim. Biophys. Acta* **1817**, 920-927

12. Brown, K. R., Brown, B. M., Hoagland, E., Mayne, C. L., and Hegg, E. L. (2004) Heme A synthase does not incorporate molecular oxygen into the formyl group of heme A. *Biochemistry* **43**, 8616-8624

13. Zhuang, J., Reddi, A. R., Wang, Z., Khodaverdian, B., Hegg, E. L., and Gibney, B. R. (2006) Evaluating the roles of the heme *a* side chains in cytochrome *c* oxidase using designed heme proteins. *Biochemistry* **45**, 12530-12538

14. Soto, I. C., Fontanesi, F., Liu, J., and Barrientos, A. (2012) Biogenesis and assembly of eukaryotic cytochrome *c* oxidase catalytic core. *Biochim. Biophys. Acta* **1817**, 883-897

15. Bundschuh, F. A., Hannappel, A., Anderka, O., and Ludwig, B. (2009) Surf1, associated with Leigh syndrome in humans, is a heme-binding protein in bacterial oxidase biogenesis. *J. Biol. Chem.* **284**, 25735-25741

16. Zara, V., Conte, L., and Trumpower, B. L. (2007) Identification and characterization of cytochrome bc_1 subcomplexes in mitochondria from yeast with single and double deletions of genes encoding cytochrome bc_1 subunits. *FEBS J.* **274**, 4526-4539

17. Khalimonchuk, O., Bird, A., and Winge, D. R. (2007) Evidence for a pro-oxidant intermediate in the assembly of cytochrome oxidase. *J. Biol. Chem.* **282**, 17442-17449

18. Pierrel, F., Khalimonchuk, O., Cobine, P. A., Bestwick, M., and Winge, D. R. (2008) Coa2 is an assembly factor for yeast cytochrome *c* oxidase biogenesis that facilitates the maturation of Cox1. *Mol. Cell Biol.* **28**, 4927-4939

19. Stuart, R. A. (2009) Chapter 11 Supercomplex organization of the yeast respiratory chain complexes and the ADP/ATP carrier proteins. *Methods Enzymol.* **456**, 191-208

20. Khalimonchuk, O., Kim, H., Watts, T., Perez-Martinez, X., and Winge, D. R. (2012) Oligomerization of heme *o* synthase in cytochrome oxidase biogenesis is mediated by cytochrome oxidase assembly factor Coa2. *J. Biol. Chem.* **287**, 26715-26726

21. Schagger, H., and Pfeiffer, K. (2000) Supercomplexes in the respiratory chains of yeast and mammalian mitochondria. *EMBO J.* **19**, 1777-1783

22. Cruciat, C. M., Brunner, S., Baumann, F., Neupert, W., and Stuart, R. A. (2000) The cytochrome bc_1 and cytochrome *c* oxidase complexes associate to form a single supracomplex in yeast mitochondria. *J. Biol. Chem.* **275**, 18093-18098

23. Solmaz, S. R. N., and Hunte, C. (2008) Structure of complex III with bound cytochrome *c* in reduced state and definition of a minimal core interface for electron transfer. *J Biol Chem* **283**, 17542-17549

24. Marechal, A., Meunier, B., Lee, D., Orengo, C., and Rich., P. R. (2012) Yeast cytochrome *c* oxidase: A model system to study mitochondrial forms of the haem-copper oxidase superfamily. *Biochim Biophys Acta* **1817**, 620-628

25. Nijtmans, L. G., Artal Sanz, M., Bucko, M., Farhoud, M. H., Feenstra, M., Hakkaart, G. A., Zeviani, M., and Grivell, L. A. (2001) Shy1p occurs in a high molecular weight complex and is required for efficient assembly of cytochrome *c* oxidase in yeast. *FEBS Lett.* **498**, 46-51

26. Mick, D. U., Wagner, K., van der Laan, M., Frazier, A. E., Perschil, I., Pawlas, M., Meyer, H. E., Warscheid, B., and Rehling, P. (2007) Shy1 couples Cox1 translational regulation to cytochrome *c* oxidase assembly. *EMBO J.* **26**, 4347-4358

27. Lazarou, M., Smith, S. M., Thorburn, D. R., Ryan, M. T., and McKenzie, M. (2009) Assembly of nuclear DNA-encoded subunits into mitochondrial complex IV, and their preferential integration into supercomplex forms in patient mitochondria. *FEBS J.* **276**, 6701-6713

28. Dowhan, W., Bibus, C. R., and Schatz, G. (1985) The cytoplasmically-made subunit IV is necessary for assembly of cytochrome *c* oxidase in yeast. *EMBO J.* **4**, 179-184

29. Taanman, J. W., and Capaldi, R. A. (1993) Subunit VIa of yeast cytochrome *c* oxidase is not necessary for assembly of the enzyme complex but modulates the enzyme activity. Isolation and characterization of the nuclear-coded gene. *J. Biol. Chem.* **268**, 18754-18761

30. Nijtmans, L. G., J.W., T., Muijsers, A. O., Speijer, D., and Van den Bogert, C. (1998) Assembly of cytochrome-*c* oxidase in cultured human cells. *Eur. J. Biochem.* **254**, 389-394

31. Fontanesi, F., Jin, C., Tzagoloff, A., and Barrientos, A. (2008) Transcriptional activators HAP/NF-Y rescue a cytochrome *c* oxidase defect in yeast and human cells. *Hum. Mol. Genet.* **17**, 775-788

32. Barrientos, A., Gouget, K., Horn, D., Soto, I. C., and Fontanesi, F. (2009) Suppression mechanisms of COX assembly defects in yeast and human: insights into the COX assembly process. *Biochim. Biophys. Acta* **1793**, 97-107

33. Vukotic, M., Oeljeklaus, S., Wiese, S., Vogtle, F. N., Meisinger, C., Meyer, H. E., Zieseniss, A., Katschinski, D. M., Jans, D. C., Jakobs, S., Warscheid, B., Rehling, P., and Deckers, M. (2012) Rcf1 mediates cytochrome oxidase assembly and respirasome formation, revealing heterogeneity of the enzyme complex. *Cell Metab.* **15**, 336-347

34. Levchenko, M., Wuttke, J. M., Römpler, K., Schmidt, B., Neifer, K., Juris, L., Wissel, M., Rehling, P., and Deckers, M. (2016) Cox26 is a novel stoichiometric subunit of the yeast cytochrome *c* oxidase. *Biochim. Biophys. Acta* **1863**, 1624-1632

35. Cui, T. Z., Conte, A., Fox, J. L., Zara, V., and Winge, D. R. (2014) Modulation of the respiratory supercomplexes in yeast: enhanced formation of cytochrome oxidase increases the stability and abundance of respiratory supercomplexes. *J. Biol. Chem.* **289**, 6133-6141

36. Chen, Y. C., Taylor, E. B., Dephoure, N., Heo, J. M., Tonhato, A., Papandreou, I., Nath, N., Denko, N. C., Gygi, S. P., and Rutter, J. (2012) Identification of a protein mediating respiratory supercomplex stability. *Cell. Metab.* **15**, 348-360

37. Strogolova, V., Furness, A., Robb-McGrath, M., Garlich, J., and Stuart, R. A. (2012) Rcf1 and Rcf2, members of the hypoxia-induced gene 1 protein family, are critical components of the mitochondrial cytochrome bc_1-cytochrome *c* oxidase supercomplex. *Mol. Cell Biol.* **32**, 1363-1373

38. Wang, Z., Wang, Y., and Hegg, E. L. (2009) Regulation of the heme A biosynthetic pathway: differential regulation of heme A synthase and heme O synthase in *Saccharomyces cerevisiae*. *J. Biol. Chem.* **284**, 839-847

39. Dienhart, M. K., and Stuart, R. A. (2008) The yeast Aac2 protein exists in physical association with the cytochrome bc_1-COX supercomplex and the TIM23 machinery. *Mol. Biol. Cell* **19**, 3934-3943

40. van der Laan, M., Wiedemann, N., Mick, D. U., Guiard, B., Rehling, P., and Pfanner, N. (2006) A role for Tim21 in membrane-potential-dependent preprotein sorting in mitochondria. *Curr. Biol.* **16**, 2271-2276

41. Saddar, S., Dienhart, M. K., and Stuart, R. A. (2008) The F_1F_0-ATP synthase complex influences the assembly state of the cytochrome bc_1-cytochrome oxidase supercomplex and its association with the TIM23 machinery. *J. Biol. Chem.* **283**, 6677-6686

42. Wiedemann, N., van der Laan, M., Hutu, D. P., Rehling, P., and Pfanner, N. (2007) Sorting switch of mitochondrial presequence translocase involves coupling of motor module to respiratory chain. *J. Cell Biol.* **179**, 1115-1122

43. Claypool, S. M., Boontheung, P., McCaffery, J. M., Loo, J. A., and Koehler, C. M. (2008) The cardiolipin transacylase, tafazzin, associates with two distinct respiratory components providing insight into Barth syndrome. *Mol. Biol. Cell* **19**, 5143-5155

44. Mick, D. U., Vukotic, M., Piechura, H., Meyer, H. E., Warscheid, B., Deckers, M., and Rehling, P. (2010) Coa3 and Cox14 are essential for negative feedback regulation of COX1 translation in mitochondria. *J. Cell Biol.* **191**, 141-154

45. Stuart, R. A. (2008) Supercomplex organization of the oxidative phosphorylation enzymes in yeast mitochondria. *J. Bioenerg. Biomembr.* **40**, 411-417

46. Vogel, F., Bornhövd, C., Neupert, W., and Reichert, A. S. (2006) Dynamic subcompartmentalization of the mitochondrial inner membrane. *J. Cell Biol.* **175**, 237-247

47. Conte, A., B., P., Ferramosca, A., and Zara, V. (2015) The dimerization of the yeast cytochrome bc_1 complex is an early event and is independent of Rip1. *Biochim. Biophys. Acta* **1853**, 987-995

48. Brandner, K., Mick, D. U., Frazier, A. E., Taylor, R. D., Meisinger, C., and Rehling, P. (2005) Taz1, an outer mitochondrial membrane protein, affects stability and assembly of inner membrane protein complexes: implications for Barth Syndrome. *Mol. Biol. Cell* **16**, 5202-5214

49. Bianchi, C., Genova, M. L., Parenti Castelli, G., and Lenaz, G. (2004) The mitochondrial respiratory chain is partially organized in a supercomplex assembly: kinetic evidence using flux control analysis. *J. Biol. Chem.* **279**, 36562-36569

50. Bestwick, M., Khalimonchuk, O., Pierrel, F., and Winge, D. R. (2010) The role of Coa2 in hemylation of yeast Cox1 revealed by its genetic interaction with Cox10. *Mol. Cell Biol.* **30**, 172-185

51. Longtine, M. S., McKenzie, A., 3rd, Demarini, D. J., Shah, N. G., Wach, A., Brachat, A., Philippsen, P., and Pringle, J. R. (1998) Additional modules for versatile and

economical PCR-based gene deletion and modification in *Saccharomyces cerevisiae*. *Yeast* **14**, 953-961

52. Gietz, R. D., and Schiestl, R. H. (2007) High-efficiency yeast transformation using the LiAc/SS carrier DNA/PEG method. *Nature Protocols* **2**, 31-34

53. Bähler, J., Wu, J. Q., Longtine, M. S., Shah, N. G., McKenzie, A. r., Steever, A. B., Wach, A., Philippsen, P., and Pringle, J. R. (1998) Heterologous modules for efficient and versatile PCR-based gene targeting in *Schizosaccharomyces pombe*. *Yeast* **14**, 943-951

54. Lange, H., Kispal, G., and Lill, R. (1999) Mechanism of iron transport to the site of heme synthesis inside yeast mitochondria. *J. Biol. Chem.* **274**, 18989-18996

55. Diekert, K., de Kroon, A., Kispal, G., and Lill, R. (2001) Isolation and subfractionation of mitochondria from the yeast *Saccharomyces cerevisiae*. *Mol. Cell Biol.* **65**, 37-51

56. Frazier, A. E., Chacinska, A., Truscott, K. N., Guiard, B., Pfanner, N., and Rehling, P. (2003) Mitochondria use different mechanisms for transport of multispanning membrane proteins through the intermembrane space. *Mol. Cell Biol.* **23**, 7818-7828

57. Shevchenko, A., Wilm, M., Vorm, O., and Mann, M. (1996) Mass spectrometric sequencing of proteins silver-stained polyacrylamide gels. *Anal. Chem.* **68**, 850-858

Chapter 3: Investigation of the catalytic mechanism of heme *a* synthase[1]

[1] K. L. Foreman performed the experiment shown in Figure 2C. E. D. Rivett performed all of the other experiments and wrote the chapter.

Abstract

In eukaryotes and many aerobic prokaryotes, the final step of aerobic respiration is catalyzed by an aa_3 cytochrome *c* oxidase. As its name implies, this type of terminal oxidase requires a modified heme cofactor known as heme *a*. Synthesis of heme *a* from heme *b*, the prototypical cellular heme, is a two-step process. First, heme *o* synthase catalyzes the conversion of a vinyl group from heme *b* to a hydroxyethylfarnesyl moiety, producing heme *o*. Then heme *a* synthase catalyzes the oxidation of a specific methyl substituent of heme *o* to an aldehyde. Previously reported data indicate that heme *a* synthase has a heme *b* cofactor and is an oxygen-activating enzyme that uses a peroxidase-like electron transfer mechanism of oxidation. However, several details of the catalytic mechanism remain unclear. In this report, we investigated the role of conserved residues from the N- and C-terminal heme binding sites of heme *a* synthase. We found that a glutamate within the N-terminal heme binding site is critical for activity, consistent with the hypothesis that a carbocation forms transiently during catalysis. We also investigated the ability of HAS to bind CO, an O_2 mimic, and found that in most instances, CO does not bind heme *a* synthase in the absence of substrate.

Introduction

Aerobic respiration is a key metabolic pathway in eukaryotes and many prokaryotes. This process uses the energy temporarily stored in metabolic intermediates, such as NADH or succinate, to generate the chemiosmotic gradient that ultimately powers ATP synthesis. This electrochemical gradient is produced via transfer of electrons through a membrane-localized electron transport chain with concomitant pumping of protons across the membrane. At the end of the electron transport chain, the electrons are transferred to oxygen, the final electron acceptor, reducing O_2 to H_2O (1). This reduction is most commonly catalyzed by an oxidase from the heme-copper oxidase superfamily (2-4).

As their name suggests, heme-copper oxidases possess a bimetallic active site with both a heme molecule and a copper ion (1,2). All eukaryotic (mitochondrial) heme-copper

oxidases and the majority of known prokaryotic heme-copper oxidases are aa_3 cytochrome *c* oxidases, meaning that the heme cofactor is a modified heme known as heme *a* (2-8). Failure to synthesize heme *a* halts assembly of cytochrome *c* oxidase, a multi-subunit protein complex. A lack of properly assembled cytochrome *c* oxidase typically hinders bacterial growth on non-fermentable carbon sources and essentially halts aerobic respiration in eukaryotes, which have unbranched electron transport chains, with severe consequences in higher eukaryotes (9-19). Despite the important role of heme *a* in aerobic respiration, many aspects of the catalytic mechanism of HAS have not yet been elucidated.

Heme *a* is synthesized from heme *b* by two enzymatic reactions. In the first reaction, the vinyl group from pyrrole ring A is converted to a hydroxyethylfarnesyl group by heme *o* synthase (HOS), producing heme *o* (20). In the second reaction, heme *a* synthase (HAS) oxidizes the C8 methyl group of pyrrole ring D, converting heme *o* to heme *a* (Figure 3.1) (19,21-28). The enzymes that catalyze these reactions, HOS and HAS, respectively, are both integral membrane proteins located either in the eukaryotic inner mitochondrial membrane or in the prokaryotic cell membrane. HOS is a member of the intramembrane aromatic prenyltransferase superfamily, which is distantly related to soluble isoprenyl pyrophosphate synthases (19,24,25,29-34). Similar to these related prenyltransferases, HOS is proposed to transfer a farnesyl group from farnesyl diphosphate to heme *b* via an ionization-condensation-hydroxylation mechanism (25,35-38). HAS, on the other hand, is an oxygen-activating enzyme that is not very closely related phylogenetically to any other enzyme families.

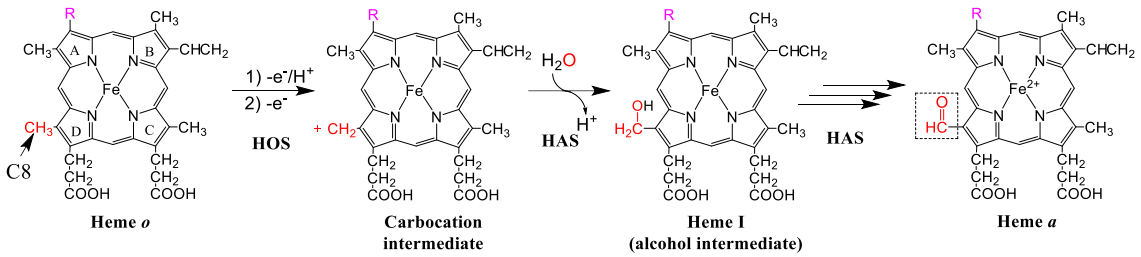

Figure 3.1: Overview of the proposed reaction mechanism for the conversion of heme *o* to heme *a*

The C-8 methyl group (shown in red) loses a proton and two electrons, generating a carbocation. An oxygen atom from water (shown in red) traps this carbocation, yielding heme I, an alcohol intermediate. A second oxidation step ultimately converts the alcohol into an aldehyde, generating heme *a*. (R group shown in pink – hydroxyethylfarnesyl group)

HAS catalyzes the stepwise oxidation of the C8 methyl group of heme *o* to an alcohol (heme I) and then to an aldehyde (heme *a*) in successive O_2-dependent reactions (Figure 3.1) (27). Although HAS was initially thought to be a monooxygenase, like cytochrome P_{450} or chlorophyll *a* oxygenase (22,26,27,39-42), isotope labelling studies indicate that HAS probably oxidizes heme *o* via electron transfer using a peroxidase-like mechanism (28). Thus, while HAS uses O_2 as an electron acceptor, H_2O is the source of the oxygen atom that is ultimately incorporated into the aldehyde group of heme *a*.

The majority of known HAS sequences are comprised of eight transmembrane (TM) helices, although certain archaea have a truncated, 4-TM HAS variant (43,44). Sequence homology between the N-terminal half of HAS (helices 1-4) and the C-terminal half (helices 5-8) indicates that an ancient gene encoding a 4-TM HAS variant was duplicated and fused to produce the more common 8-TM variant. There are four highly conserved His residues in HAS, two located in the N-terminal half of the protein (located on TM2 and TM4) and two located at analogous positions in the C-terminal half (located on TM6 and TM8) (43,45,46). Because *Bacillus subtilis* HAS (*Bs*HAS) co-purifies with heme *b* and heme *a*, both of which are *bis*-histidine axially ligated, it was proposed that all four conserved histidines could serve as heme ligands (22,23,39,43,45,46). Mutagenesis of each of these conserved histidines

indicates that they are all important for activity, although subtle variations in the activity and stability of each singly substituted variant suggest that each histidine has a unique role (43,45-49).

Recently, the structure of *Bacillus subtilis* HAS was solved by X-ray crystallography, showing that the N-terminal and C-terminal halves of HAS each form a four-helical bundle (50). Heme *b* was bound within the C-terminal bundle, ligated by two of the conserved histidines. The N-terminal bundle was empty, but the position of the two conserved N-terminal histidines indicates that they could also serve as heme ligands. In addition, the cryo electron microscopy (cryo-EM) structure of *Aquifex aeolicus* HAS also appears to show density for a heme in the center of the C-terminal four-helical bundle (51). Thus, the currently available structural and biochemical data indicates that HAS contains two heme binding sites that, despite being structurally very similar, seem to be specific for either binding heme *o* (substrate) or heme *b* (presumably a cofactor). However, biochemical data that conclusively demonstrates the function of each heme binding site is lacking.

In addition to the four histidine ligands, there are only a few residues that are highly conserved across all know HAS sequences. Of these, one particularly intriguing residue is a glutamate that precedes the second highly conserved histidine as part of the short EXXHR motif located within the N-terminal heme binding site (TM2). This glutamate (97% conservation) is the only highly conserved negatively charged residue within the transmembrane domain. The residue at the corresponding position in the C-terminal heme binding site is either glutamine (~57% conservation) or histidine (~37% conservation), forming the motif Q/HXXHR (TM6). Due to its location and high degree of conservation, one intriguing possibility is that this glutamate plays a role in stabilizing a carbocation that forms transiently at the C8 position of heme *o* as part of a reaction mechanism similar to the proposed mechanism of mammalian peroxidases (Figure 3.1) (28,50,52,53).

In this chapter, I probe the function of each heme binding site via mutagenesis of conserved residues in the N- and C-terminal halves of *Shewanella oneidensis* HAS (*So*HAS). Homologous expression of *So*HAS in *S. oneidensis* does not suffer from some of the heterogeneity we have observed previously when expressing *Bs*HAS variants in *Escherichia coli*. Our results support the hypothesis that the C-terminal four-helical bundle specifically functions as a heme *b* binding site. Furthermore, analysis of the *in vivo* activity of *So*HAS variants suggests that the highly conserved glutamate (E72) in the N-terminal heme binding site plays a unique role in catalysis, unlike the corresponding C-terminal residue, H241. Similar results were also obtained when this conserved glutamate (E166) was substituted to alanine in a representative eukaryotic HAS from *Saccharomyces cerevisiae* (*Sc*HAS). Additionally, preliminary UV-Visible (UV-Vis) spectrophotometry studies indicate that HAS can bind CO (an O_2 mimic) under certain circumstances. Overall, our results shed light on the potential mechanism of HAS.

Results

Substitution of a conserved glutamate in the N-terminal heme binding site of HAS indicates that a negatively charged residue is necessary at this position

To understand the role of conserved residues in HAS, we expressed wild-type (WT) and amino acid substituted *So*HAS (CtaA) variants in *S. oneidensis* and assessed the *in vivo* activity of each variant. Although the genome of *S. oneidensis* includes genes for HOS and HAS, as well as the structural genes for an aa_3 cytochrome *c* oxidase, under normal growth conditions *S. oneidensis* does not express these genes and therefore does not produce detectable levels of heme *o* or heme *a* (Table 3.1) (54,55). Thus, the activity of overexpressed *So*HAS could be assessed by the presence of heme *a* in the cell pellet. Heme *o*, the substrate for HAS, was provided by co-expressing *So*HAS with *S. oneidensis* HOS (*So*HOS). When we expressed an *So*HAS variant with C-terminal V5 and His_6 epitope tags, *So*HAS-V5-His_6

could be isolated from the cell membrane (Figure 3.2C), confirming that *So*HAS was properly inserted into the membrane. Importantly, a small amount of heme *a* (5% ± 2) was detectable in the lysate, indicating that both overexpressed proteins, *So*HOS and *So*HAS-V5-His_6, were active (Table 3.1). (The relative amounts of hemes *b*, *o*, I, and *a* are expressed as a percentage of the total extractable heme, *e.g.*, non-covalently bound heme.) After confirming that our co-expression system worked, we proceeded with the investigation of *So*HAS-V5-His_6 variants.

To study the role of the highly conserved glutamate in the N-terminal heme binding site (E72 in *So*HAS), this residue was substituted to alanine (E72A), glutamine (E72Q), and aspartate (E72D) (Figure 3.2A). Our goal was to determine if another negatively charged residue (aspartate) or a residue of a similar size and shape (glutamine) could perform the role of E72 in the catalytic mechanism. The E72A and E72Q variants were completely inactive, as judged by the lack of heme *a* or the heme I intermediate in the lysate. However, when the E72D variant was expressed, small amounts of heme I (5% ± 1) and heme *a* (3% ± 0) were detectable, indicating that the E72D variant was partially active. (Heme I did not accumulate when WT *So*HAS-V5-His_6 was expressed.) The observation that only the E72D variant had any level of activity suggests that the presence of a negatively charged residue at this position within the N-terminal heme binding site is important for the catalytic activity of HAS.

Because this N-terminal glutamate is highly conserved and seems to be important for catalysis, we also investigated the significance of this residue in *S. cerevisiae*, a model eukaryote frequently used in the study of mitochondrial aa_3 cytochrome *c* oxidase. To assess the *in vivo* activity of *Sc*HAS (Cox15) variants, plasmids carrying *Sc*HAS-FLAG (WT, E166A, or E166D) were expressed in a *Δcox15* background, followed by extraction of non-covalently bound hemes from isolated mitochondria. Expression of WT *Sc*HAS-FLAG, which has been shown to restore respiratory competence in the *Δcox15* strain, produced

detectable levels of heme *a* (Table 3.1). However, both the E166A and E166D variants were inactive, despite having expression levels similar to that of the WT enzyme (Figure 3.2B). This result indicates that the presence of a glutamate in the N-terminal heme binding site is also important in eukaryotic HAS.

Sample	[Heme *b*] (μM)[a]	Heme *b* (%)[b]	Heme *o* (%)[b]	Heme I (%)[b]	Heme *a* (%)[b]	*n*
***S. oneidensis* whole cell**[c]						
*So*HOS *So*HAS WT	13 ± 4	95 ± 2	—	—	5 ± 2	4
*So*HOS	7 ± 0.5	100 ± 0	—	—	—	2
*So*HAS	12 ± 3	100 ± 0	—	—	—	2
No plasmid	8	100	—	—	—	1
*So*HOS *So*HAS E72A	19 ± 1	93 ± 0.1	7 ± 0.3	—	—	2
*So*HOS *So*HAS E72D	14 ± 3	90 ± 3	3 ± 3	5 ± 1	3 ± 0.2	3
*So*HOS *So*HAS E72Q	17 ± 1	89 ± 1	11 ± 1	—	—	2
*So*HOS *So*HAS H241A	13 ± 0.1	97 ± 0.1	—	—	3 ± 0.1	2
*So*HOS *So*HAS H241E	16 ± 2	95 ± 3	—	—	5 ± 3	2
*So*HOS *So*HAS-MBP-V5-His_6	21 ± 0.2	96 ± 4	—	—	4 ± 4	3
***S. cerevisiae* mitochondria**[d]						
*Sc*HAS-FLAG WT	7 ± 2	91 ± 5	—	—	9 ± 5	2
pRS426 empty	8	100	—	—	—	1
*Sc*HAS-FLAG E166A	9	78	22	—	—	1
*Sc*HAS-FLAG E166D	13	81	19	—	—	1

Table 3.1: Hemes extracted from *S. oneidensis* expressing *So*HAS-V5-His_6 variants or *S. cerevisiae* expressing *Sc*HAS-FLAG variants

[a]The concentration of heme *b* was calculated by comparing the heme *b* peak area to a standard curve prepared for hemin (heme *b* chloride).

[b]The approximate percentage of each heme relative to the total amount of all extractable hemes was calculated using the area under the curve of each elution peak in the chromatogram. The average percentage and standard deviation for *n* samples are shown.

[c]*So*HOS and *So*HAS were expressed in a WT *S. oneidensis* background. *So*HOS (untagged) was constitutively expressed from the vector pBBR1-RBS *So ctaB*. *So*HAS-V5-His_6 was expressed from the vector pBAD *So ctaA-V5-His*$_6$.

[d]*Sc*HAS-FLAG was expressed from the vector pRS426 *COX15-FLAG* in a *Δcox15* DY5113 background.

Because the structures of the N-terminal and C-terminal heme binding sites are similar, the conserved N-terminal glutamate has a C-terminal counterpart. This corresponding C-terminal residue is less highly conserved and is usually either glutamine (~58% conservation) or histidine (~38% conservation). In *So*HAS, this residue is H241. To test the hypothesis that the N-terminal heme binding site and C-terminal binding site have distinct roles, H241 was substituted with alanine or glutamate (Figure 3.2A). Both the H241A and the H241E variants were active (Table 3.1), indicating that this residue is not necessary for activity in *So*HAS. Substitution of the analogous residue in *Sc*HAS (Q365) to alanine also appears to rescue the respiratory deficiency of *Δcox15*, indicating that this residue is also not critical in eukaryotic HAS[2]. Thus, compared to the glutamate in the N-terminal heme binding site, the corresponding C-terminal glutamine or histidine is relatively unimportant, supporting the hypothesis that the N-terminal and C-terminal heme binding sites are not interchangeable.

[2] Dr. Oleh Khalimonchuk, personal communication.

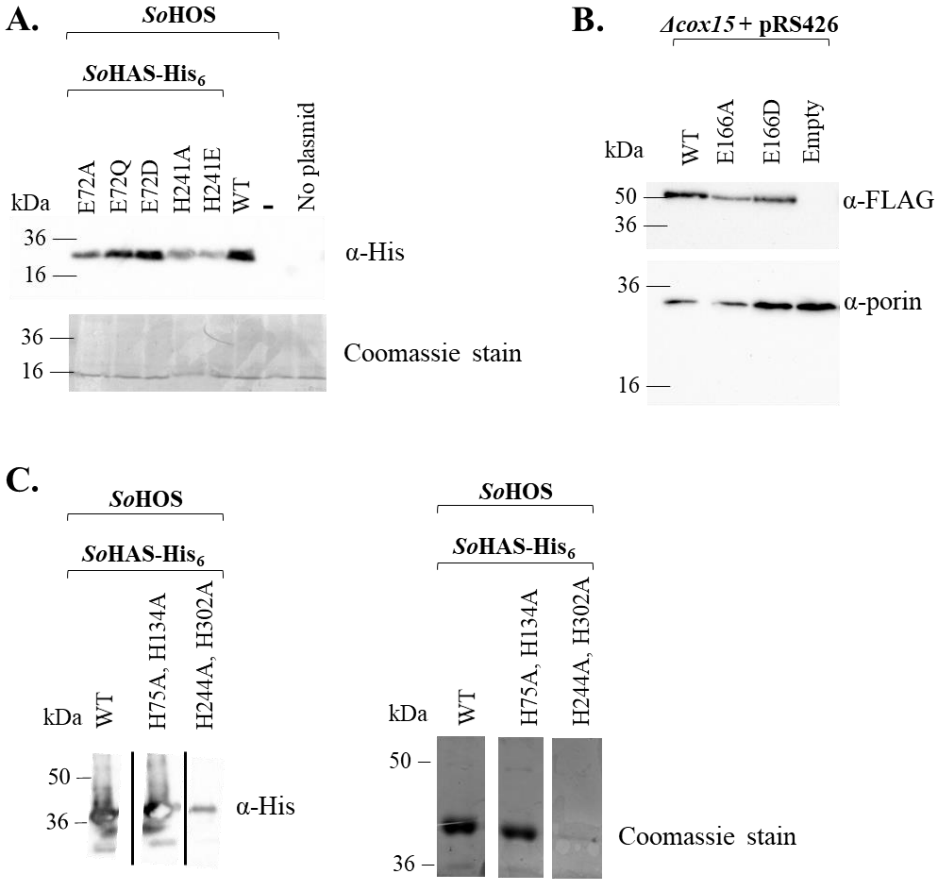

Figure 3.2: SDS-PAGE experiments showing the relative expression levels of *So*HAS-V5-His$_6$ variants and *Sc*HAS-FLAG variants

A. SDS-PAGE of *S. oneidensis* lysate (~1 μg total protein) expressing WT SoHAS-V5-His$_6$, or a HAS variant with the conserved N-terminal glutamate substituted (E72A, E72Q, E72D), or a HAS variant with the analogous C-terminal residue substituted (H241A, H241E). After immunoblotting, the PVDF membrane was stained with Coomassie brilliant blue to show the total amount of protein loaded. (Experiment repeated in one biological replicate.) B. SDS-PAGE of *Sc*HAS-FLAG mitochondria (10 μg total protein) expressed from pRS426 in a *Δcox15* background. A second immunoblot probed with anti porin is also shown as a loading control. C. SDS-PAGE of *So*HAS-V5-His$_6$ isolated from *S. oneidensis*. SoHAS-V5-His$_6$ was isolated from *S. oneidensis* coexpressing *So*HOS and WT *So*HAS-V5-His$_6$ or a doubly substituted variant (H75A, H134A or H244A, H303A). Equal volumes of eluate from nickel-nitrilotriacetic acid (NTA) resin were loaded. (Experiment repeated in four biological replicates.)

*Substitutions in the C-terminal heme binding site destabilize prokaryotic HAS (*So*HAS) to a greater extent than substitutions in the N-terminal heme binding site*

Over the course of our investigations, we noticed that substitutions in the C-terminal heme binding site of *So*HAS-V5-His_6 seem to decrease the steady-state expression level of HAS. This trend can be observed by comparing the expression levels of the N-terminally substituted variants (E72A, E72D, and E72Q) with the those of the C-terminally substituted variants (H241A and H241E) (Figure 3.2A). Although the amount of the E72A variant was slightly decreased compared to WT, the other two variants, E72Q and E72D, were expressed to approximately the same level as WT HAS. In contrast, expression of the H241A and H241E variants was decreased compared to WT HAS.

The destabilizing effect of mutations in the C-terminal heme binding site was also apparent when the N-terminal and C-terminal histidines were substituted with alanine in *So*HAS. The N-terminal and C-terminal heme binding sites both have two highly conserved histidines that all seem to serve as axial heme ligands. Structural data indicate that the C-terminal histidines ligate heme *b*, a cofactor. The N-terminal histidines are expected to ligate heme *o*, the substrate. To test the importance of these residues, we constructed doubly substituted *So*HAS-V5-His_6 variants which either had both N-terminal histidines (H75 and H134) or both C-terminal histidines (H244 and H302) substituted with alanine. Consistent with previous studies of *Bs*HAS and *Sc*HAS, both variants were inactive (data not shown). A striking difference between the two variants however, was their apparent stability. The N-terminal double variant (H75A, H134A) was similar to that of WT HAS, while expression of the C-terminal double variant (H244A, H302A) was significantly diminished (Figure 3.2C). The marked instability of C-terminal *So*HAS-V5-His_6 variants when compared to their N-terminal counterparts seems to support the hypothesis that the C-terminal half of HAS binds heme *b* while the N-terminal half binds heme *o*. Because the heme *b* cofactor is probably not

released, the C-terminal four-helical bundle is presumably relatively static. On the other hand, the N-terminal half of HAS is expected to be more dynamic since it must bind substrate (heme *o*) and release product (heme *a*). Thus, it seems logical that substitutions in the N-terminal heme binding site do not affect HAS stability to the same extent as mutations in the C-terminal heme binding site, as the C-terminal substitutions presumably disrupt cofactor binding and the overall structure.

In an attempt to confirm that the conserved histidines in the N-terminal heme binding site ligate heme *o*, we analyzed the hemes that co-purified with the H75A, H134A variant and with the H244A, H302A variant. WT HAS typically co-purifies with heme *a* and heme *b*, leading to the hypothesis that each heme binding site binds a specific heme type. Because previous work has shown that individually substituting each conserved histidine with a non-ligating residue does not clarify which histidine ligates which heme (43,45,46), we tried expressing doubly substituted *So*HAS-V5-His_6 variants. The rationale behind this approach was that substitution of both histidine ligands in a heme binding site might disrupt the site enough to prevent heme from binding at that location. Ideally, this would allow us to verify which type of heme binds to each heme binding site, as any heme that co-purifies with the H75A, H134A variant must be bound to the C-terminal heme binding site, and vice versa. However, we found that the H75A, H134A variant co-purifies with both heme *b* and a small amount of heme *o* (data not shown). The presence of heme *o* suggests that substituting both N-terminal histidines does not completely abolish the heme binding capability of the N-terminal heme binding site. Although poor expression of the H244A, H302A variant made it difficult to analyze co-purifying hemes, a small amount of heme *b* was detected in some preparations of this variant. This could either indicate that some heme *b* can bind the N-terminal site or that a small portion of heme *b* can bind the disrupted C-terminal heme binding site. The first scenario could be interpreted as evidence that the N-terminal binding

site normally binds heme *b*. However, since the crystal structure of *Bs*HAS indicates that the C-terminal heme binding site is occupied by heme *b* (50), we tend to favor the second scenario.

Ferrous CO optical absorbance spectra suggest that HAS can bind CO (an O_2 mimic) under certain circumstances

When expressed in *B. subtilis*, *Bs*HAS co-purified with heme *a* and heme *b*, and spectroscopic data suggested that both hemes were ligated by two axial histidines (22). The crystal structure of *Bs*HAS is also consistent with the hypothesis that both the prenylated hemes (heme *o* and heme *a*) and heme *b* and are ligated by the four most highly conserved histidines in HAS, located in the N- and C-terminal heme binding sites, respectively (50). However, HAS is an oxygen-activating enzyme, which suggests that during the catalysis, one of these histidines must be displaced in order for O_2 to bind. However, it is unclear which heme binds O_2 and which histidine is displaced. To help address this question, we assessed the ability of *So*HAS to bind CO when the only heme present in *So*HAS was heme *b*. Our goal was to determine if the presence of heme *o* is required in order for CO to bind HAS.

To improve expression of *So*HAS, we added a maltose binding protein (MBP) tag to the C-terminal end of *So*HAS, producing the construct *So*HAS-MBP-V5-His_6. MBP-tagged *So*HAS was more highly expressed than *So*HAS-V5-His_6 and could be isolated on amylose resin instead of nickel resin, allowing us to obtain purer preparations of *So*HAS-MBP-V5-His_6. Coexpression of *So*HAS-MBP-V5-His_6 and HOS confirmed that the MBP-tagged *So*HAS was active *in vivo* (Table 1). *So*HAS-MBP-V5-His_6 co-purified with heme *b* and heme *a* (data not shown), similar to *Bs*HAS when expressed in *B. subtilis* (22,23,43). Therefore, we used *So*HAS-MBP-V5-His_6 for our initial CO binding tests.

To obtain *So*HAS-MBP-V5-His_6 preparations with only heme *b*, *So*HAS was expressed in *S. oneidensis* without coexpression of *So*HOS. HPLC analysis of the hemes

extracted from purified *So*HAS-MBP-V5-His_6 confirmed that only heme *b* was present. The heme/protein molar ratio of these samples ranged from 0.5-0.7, indicating that at most 50-70% of one heme binding site, presumably the C-terminal heme binding site, was occupied by heme *b*. To assess the CO-binding capablity of heme *b* bound to *So*HAS-MBP-V5-His_6 in the absence of heme *o*, the sample was reduced and the optical absorbance spectrum of the protein sample was measured before and after purging with CO (Figure 3.3A). As expected, addition of reductant shifted the Soret peak absorbance maximum from 416 nm to 428 nm. Upon introduction of CO, the absorbance maximum shifted to 423 nm, which is indicative of CO binding.

The observation that CO could bind *So*HAS-MBP-V5-His_6 when only heme *b* was present is in direct contrast to previously collected data from our lab[3], which indicated that in order for *Bs*HAS-His_6 to bind CO, both heme *b* and heme *o* must be present. To determine if the addition of the MBP tag was responsible for this discrepancy, we repeated the CO binding experiment with *So*HAS-V5-His_6 (Figure 3.3B). Unlike the MBP-tagged version, SoHAS-V5-His_6 did not appear to bind CO, as the absorbance maximum of the reduced peak did not shift after the introduction of CO. Thus, it appears that fusing MBP to the C-terminus of *So*HAS alters *So*HAS in some way that allows CO to bind heme *b*.

[3] Data collected by Dr. Shipra Gupta

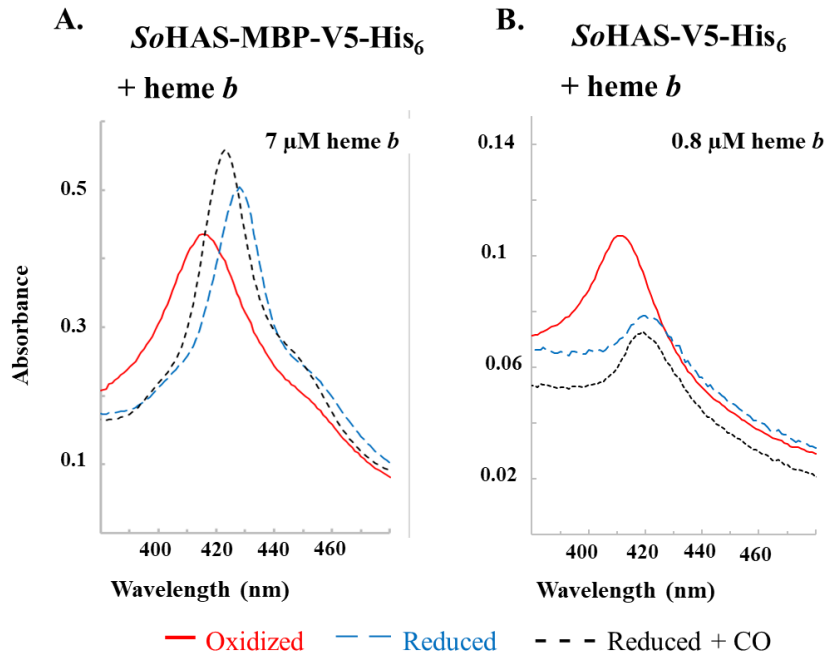

Figure 3.3: Optical absorbance spectra of *So*HAS (with or without an MBP tag) bound to only heme *b*

Oxidized (solid red line), reduced (blue dashed line), and reduced + CO absorbance spectra are shown for *So*HAS-MBP-V5-His_6 (A) and *So*HAS-V5-His_6 (B). The concentration of heme *b* in each sample was determined by HPLC analysis. Formation of a ferrous-CO derivative (seen in A but not in B) results in a sharpening of the Soret peak and a slight blue shift relative to the reduced spectrum. The experiment shown in panel A was repeated three times. The experiment shown in panel B was performed once.

Discussion

Ever since it was reported that HAS co-purifies with both heme *a* and heme *b*, it has been theorized that HAS forms two four-helical bundles, each with a heme binding site. The crystal structure of *Bs*HAS, which revealed heme *b* in the C-terminal heme binding site and an empty N-terminal heme binding site, strongly suggests that the C-terminal heme binding site specifically binds the heme *b* cofactor, while the N-terminal four-helical bundle presumably forms the binding site for the substrate heme. Although direct biochemical evidence showing where heme *o* binds remains elusive, our mutagenesis data on the stability and catalytic activity of HAS support the idea that the N-terminal four-helical bundle is the site of substrate binding.

We observed that substitution of conserved residues in the C-terminal heme binding site decreased the steady-state expression levels of *So*HAS, presumably due to a decrease in stability. In contrast, substitution of analogous residues in the N-terminal heme binding site did not significantly affect protein stability, even when these substitutions rendered *So*HAS completely inactive. Similarly, previous studies with *Bs*HAS have shown that substitutions of C-terminal residues, such as the C-terminal histidine ligands, seem to decrease the stability of these variants relative to WT *Bs*HAS (45,46). The observation that substitutions in the C-terminal heme binding site generally reduce the stability of prokaryotic HAS is consistent with the hypothesis that the C-terminal heme binding site is occupied by heme *b*, as structural changes to the cofactor heme binding site would likely have a greater effect on protein stability than analogous alterations in the substrate heme binding site.

Interestingly, HAS from the hyperthermophilic bacterium *A. aeolicus* (*Aa*HAS) was recently shown to form trimers that are quite stable in solution (51). The cryo-EM structure of *A. aeolicus* HAS (*Aa*HAS) revealed that the protein forms trimers with two C-terminal helices from each monomer at the core of the trimer. Electron density from the cryo-EM structure also suggested that a heme (likely heme *b*) was present at the center of each C-terminal four-helical bundle. Again, this finding suggests that the C-terminal half of HAS binds heme *b* and remains relatively static (51).

A recently published heme *o* binding model of *Bs*HAS (based on the crystal structure of this protein) suggests that a conserved N-terminal glutamate is positioned near the C8 methyl group of heme *o* when this substrate binds (50). We found this prediction intriguing because it suggests that this glutamate could stabilize a carbocation intermediate that is proposed to form transiently at the C8 position during catalysis (Figure 3.1). To probe the function of this highly conserved glutamate in the N-terminal heme binding site, we made substitutions at this position in prokaryotic HAS (*So*HAS-V5-His_6 and eukaryotic HAS

(*Sc*HAS-FLAG) and assessed the *in vivo* activity of each variant. Overexpression of HOS and HAS in a bacterial expression system allows for the detection of the heme I intermediate, which otherwise does not typically accumulate to high concentrations (27,28,43,45,46). Expression of *Sc*HAS variants in *S. cerevisiae*, on the other hand, allowed us to assess the activity of eukaryotic HAS variants by analysis of extracted mitochondrial hemes and by analysis of each variant's ability to rescue respiration in a yeast strain with the genomic copy of HAS knocked out (*Δcox15*).

Our results indicate that replacing E72 with alanine or glutamine abolished the catalytic activity of *So*HAS. Analogous substitutions in *Bs*HAS (E57A and E57Q) have also been reported to inactivate *Bs*HAS without affecting the enzyme's ability to bind heme *o* (43,46). Similarly, the E166A variant of *Sc*HAS was inactive and failed to rescue respiration in a *Δcox15* background. In contrast to the E72A and E72Q variants of *So*HAS, the E72D variant was partially active *in vivo*, as judged by the presence of detectable levels of heme I and heme *a* in *S. oneidensis* cells expressing this variant. The C-terminal counterpart of the highly conserved glutamate is typically either histidine or glutamine. Substitution of this analogous C-terminal residue (H241 in *So*HAS and Q365 in *Sc*HAS) did not significantly alter the *in vivo* activity of HAS, bolstering the hypothesis that the N-terminal glutamate plays a unique role in catalysis. Overall, our mutagenesis data indicate that the conserved glutamate in the N-terminal heme binding site is important for the catalytic activity of HAS and suggests that this importance stems from its negative charge. The necessity of an anionic residue near the heme *o* substrate and the accumulation of heme I in the case of the E72D variant are both consistent with the proposed catalytic mechanism of HAS, which is discussed below.

HAS catalyzes successive O_2-dependent oxidations that convert the C8 methyl group of heme *b* first to an alcohol (heme I) and then to an aldehyde (heme *a*) (27). Because the

oxygen atom that is incorporated into the aldehyde group is derived from H_2O, not O_2, it has been proposed that HAS uses a peroxidase-like electron transfer mechanism of oxidation (Figure 3.4) (28). A key feature of this mechanism is the formation of an Fe(IV)=O porphyrin cation radical (similar to compound I in peroxidases) (40,56,57). This high-valent iron-oxo species can remove one electron from the C8 methyl group of heme *o*, generating a radical at the C8 position and converting compound I to compound II. Compound II then removes a second electron from the radical, converting it to a carbocation that is ultimately trapped by H_2O to yield the hydroxylated intermediate, heme I. This process can then be repeated to oxidize the primary alcohol group of heme I to a geminal diol, which dehydrates to the aldehyde. Notably, both oxidation steps in this proposed mechanism for HAS involve the transient formation of a carbocation intermediate.

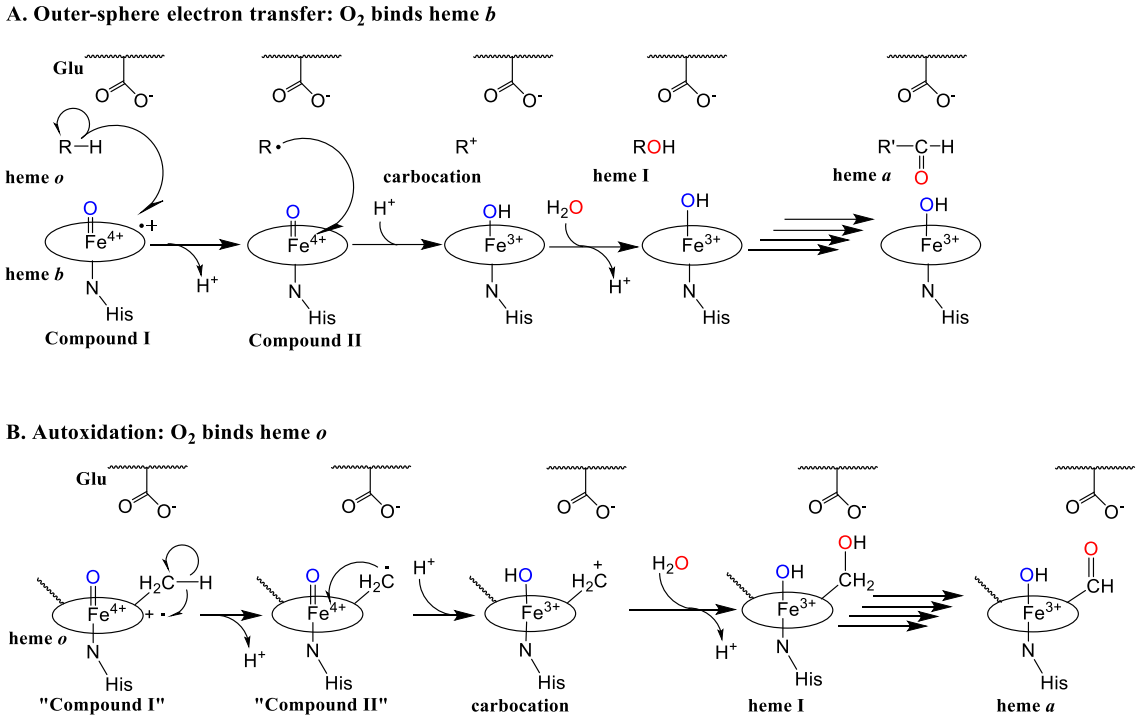

Figure 3.4: Possible mechanisms of oxygen activation by HAS

In HAS, O_2 activation may occur at heme *b* (A) or heme *o* (B). Either proposed mechanism would likely require the displacement of a histidine ligand to allow O_2 to bind. A. Outer-sphere electron transfer. O_2 activation leads to the formation of a high-valent iron-oxo species (compound I, far left) that removes an electron from the C8 methyl group of heme *o* (shown as R-H). This leads to the formation of a radical intermediate and compound II. Compound II then removes another electron from the substrate radical, forming a carbocation intermediate. Water traps the carbocation intermediate to form heme I. This process can then be repeated with heme I as the substrate to form a geminal diol (not shown), which readily dehydrates to form the aldehyde in heme *a*, the final product. A conserved glutamate positioned near the heme *o* binding site is proposed to stabilize the carbocation intermediate. B. Autoxidation mechanism. Heme *o* activates O_2 to form a compound I-like species. "Compound I" of heme *o* then oxidizes its own C8 methyl group using the general mechanism described in mechanism A.

Based on the apparent proximity of the N-terminal glutamate to the C8 position of heme *o* (50), it seems likely that this glutamate stabilizes the carbocation intermediates that are predicted to form during the catalytic mechanism of HAS. A similar mechanism has been proposed for mammalian peroxidases. Like HAS, the heme from this family of peroxidases catalyzes the modification of its own methyl substituent via a mechanism that is proposed to involve formation of a carbocation (52,53). Normally, this carbocation is trapped by a nearby

glutamate, forming an ester crosslink to the heme. However, if the crosslinking glutamate is substituted for aspartate, the heme is hydroxylated. This observation indicates that the negatively charged aspartate can still stabilize the formation of the carbocation intermediate, but, because aspartate is too short to crosslink to the heme, water traps the carbocation instead.

Like mammalian peroxidases, WT HAS produces a hydroxylated heme intermediate (heme I) that is most likely formed when a carbocation intermediate is trapped by water. Therefore, it seems logical that the N-terminal glutamate positioned near heme *o* may also be involved in stabilizing a carbocation intermediate. Substitution of E72 for D in *So*HAS presumably decreases the electrostatic stabilization of the putative carbocation intermediate that forms during each oxidation step because the shorter side chain of aspartate would be farther away from the C8 carbocation. Although both oxidation steps are expected to involve a carbocation intermediate, carbocation formation during the second oxidation would be more difficult due to the presence of the electron withdrawing hydroxyl group on the C8 carbon. Thus, the E72D substitution might be expected to have a more significant impact on the rate of the second oxidation if both oxidation steps require carbocation formation. This observation may explain why the product of the first oxidation step, heme I, accumulated in cells expressing the E72D variant of *So*HAS. Overall, our mutagenesis data are consistent with a mechanism consisting of two consecutive oxidations, both involving formation of carbocation intermediates that are stabilized by a highly conserved glutamate in the N-terminal heme binding site.

Another interesting aspect of the proposed mechanism of HAS is the question of which heme binds O_2. In other classes of heme enzymes that form compound I, one of the heme's axial coordination sites is vacant, making it obvious where O_2 or peroxide binds. However, as-purified *Bs*HAS contains heme *b* and heme *a*, which are both *bis*-histidyl axially

ligated, making it unclear where O_2 binds. Presumably, one of the histidine ligands dissociates to allow O_2 to bind either heme *b* or heme *o* in order to form compound I or a prenylated compound I-like species (28). If compound I forms at heme *b*, the oxidation of heme *o* would proceed via outer sphere electron transfer between heme *o* and heme *b* (Figure 3.4A). Alternatively, O_2 could bind heme *o* and form a compound I-like species that autocatalytically oxidizes its own methyl group, similar to mammalian peroxidases (Figure 3.4B) (52,53). In this second scenario, heme *b* would be limited to a role in electron transfer.

To investigate the potential binding site of O_2, we tested the CO-binding capability of *So*HAS bound only to heme *b*. Currently, our results indicate that CO does not bind *So*HAS-V5-His_6 in the absence of heme *o*. The lack of CO binding suggests either that CO binds heme *o* or that the presence of heme *o* in the N-terminal domain alters the conformation of the C-terminal domain so that heme *b* binds CO only in the presence of substrate. Curiously, the addition of an MBP tag to the C-terminus of *So*HAS allows heme *b* bound to *So*HAS to bind CO, but this is presumably due to some alteration in the structure of the fusion protein. Future work will be needed to determine if the presence of heme *o* in *So*HAS-V5-His_6 allows CO (and by analogy O_2) to bind.

Although my current CO binding data is consistent with both the outer-sphere electron transfer mechanism and autoxidation mechanism of O_2 activation (Figure 3.4), I tend to favor the second scenario, in which O_2 binds heme *o* within the N-terminal domain. The N-terminal half of HAS contains more conserved residues than the C-terminal half, and the conservation levels of these N-terminal residues are generally higher than their C-terminal counterparts (where present) (43,58). This trend holds true even for the histidine ligands. Although all four histidines are very highly conserved, phylogenetic analysis reveals that the histidines from the C-terminal heme binding site are more likely to be replaced by other residues than their N-terminal counterparts (58). The greater number of conserved residues in

the N-terminal domain suggests that this domain is dedicated to O_2 activation. Other heme enzymes that are capable of O-O bond cleavage, such as peroxidases and cytochromes P_{450}, also require a set of highly conserved residues in the heme binding pocket (40,56,57,59-62). Substitution of these residues typically has a severe effect on catalytic activity (40,56,57,60-62). In contrast, substitutions in electron transfer hemoproteins are often better tolerated (63-66).

Additional support for the autoxidation method comes from previously published reports on the effects of substituting the histidine residues that serve as heme ligands in *Bs*HAS. These studies show that replacing one of the N-terminal histidine ligands (H60 and H123) with alanine or leucine completely abolishes activity, while substituting either of the C-terminal histidines with a non-ligating residue often results in a HAS variant that retains partial activity (43,45,46,67). Furthermore, catalytic activity of *Bs*HAS is lost if H123 is replaced with methionine, an alternate heme ligand, while partial activity is retained if any of the other three histidine ligands is substituted with methionine (45). Replacing a histidine axial ligand with methionine generally increases the redox potential of the heme in question, a change which will alter the electron transfer capability of the cytochrome but may not render it inactive (63,68-70). Notably, the H123M variant co-purifies with heme *o*, ruling out ineffective substrate binding as the culprit behind loss of catalytic activity. Thus, the available experimental data strongly suggests that H123, one of the histidines in the N-terminal heme binding pocket, plays a role in HAS catalytic activity beyond that of simply ligating the substrate heme.

The unique importance of the histidines in the N-terminal heme binding site of *Bs*HAS is reminiscent of peroxidases, which use proximal and distal histidine residues to generate compound I via a push-pull mechanism. In peroxidases, the proximal histidine ligates the heme iron and provides an electron-donating “push.” The distal histidine, located

on the other side of the heme, is not close enough to ligate the heme iron (71). Instead, this residue acts as a general acid-base catalyst, assisting in the deprotonation of the proximal oxygen and protonation of the distal oxygen prior to O-O bond scission, thus providing the "pull" of the push-pull mechanism (40,56,57,59). Thus, both histidines are important for compound I formation and catalysis in peroxidases (40,56,57,72,73). Similarly, one potential explanation for the necessity of both N-terminal histidine ligands in HAS for full catalytic activity is that these residues participate directly in compound I formation via a push-pull mechanism similar to that of peroxidases. Based on the available data on *Bs*HAS, it is tempting to speculate that H123 is the "proximal" ligand in HAS and H60 is the "distal" ligand. In the crystal structure of *Bs*HAS, H60 is located on a transmembrane helix that is bent away from the center of the N-terminal four-helical bundle, making it seem likely that this residue could dissociate from the heme *o* iron to allow O_2 to bind (50). A similar mechanism has been proposed for diheme cytochrome *c* peroxidase, an enzyme that is activated by conformational changes that cause the distal histidine to dissociate from the active site heme (74,75). This hypothesis would also explain the inactivity of the H123M variant, as replacing the proximal histidine ligand with methionine would probably increase the redox potential of the heme and prevent compound I formation. Future structural and biochemical analyses will be needed to confirm the location of the O_2 binding site and the role of the histidine ligands in O_2 activation.

Summary and future directions

In this report, we present data that has broadened our understanding of the reaction mechanism of heme *a* synthase. Specifically, our results support the hypothesis that the N- and C-terminal domains of HAS serve distinct roles as the binding sites for substrate and cofactor heme, respectively. In particular, our results are consistent with a model of heme *o* binding that positions the C8 group of heme *o* near a highly conserved glutamate in the N-

terminal heme binding site. (Additional replicates will need to be obtained for analysis of the *in vivo* activity of *Sc*HAS variants.) Finally, initial CO binding studies seem to indicate that heme o must be bound to HAS in order for CO to bind. However, future work with *So*HAS bound to both heme *o* and heme *b* will be needed to confirm this hypothesis.

Experimental procedures

Cloning

The gene encoding *S. oneidensis* HAS (*ctaA*) was inserted into the vector pBAD202/D-TOPO (Invitrogen) with the sequence encoding the N-terminal thioredoxin tag removed. Specifically, *ctaA* was inserted downstream of an arabinose-inducible promoter (*araBAD*). The *ctaA* gene was amplified from *S. oneidensis* genomic DNA with primers that added NcoI and HindIII restriction sites to the 5′ and 3′ ends of the gene, respectively, and then ligated into pBAD. This produced the vector pBAD *So ctaA-V5-*His_6, in which the encoded HAS had (a) a V5 epitope tag and a hexahistidyl (His_6) tag appended to the C-terminus and (b) the amino acid sequence MG added to the N-terminus preceding the native amino acid sequence (Table 3.2). This plasmid was used as the template for site-directed mutagenesis to produce *So*HAS variants with a single substitution (E72A, E72Q, E72D, H241A, and H241E) or two substitutions (H75A, H134A and H244A, H302A). To add the MBP tag to the C-terminus of WT *So*HAS, a gene encoding MBP from *E. coli* (without the native signal sequence) was fused to the 3′ end of *ctaA* and ligated into pBAD, producing an *So*HAS construct with three C-terminal tags (*So*HAS-MBP-V5-His_6).

The gene encoding HOS from *S. oneidensis* (*ctaB*) was amplified from genomic DNA by PCR and inserted into the KpnI/SacI site of pBBR1 MCS3 (Table 3.2). A ribosomal binding site (RBS) was added just upstream of the start codon as previously described (76) to allow for better expression in *S. oneidensis*. The pBAD constructs were introduced into *S. oneidensis* by electroporation (77,78) and selected for by resistance to 50 μg/mL kanamycin

(Luria-Bertani (LB) agar plates). The pBBR1 construct was introduced into *S. oneidensis* via conjugation with donor strain WM3064 (79,80) and selected for resistance to 5 μg/mL tetracycline (LB agar plates).

Strain	**Description**	**Source or reference**
E. coli WM3064	*thrB1*004 *pro thi rpsL hsdS lacZ*ΔM15 RP4-1360 Δ(*araBAD*)*567* Δ*dapA*1341::[*erm pir*]	William Metcalf, University of Illinois
S. oneidensis MR-1	WT *S. oneidensis* strain	(81)
S. cerevisiae DY5113 *Δcox15*	*MATa, ade2-, can1-, leu2-, ura3-, trp1-, his3-, cox15::KanMX*; derived from *W303a*	(82)
Plasmid	**Description**	**Source or reference**
pBAD *So ctaA-V5-His$_6$*	pBAD with *S. oneidnesis ctaA-V5-His$_6$; araBAD* promoter	This study
pBAD *So ctaA-V5-His$_6$ E72A*	pBAD *So ctaA-V5-His$_6$* with E72A substitution	This study
pBAD *So ctaA-V5-His$_6$ E72D*	pBAD *So ctaA-V5-His$_6$* with E72D substitution	This study
pBAD *So ctaA-V5-His$_6$ E72Q*	pBAD *So ctaA-V5-His$_6$* with E72Q substitution	This study
pBAD *So ctaA-V5-His$_6$ H241A*	pBAD *So ctaA-V5-His$_6$* with H241A substitution	This study
pBAD *So ctaA-V5-His$_6$ H241E*	pBAD *So ctaA-V5-His$_6$* with H241E substitution	This study
pBAD *So ctaA-V5-His$_6$ H75A, H134A*	pBAD *So ctaA-V5-His$_6$* with H75A, H134A substitutions	This study
pBAD *So ctaA-V5-His$_6$ H244A, H302A*	pBAD *So ctaA-V5-His$_6$* with H244A, H302A substitutions	This study
pBAD *So ctaA-MBP-V5-His$_6$*	pBAD with *S. oneidnesis ctaA-MBP-V5-His$_6$*; *araBAD* promoter; linker between CtaA and MBP: NSSSVPG	This study
pBBR1 MCS3	Empty pBBR1 MCS3	(83)
pBBR1-RBS *So ctaB*	pBBR1-MCS3 with *S. oneidensis ctaB* preceded by a new RBS; *lac* promoter (constitutive expression in *S. ondeidensis*)	This study
pRS426 empty	Empty pRS426 vector	(84)
pRS426 *COX15-FLAG*	pRS426 with *S. cerevisiae COX15-FLAG*; *MET25 promoter, CYC1 terminator*	(47)
pRS426 *COX15-FLAG E166A*	pRS426 *COX15-FLAG* with E166A substitution	Oleh Khalimonchuk, University of Nebraska-Lincoln
pRS426 *COX15-FLAG E166D*	pRS426 *COX15-FLAG* with E166D substitution	
pRS426 *COX15-FLAG R369C*	pRS426 *COX15-FLAG* with R369C substitution	

Table 3.2: Bacterial and yeast plasmids and strains used in this study

Protein expression in S. oneidensis

For purification of His-tagged *So*HAS, a 5 mL-inoculum of transformed *S. oneidensis* culture (grown overnight) was used to inoculate 500 mL of LB in a 2 L baffled flask. When necessary, the medium was supplemented with 50 mg/mL kanamycin to select for pBAD and 1 mg/mL tetracycline to select for pBBR1. After the cultures reached an OD_{600} of approximately 1, protein expression was induced by the addition of 0.2% arabinose followed by incubation overnight (16-20 h) at 30 °C. The equivalent of 10-20 mL of cells at OD = 1 was collected by centrifugation and flash frozen for heme extraction. The remaining culture was harvested by low-speed centrifugation (12,000 x *g*) at 4 °C.

In some cases, small-scale *S. oneidensis* cultures were grown for the purpose of whole cell heme extraction. In this case, approximately 0.25 mL of a transformed *S. oneidensis* culture grown overnight was used to inoculate 25 mL of LB in a 250 mL Erlenmeyer flask. Expression of *So*HAS was induced as described above, and the equivalent of 20 mL at OD_{600} = 1 was harvested for heme extraction. The remaining culture was also harvested so that expression levels of *So*HAS could be evaluated. Cell pellets were flash frozen and stored at -80 °C.

Protein purification from S. oneidensis

Samples were kept cold (at 4 °C or on ice) for the entire procedure. The cell pellet from a large-scale (500 mL) *S. oneidensis* culture was resuspended in 10 mL of Buffer 1 (25 mM Tris-HCl, pH 8.0, 50 mM NaCl, 10% glycerol, 1 mM phenylmethylsulfonyl fluoride (PMSF), 1 mM EDTA, 0.02% NaN_3). At this point, the cell suspension was either immediately used for protein purification or frozen and stored at -80 °C. Cells were lysed via sonication ten times for 10 s each and then centrifuged at 22,000 x *g* for 30 min. The supernatant was transferred to a new centrifuge tube and centrifuged at 100,600 x *g* for 60 min to pellet the membrane fraction. The membrane pellet was resuspended in 9 mL of Buffer 2 (50 mM Tris-

HCl, pH 8.0, 300 mM NaCl, 10% glycerol, 1 mM PMSF, 0.02% NaN_3) and homogenized (ten strokes). Either *n*-dodecyl-β-D-maltopyranoside (DDM) (His tag purifications) or Triton X-100 (MBP tag purifications) was added to a final concentration of 1%, and the samples were incubated on a rocking platform 1-2 h and centrifuged again for 30 min at 100,600 x *g*. The supernatant was incubated with either 0.5 mL of nickel-nitrilotriacetic acid (Ni-NTA) resin for His tag purifications or with 0.25 mL of amylose resin for MBP tag purifications. For His tag purifications, 10 mM imidazole was also added to decrease non-specific binding. Following 1-2 h of incubation, the resin was transferred to a column, washed, and eluted. For His tag purifications, the resin was washed first with 10 column volumes of Buffer 2 supplemented with 10 mM imidazole and 0.02% DDM, and then with 10 column volumes of Buffer 2 supplemented with 25 mM imidazole and 0.02% DDM. Finally, the His-tagged protein was eluted with 200 mM imidazole and 0.02% DDM. For MBP tag purifications, the amylose resin was washed with 12 column volumes of Buffer 2 supplemented with 0.02% Triton X-100 and eluted with Buffer 2 supplemented with 10 mM maltose and 0.02% Triton X-100.

Yeast growth and mitochondrial isolation

All experiments with *S. cerevisiae* were performed in a *Δcox15* DY5113 background (*MATa, ade2-, can1-, leu2-, ura3-, trp1-, his-, COX15::KanMX*), in which the *COX15* gene was replaced by the *KanMX* cassette (Table 3.2) (82,85,86). This strain was transformed with the episomal vector pRS426 inserted with either the gene for WT Cox15-FLAG or the gene for a Cox15-FLAG variant (E166A, E166D) under the control of the native *MET25* promoter. An empty pRS426 vector lacking *COX15* was used as a negative control. Yeast cells were grown in synthetic medium (2% glucose); uracil was omitted from the medium to select for the presence of pRS426. All plasmids used in the Cox15 mutant studies were a kind gift from Dr. Oleh Khalimonchuk (University of Nebraska-Lincoln).

Yeast cultures were grown in synthetic medium (2% glucose) lacking uracil. Small (250 mL) cultures were grown for 20 h and used to inoculate a larger (1 L) culture (initial OD_{600} 0.1) which was grown for 2 days (~44 h). The cells were harvested by centrifugation for 10 min at 4696 x *g*, washed once with 40 mL of ice-cold water, and flash frozen. Crude mitochondria were isolated following previously published procedures (87,88).

Heme extraction

Extraction of non-covalently bound hemes was performed using a modified version of previously described protocols (89). Briefly, a hydrochloric acid-acetone mixture (HCl-acetone) was prepared by mixing 0.5 mL of concentrated (~33% w/w or 12 M) HCl with 9.5 mL acetone (final HCl concentration ~1.7%). An aqueous, heme-containing sample (purified protein, *S. oneidensis* cell suspension, or *S. cerevisiae* crude mitochondria) was then combined with HCl-acetone in a 2:3 ratio. This mixture was incubated on ice for 20 min with brief vortexing at 0, 10, and 20 min. The sample was then centrifuged at 21,130 x *g* for 10 min at room temperature. The supernatant was transferred to a new 1.7 mL microfuge tube and centrifuged again to remove any remaining insoluble material. The supernatant was then removed and analyzed by reversed-phase HPLC.

Typically, 30-50 μL of purified HAS was used in an extraction. To analyze the non-covalently bound hemes in *S. oneidensis*, frozen cell pellets were thawed and resuspended in 200 μL of water. A 100 μL aliquot was then transferred to a 1.7 mL microfuge tube containing 150 μL of 5% HCl-acetone. To analyze the heme content in *S. cerevisiae* crude mitochondrial extracts, 0.25-0.5 mg of total protein (suspended in 600 mM sorbitol, 20 mM HEPES buffer, pH 7.4) was added to an appropriate volume of HCl-acetone.

Heme analysis by HPLC

Hemes were separated and analyzed on an Agilent HPLC system (1260 Infinity) equipped with a diode array detector (Agilent G1315D) using a modified version of a previously

published reversed-phase HPLC procedure (18,90). The extracted hemes (10 μL) were injected onto a C18 column (Agilent 699975-902) and resolved using a gradient of solvent A (water, 0.1% trifluoracetic acid (TFA)) and solvent B (acetonitrile, 0.1% TFA). The chromatography conditions were as follows: 1-2.67 min: 75% A, 25% B; 2.67-12.67 min: gradient from 75% A, 25% B to 100% B; 12.67-20 min 100% B; 20-23 min gradient to return to starting conditions, 75% A, 25% B; with a constant 1.18 mL /min flow rate throughout. Each heme type was identified by its retention time and Soret peak (27). Retention times were determined by the analysis of known standards. hemin (heme *b* chloride) (Sigma H9039) and protoporphyrin IX (Frontier Scientific Porphyrin Products P562-9) were commercially available. Heme *o* and heme *a* standards were isolated from *E. coli* expressing the bo_3 quinol oxidase and bovine heart, respectively, as previously described (27).

Carbon monoxide binding

CO binding experiments were performed with as-isolated *So*HAS-His_6 (0.75 μM heme *b*, 0.7 mg/mL total protein, minimum heme/HAS molar ratio 0.04[4]) or *So*HAS-MBP-His_6 (0.4-7 μM heme *b*, 0.4-1.0 mg/mL total protein, minimum heme/HAS molar ratio 0.5-0.7) using a protocol based on previously published assays (91,92). All UV-Vis absorption spectra were measured using an HP 8453 spectrophotometer. A 500 μL aliquot of HAS was centrifuged at 17,000 x *g* for 15 min at 4 °C to pellet insoluble material. The clarified protein solution was transferred to a Schlenk cuvette, and the cuvette was sealed with a rubber septum. After the head space of the cuvette was purged with argon and mixed, the initial air-oxidized absorbance spectrum was measured. To reduce the heme, 1-5 μL of a 50 mM sodium

[4] Heme/HAS ratio was calculated by assuming that all of the protein in a given sample was HAS. Since some contaminating proteins were present (as judged by Coomassie stain), especially in the *So*HAS-His_6 sample, the calculated ratio represents the minimum heme/HAS ratio.

dithionite (prepared in degassed Buffer 2) was added to the cuvette via a gastight syringe. Reduction was judged to be complete when the Soret peak shifted and the peak for sodium dithionite at ~320 nm appeared. Finally, the cuvette was purged with CO in a fume hood by introducing CO via the side arm of the cuvette at a low flow rate from a gas cylinder equipped with a regulator. An exit needle was added to the septum sealing the cuvette to allow for head space exchange. After mixing, the absorbance spectrum was measured again to obtain the ferrous CO spectrum. As a positive control, the ferrous CO spectra of different concentrations of myoglobin (1 μM and 10 μM) were also measured (data not shown).

SDS-PAGE, Coomassie staining, and immunodetection

Protein samples were separated on 10% acrylamide SDS-PAGE gels. Following SDS-PAGE separation, protein was either visualized by Coomassie staining or transferred to a polyvinylidene difluoride (PVDF) membrane. The PVDF membranes were then immunodecorated with the appropriate primary and secondary antibodies. The following primary antibodies were used: anti His (Lifetein LT0426), anti FLAG (Sigma F7425), and anti-porin (Thermo 459500). The secondary antibody used following decoration with anti His or anti porin antibodies was goat anti mouse (Pierce #31430; lot PF202430). The secondary antibody used following the anti FLAG antibody was the goat anti rabbit (Abcam #6721; lot GR169100-2) antibody. All blots were imaged with a Chemi-Doc MP imager (Bio-Rad).

REFERENCES

REFERENCES

1. Ferguson-Miller, S., and Babcock, G. T. (1996) Heme/copper terminal oxidases. *Chem Rev* **96**, 2889-2908

2. Garcia-Horsman, J. A., Barquera, B., Rumbley, J., Ma, J., and Gennis, R. B. (1994) The superfamily of heme-copper respiratory oxidases. *J Bacteriol* **176**, 5587-5600

3. Schafer, G., Engelhard, M., and Muller, V. (1999) Bioenergetics of the Archaea. *Microbiol Mol Biol Rev* **63**, 570-620

4. Refojo, P. N., Sena, F. V., Calisto, F., Sousa, F. M., and Pereira, M. M. (2019) Chapter six: the plethora of membrane respiratory chains in the phyla of life. in *Advances in Microbial Physiology* (Poole, R. K. ed.), Academic Press. pp 331-414

5. Borisov, V. B., Gennis, R. B., Hemp, J., and Verkhovsky, M. I. (2011) The cytochrome *bd* respiratory oxygen reductases. *Biochim Biophys Acta* **1807**, 1398-1413

6. Hemp, J. G., Robert, B. (2008) Bioenergetics: energy conservation and conversion. in *Bioenergetics: Energy Conservation and Conversion* (Schäfer, G. n. P., Harvey S. ed., 2008 Ed., Springer, Berlin

7. Pereira, M. M., Santana, M., and Teixeira, M. (2001) A novel scenario for the evolution of haem-copper oxygen reductases. *Biochim Biophys Acta* **1505**, 185-208

8. Pereira, M. M., Sousa, F. L., Veríssimo, A. F., and Teixeira, M. (2008) Looking for the minimum common denominator in haem-copper oxygen reductases: towards a unified catalytic mechanism. *Biochim Biophys Acta* **1777**, 929-934

9. Quadalti, C., Brunetti, D., Lagutina, I., Duchi, R., Perota, A., Lazzari, G., Cerutti, R., Di Meo, I., Johnson, M., Bottani, E., Crociara, P., Corona, C., Grifoni, S., Tiranti, V., Fernandez-Vizarra, E., Robinson, A. J., Viscomi, C., Casalone, C., Zeviani, M., and Galli, C. (2018) SURF1 knockout cloned pigs: Early onset of a severe lethal phenotype. *Biochimica et biophysica acta. Molecular basis of disease* **1864**, 2131-2142

10. Robinson, B. H. (2000) Human cytochrome oxidase deficiency. *Pediatric research* **48**, 581-585

11. Fontanesi, F., Soto, I. C., Horn, D., and Barrientos, A. (2006) Assembly of mitochondrial cytochrome c-oxidase, a complicated and highly regulated cellular process. *American journal of physiology. Cell physiology* **291**, C1129-1147

12. Kim, H. J., Khalimonchuk, O., Smith, P. M., and Winge, D. R. (2012) Structure, function, and assembly of heme centers in mitochondrial respiratory complexes. *Biochim Biophys Acta* **1823**, 1604-1616

13. Timón-Gómez, A., Nývltová, E., Abriata, L. A., Vila, A. J., Hosler, J., and Barrientos, A. (2018) Mitochondrial cytochrome *c* oxidase biogenesis: recent developments. *Seminars in cell & developmental biology* **76**, 163-178

14. Antonicka, H., Leary, S. C., Guercin, G. H., Agar, J. N., Horvath, R., Kennaway, N. G., Harding, C. O., Jaksch, M., and Shoubridge, E. A. (2003) Mutations in *COX10* result in a defect in mitochondrial heme A biosynthesis and account for multiple, early-onset clinical phenotypes associated with isolated COX deficiency. *Human molecular genetics* **12**, 2693-2702

15. Antonicka, H., Mattman, A., Carlson, C. G., Glerum, D. M., Hoffbuhr, K. C., Leary, S. C., Kennaway, N. G., and Shoubridge, E. A. (2003) Mutations in *COX15* produce a defect in the mitochondrial heme biosynthetic pathway, causing early-onset fatal hypertrophic cardiomyopathy. *American journal of human genetics* **72**, 101-114

16. Oquendo, C. E., Antonicka, H., Shoubridge, E. A., Reardon, W., and Brown, G. K. (2004) Functional and genetic studies demonstrate that mutation in the *COX15* gene can cause Leigh syndrome. *Journal of medical genetics* **41**, 540-544

17. Khalimonchuk, O., Bestwick, M., Meunier, B., Watts, T. C., and Winge, D. R. (2010) Formation of the redox cofactor centers during Cox1 maturation in yeast cytochrome oxidase. *Molecular and cellular biology* **30**, 1004-1017

18. Del Arenal, I. P., Contreras, M. L., Svlateorova, B. B., Rangel, P., Lledías, F., Dávila, J. R., and Escamilla, J. E. (1997) Haem O and a putative cytochrome *bo* in a mutant of *Bacillus cereus* impaired in the synthesis of haem A. *Archives of microbiology* **167**, 24-31

19. van der Oost, J., von Wachenfeld, C., Hederstedt, L., and Saraste, M. (1991) *Bacillus subtilis* cytochrome oxidase mutants: biochemical analysis and genetic evidence for two aa_3-type oxidases. *Molecular microbiology* **5**, 2063-2072

20. Puustinen, A., and Wikstrom, M. (1991) The heme groups of cytochrome *o* from *Escherichia coli*. *Proceedings of the National Academy of Sciences* **88**, 6122-6126

21. Mueller, J. P., and Taber, H. W. (1989) Structure and expression of the cytochrome aa_3 regulatory gene *ctaA* of *Bacillus subtilis*. *Journal of Bacteriology* **171**, 4979-4986

22. Svensson, B., Andersson, K. K., and Hederstedt, L. (1996) Low-spin heme A in the heme A biosynthetic protein CtaA from *Bacillus subtilis*. *European journal of biochemistry* **238**, 287-295

23. Svensson, B., and Hederstedt, L. (1994) *Bacillus subtilis* CtaA is a heme-containing membrane protein involved in heme A biosynthesis. *J Bacteriol* **176**, 6663-6671

24. Svensson, B., Lübben, M., and Hederstedt, L. (1993) *Bacillus subtilis* CtaA and CtaB function in haem A biosynthesis. *Molecular microbiology* **10**, 193-201

25. Mogi, T., Saiki, K., and Anraku, Y. (1994) Biosynthesis and functional role of haem O and haem A. *Molecular microbiology* **14**, 391-398

26. Barros, M. H., Carlson, C. G., Glerum, D. M., and Tzagoloff, A. (2001) Involvement of mitochondrial ferredoxin and Cox15p in hydroxylation of heme O. *FEBS letters* **492**, 133-138

27. Brown, K. R., Allan, B. M., Do, P., and Hegg, E. L. (2002) Identification of novel hemes generated by heme A synthase: evidence for two successive monooxygenase reactions. *Biochemistry* **41**, 10906-10913

28. Brown, K. R., Brown, B. M., Hoagland, E., Mayne, C. L., and Hegg, E. L. (2004) Heme A synthase does not incorporate molecular oxygen into the formyl group of heme A. *Biochemistry* **43**, 8616-8624

29. Hill, J., Goswitz, V. C., Calhoun, M., Garcia-Horsman, J. A., Lemieux, L., Alben, J. O., and Gennis, R. B. (1992) Demonstration by FTIR that the *bo*-type ubiquinol oxidase of *Escherichia coli* contains a heme-copper binuclear center similar to that in cytochrome *c* oxidase and that proper assembly of the binuclear center requires the *cyoE* gene product. *Biochemistry* **31**, 11435-11440

30. Saiki, K., Mogi, T., and Anraku, Y. (1992) Heme O biosynthesis in *Escherichia coli*: the *cyoE* gene in the cytochrome *bo* operon encodes a protoheme IX farnesyltransferase. *Biochemical and biophysical research communications* **189**, 1491-1497

31. Saiki, K., Mogi, T., Ogura, K., and Anraku, Y. (1993) *In vitro* heme O synthesis by the *cyoE* gene product from *Escherichia coli*. *J. Biol. Chem.* **268**, 26041-26044

32. Glerum, D. M., and Tzagoloff, A. (1994) Isolation of a human cDNA for heme A:farnesyltransferase by functional complementation of a yeast *cox10* mutant. *Proceedings of the National Academy of Sciences* **91**, 8452-8456

33. Nobrega, M. P., Nobrega, F. G., and Tzagoloff, A. (1990) *COX10* codes for a protein homologous to the ORF1 product of *Paracoccus denitrificans* and is required for the synthesis of yeast cytochrome oxidase. *J. Biol. Chem.* **265**, 14220-14226

34. Li, W. (2016) Bringing bioactive compounds into membranes: the UbiA superfamily of intramembrane aromatic prenyltransferases. *Trends in biochemical sciences* **41**, 356-370

35. Poulter, C. D., and Rilling, H. C. (1978) The prenyl transfer reaction: enzymatic and mechanistic studies of the 1'-4 coupling reaction in the terpene biosynthetic pathway. *Accounts of Chemical Research* **11**, 307-313

36. Hosfield, D. J., Zhang, Y., Dougan, D. R., Broun, A., Tari, L. W., Swanson, R. V., and Finn, J. (2004) Structural basis for bisphosphonate-mediated inhibition of isoprenoid biosynthesis. *J. Biol. Chem.* **279**, 8526-8529

37. Kavanagh, K. L., Dunford, J. E., Bunkoczi, G., Russell, R. G., and Oppermann, U. (2006) The crystal structure of human geranylgeranyl pyrophosphate synthase reveals a novel hexameric arrangement and inhibitory product binding. *J. Biol. Chem.* **281**, 22004-22012

38. Saiki, K., Mogi, T., Hori, H., Tsubaki, M., and Anraku, Y. (1993) Identification of the functional domains in heme O synthase: site-directed mutagenesis studies on the *cyoE* gene of the cytochrome *bo* operon in *Escherichia coli*. *J. Biol. Chem.* **268**, 26927-26934

39. Sakamoto, J., Hayakawa, A., Uehara, T., Noguchi, S., and Sone, N. (1999) Cloning of *Bacillus stearothermophilus ctaA* and heme A synthesis with the CtaA protein produced in *Escherichia coli*. *Bioscience, biotechnology, and biochemistry* **63**, 96-103

40. Sono, M., Roach, M. P., Coulter, E. D., and Dawson, J. H. (1996) Heme-containing oxygenases. *Chem Rev* **96**, 2841-2888

41. Schneegurt, M. A., and Beale, S. I. (1992) Origin of the chlorophyll *b* formyl oxygen in *Chlorella vulgaris*. *Biochemistry* **31**, 11677-11683

42. Porra, R. J., Schäfer, W., Cmiel, E., Katheder, I., and Scheer, H. (1993) Derivation of the formyl-group oxygen of chlorophyll *b* from molecular oxygen in greening leaves of a higher plant (*Zea mays*). *FEBS letters* **323**, 31-34

43. Hederstedt, L. (2012) Heme A biosynthesis. *Biochim Biophys Acta* **1817**, 920-927

44. Lewin, A., and Hederstedt, L. (2006) Compact archaeal variant of heme A synthase. *FEBS letters* **580**, 5351-5356

45. Hederstedt, L., Lewin, A., and Throne-Holst, M. (2005) Heme A synthase enzyme functions dissected by mutagenesis of *Bacillus subtilis* CtaA. *J Bacteriol* **187**, 8361-8369

46. Mogi, T. (2009) Probing structure of heme A synthase from *Bacillus subtilis* by site-directed mutagenesis. *Journal of biochemistry* **145**, 625-633

47. Swenson, S., Cannon, A., Harris, N. J., Taylor, N. G., Fox, J. L., and Khalimonchuk, O. (2016) Analysis of oligomerization properties of heme *a* synthase provides insights into its function in eukaryotes. *J. Biol. Chem.* **291**, 10411-10425

48. Bareth, B., Dennerlein, S., Mick, D. U., Nikolov, M., Urlaub, H., and Rehling, P. (2013) The heme *a* synthase Cox15 associates with cytochrome *c* oxidase assembly intermediates during Cox1 maturation. *Molecular and cellular biology* **33**, 4128-4137

49. Merli, M. L., Cirulli, B. A., Menéndez-Bravo, S. M., and Cricco, J. A. (2017) Heme A synthesis and C*c*O activity are essential for *Trypanosoma cruzi* infectivity and replication. *The Biochemical journal* **474**, 2315-2332

50. Niwa, S., Takeda, K., Kosugi, M., Tsutsumi, E., Mogi, T., and Miki, K. (2018) Crystal structure of heme A synthase from *Bacillus subtilis*. *Proceedings of the National Academy of Sciences of the United States of America* **115**, 11953-11957

51. Zeng, H., Zhu, G., Zhang, S., Li, X., Martin, J., Morgner, N., Sun, F., Peng, G., Xie, H., and Michel, H. (2020) Isolated heme A synthase from *Aquifex aeolicus* is a trimer. *mBio* **11**

52. Colas, C., Kuo, J. M., and Ortiz de Montellano, P. R. (2002) Asp-225 and Glu-375 in autocatalytic attachment of the prosthetic heme group of lactoperoxidase. *J. Biol. Chem.* **277**, 7191-7200

53. Ortiz de Montellano, P. R. (2008) Mechanism and role of covalent heme binding in the CYP4 family of P_{450} enzymes and the mammalian peroxidases. *Drug metabolism reviews* **40**, 405-426

54. Le Laz, S., Kpebe, A., Bauzan, M., Lignon, S., Rousset, M., and Brugna, M. (2014) A biochemical approach to study the role of the terminal oxidases in aerobic respiration in *Shewanella oneidensis* MR-1. *PloS one* **9**, e86343

55. Le Laz, S., Kpebe, A., Bauzan, M., Lignon, S., Rousset, M., and Brugna, M. (2016) Expression of terminal oxidases under nutrient-starved conditions in *Shewanella oneidensis*: detection of the A-type cytochrome *c* oxidase. *Scientific reports* **6**, 19726

56. Hiner, A. N., Raven, E. L., Thorneley, R. N., García-Cánovas, F., and Rodríguez-López, J. N. (2002) Mechanisms of compound I formation in heme peroxidases. *Journal of inorganic biochemistry* **91**, 27-34

57. Poulos, T. L. (2010) Thirty years of heme peroxidase structural biology. *Archives of biochemistry and biophysics* **500**, 3-12

58. He, D., Fu, C. J., and Baldauf, S. L. (2016) Multiple origins of eukaryotic *cox15* suggest horizontal gene transfer from bacteria to jakobid mitochondrial DNA. *Molecular biology and evolution* **33**, 122-133

59. Furtmüller, P. G., Zederbauer, M., Jantschko, W., Helm, J., Bogner, M., Jakopitsch, C., and Obinger, C. (2006) Active site structure and catalytic mechanisms of human peroxidases. *Archives of biochemistry and biophysics* **445**, 199-213

60. Denisov, I. G., Makris, T. M., Sligar, S. G., and Schlichting, I. (2005) Structure and chemistry of cytochrome P_{450}. *Chem Rev* **105**, 2253-2277

61. Erman, J. E., and Vitello, L. B. (2002) Yeast cytochrome *c* peroxidase: mechanistic studies via protein engineering. *Biochim Biophys Acta* **1597**, 193-220

62. Nicolussi, A., Auer, M., Sevcnikar, B., Paumann-Page, M., Pfanzagl, V., Zámocký, M., Hofbauer, S., Furtmüller, P. G., and Obinger, C. (2018) Posttranslational modification of heme in peroxidases: impact on structure and catalysis. *Archives of biochemistry and biophysics* **643**, 14-23

63. Matsson, M., Tolstoy, D., Aasa, R., and Hederstedt, L. (2000) The distal heme center in *Bacillus subtilis* succinate:quinone reductase is crucial for electron transfer to menaquinone. *Biochemistry* **39**, 8617-8624

64. Zaidi, S., Hassan, M. I., Islam, A., and Ahmad, F. (2014) The role of key residues in structure, function, and stability of cytochrome-*c*. *Cellular and molecular life sciences : CMLS* **71**, 229-255

65. Winkler, J. R., and Gray, H. B. (2014) Electron flow through metalloproteins. *Chem Rev* **114**, 3369-3380

66. Wen, X., Patel, K. M., Russell, B. S., and Bren, K. L. (2007) Effects of heme pocket structure and mobility on cytochrome *c* stability. *Biochemistry* **46**, 2537-2544

67. Lewin, A., and Hederstedt, L. (2016) Heme A synthase in bacteria depends on one pair of cysteinyls for activity. *Biochim Biophys Acta* **1857**, 160-168

68. Liu, J., Chakraborty, S., Hosseinzadeh, P., Yu, Y., Tian, S., Petrik, I., Bhagi, A., and Lu, Y. (2014) Metalloproteins containing cytochrome, iron–sulfur, or copper redox centers. *Chemical Reviews* **114**, 4366-4469

69. Zoppellaro, G., Bren, K. L., Ensign, A. A., Harbitz, E., Kaur, R., Hersleth, H.-P., Ryde, U., Hederstedt, L., and Andersson, K. K. (2009) Review: studies of ferric heme proteins with highly anisotropic/highly axial low spin (S = 1/2) electron paramagnetic resonance signals with *bis*-histidine and histidine-methionine axial iron coordination. *Biopolymers* **91**, 1064-1082

70. Stein, N., Love, D., Judd, E. T., Elliott, S. J., Bennett, B., and Pacheco, A. A. (2015) Correlations between the electronic properties of *Shewanella oneidensis* cytochrome *c* nitrite reductase (ccNiR) and its structure: effects of heme oxidation state and active site ligation. *Biochemistry* **54**, 3749-3758

71. Berglund, G. I., Carlsson, G. H., Smith, A. T., Szöke, H., Henriksen, A., and Hajdu, J. (2002) The catalytic pathway of horseradish peroxidase at high resolution. *Nature* **417**, 463-468

72. Regelsberger, G., Jakopitsch, C., Rüker, F., Krois, D., Peschek, G. A., and Obinger, C. (2000) Effect of distal cavity mutations on the formation of compound I in catalase-peroxidases. *J. Biol. Chem.* **275**, 22854-22861

73. Choudhury, K., Sundaramoorthy, M., Mauro, J. M., and Poulos, T. L. (1992) Conversion of the proximal histidine ligand to glutamine restores activity to an inactive mutant of cytochrome *c* peroxidase. *J. Biol. Chem.* **267**, 25656-25659

74. Hsiao, H. C., Boycheva, S., Watmough, N. J., and Brittain, T. (2007) Activation of the cytochrome *c* peroxidase of *Pseudomonas aeruginosa*. The role of a heme-linked protein loop: a mutagenesis study. *Journal of inorganic biochemistry* **101**, 1133-1139

75. Dias, J. M., Alves, T., Bonifácio, C., Pereira, A. S., Trincão, J., Bourgeois, D., Moura, I., and Romão, M. J. (2004) Structural basis for the mechanism of Ca^{2+} activation of the di-heme cytochrome *c* peroxidase from *Pseudomonas nautica* 617. *Structure (London, England : 1993)* **12**, 961-973

76. Sybirna, K., Antoine, T., Lindberg, P., Fourmond, V., Rousset, M., Méjean, V., and Bottin, H. (2008) *Shewanella oneidensis*: a new and efficient system for expression and maturation of heterologous [Fe-Fe] hydrogenase from *Chlamydomonas reinhardtii*. *BMC biotechnology* **8**, 73

77. Ozawa, K., Yasukawa, F., Fujiwara, Y., and Akutsu, H. (2001) A simple, rapid, and highly efficient gene expression system for multiheme cytochromes *c*. *Bioscience, biotechnology, and biochemistry* **65**, 185-189

78. Corts, A. D., Thomason, L. C., Gill, R. T., and Gralnick, J. A. (2019) A new recombineering system for precise genome-editing in *Shewanella oneidensis* strain MR-1 using single-stranded oligonucleotides. *Scientific reports* **9**, 39

79. Coursolle, D., and Gralnick, J. A. (2012) Reconstruction of extracellular respiratory pathways for iron(III) reduction in *Shewanella oneidensis* strain MR-1. *Frontiers in microbiology* **3**, 56

80. Saltikov, C. W., and Newman, D. K. (2003) Genetic identification of a respiratory arsenate reductase. *Proceedings of the National Academy of Sciences of the United States of America* **100**, 10983-10988

81. Myers, C. R., and Nealson, K. H. (1988) Bacterial manganese reduction and growth with manganese oxide as the sole electron acceptor. *Science (New York, N.Y.)* **240**, 1319-1321

82. Herwaldt, E. J., Rivett, E. D., White, A. J., and Hegg, E. L. (2018) Cox15 interacts with the cytochrome bc_1 dimer within respiratory supercomplexes as well as in the absence of cytochrome *c* oxidase. *J. Biol. Chem.* **293**, 16426-16439

83. Kovach, M. E., Elzer, P. H., Hill, D. S., Robertson, G. T., Farris, M. A., Roop, R. M., 2nd, and Peterson, K. M. (1995) Four new derivatives of the broad-host-range cloning vector pBBR1MCS, carrying different antibiotic-resistance cassettes. *Gene* **166**, 175-176

84. Christianson, T. W., Sikorski, R. S., Dante, M., Shero, J. H., and Hieter, P. (1992) Multifunctional yeast high-copy-number shuttle vectors. *Gene* **110**, 119-122

85. Longtine, M. S., McKenzie, A., 3rd, Demarini, D. J., Shah, N. G., Wach, A., Brachat, A., Philippsen, P., and Pringle, J. R. (1998) Additional modules for versatile and economical PCR-based gene deletion and modification in *Saccharomyces cerevisiae*. *Yeast* **14**, 953-961

86. Gietz, R. D., and Schiestl, R. H. (2007) High-efficiency yeast transformation using the LiAc/SS carrier DNA/PEG method. *Nature protocols* **2**, 31-34

87. Lange, H., Kispal, G., and Lill, R. (1999) Mechanism of iron transport to the site of heme synthesis inside yeast mitochondria. *J. Biol. Chem.* **274**, 18989-18996

88. Diekert, K., de Kroon, A. I., Kispal, G., and Lill, R. (2001) Isolation and subfractionation of mitochondria from the yeast *Saccharomyces cerevisiae*. *Methods in cell biology* **65**, 37-51

89. Weinstein, J. D., and Beale, S. I. (1983) Separate physiological roles and subcellular compartments for two tetrapyrrole biosynthetic pathways in *Euglena gracilis*. *J. Biol. Chem.* **258**, 6799-6807

90. Lübben, M., and Morand, K. (1994) Novel prenylated hemes as cofactors of cytochrome oxidases: archaea have modified hemes A and O. *J. Biol. Chem.* **269**, 21473-21479

91. Guengerich, F. P., Martin, M. V., Sohl, C. D., and Cheng, Q. (2009) Measurement of cytochrome P_{450} and NADPH-cytochrome P_{450} reductase. *Nature protocols* **4**, 1245-1251

92. Bailey, J. A. (2011) An undergraduate laboratory experiment in bioinorganic chemistry: ligation states of myoglobin. *Journal of Chemical Education* **88**, 995-998

Chapter 4: Conclusions and future outlook

Heme *a* synthase (HAS) is a fascinating but still somewhat enigmatic enzyme. The primary role of this enzyme is fairly clear: HAS catalyzes the second step of the heme *a* biosynthetic pathway to provide a cofactor for heme-copper oxidases. However, a detailed understanding of the catalytic mechanism of HAS and its role in prenylated heme trafficking has remained elusive, partly due to the difficulties in expressing and purifying HAS. Despite these challenges, the recent structural advances made by other groups in the last few years (discussed in Chapter 1) (1,2), and the insight into the protein-protein interactions and mechanism of HAS presented in Chapters 2 (3) and 3 have helped expand our understanding of the catalytic mechanism of HAS and its role within the cell. As is often the case with research projects, these new data have both informed previous hypotheses about the function of HAS and raised new intriguing questions.

From a mechanistic standpoint, HAS is somewhat unusual. Previous isotopic studies indicate that HAS is an oxygen-activating enzyme that uses a peroxidase-like mechanism (4), and my mutagenesis data highlighting the need for a negatively charged residue in the N-terminal heme binding pocket (Chapter 3) is consistent with this proposed mechanism. However, many questions about the catalytic mechanism remain. For example, the site of O_2 binding has not been conclusively demonstrated. Most peroxidases have a pentacoordinate heme with a proximal histidine ligand, while the distal coordination site of the heme is vacant and thus available for peroxide binding. In contrast, both heme *a* and heme *b* appear to be hexacoordinate in as-purified *Bacillus subtilis* HAS (*Bs*HAS) (5), making it unclear where O_2 binds. Presumably, one of the histidine ligands dissociates to allow O_2 to bind either heme *o* or heme *b*. The observation that the N-terminal half of HAS has more conserved residues than the C-terminal half suggests that the N-terminal domain is the site of O_2 binding, as a set of highly conserved residues is typically required for O-O bond cleavage in peroxidases (6-8). This hypothesis is strengthened by *in vivo* activity assays performed with *Bs*HAS

expressed in *B. subtilis*, which indicate the two N-terminal histidines are more critical for catalytic activity than the C-terminal histidines (9,10). While not definitive, our current CO binding data are also consistent with the hypothesis that the N-terminal heme *o* binding pocket is the site of oxygen activation.

Assuming that this autocatalytic method of O_2 activation is correct, this leads to another question: Which histidine is the "proximal" ligand that remains bound to the heme iron throughout the catalytic mechanism, and which is the "distal" ligand that dissociates from the heme iron in order to allow O_2 to bind? Based on the crystal structure of *Bs*HAS, it could be argued that H60 is the distal ligand, as this residue is located on transmembrane (TM) helix 2, which is bent away from the center of the N-terminal four-helical bundle and would presumably be positioned farther away from the heme iron when heme *o* binds. However, additional biochemical and spectroscopic data will be needed to test this hypothesis.

In addition to the mechanism of oxygen activation and catalysis, other aspects of HAS structure and function remain largely unexplored. For example, the elongated extracellular loop between transmembrane helices 1 and 2 includes a few nearly invariant residues, indicating that this loop plays an essential, albeit currently unidentified, role in the function of HAS. In the crystal structure, this loop plugs the top of the empty heme *o* binding site (1). Substrate binding would necessitate the movement of this loop out of the N-terminal heme binding pocket, but the structure L1-2 adopts in substrate-bound HAS is unknown, as is its potential function. Interestingly, a pair of cysteines in this loop that is strictly conserved and required for catalytic activity in type-1 HAS is replaced by hydrophobic residues in type-2 HAS, suggesting that this loop may play slightly different roles in the two different types of HAS (10-12). Obtaining the structure of type-2 HAS and HAS bound to substrate analogs

may help clarify the function of L1-2 and reveal any potential differences between the two major classes of HAS.

In addition to further structural characterization, an *in vitro* activity assay would be useful for elucidating the catalytic mechanism of HAS. Several challenges will have to be overcome to develop a viable *in vitro* activity assay. Besides requiring a substantial amount of purified HAS, such an assay would require successful delivery of heme *o* to the substrate heme binding site. Heme *o* delivery could be difficult because HAS often co-purifies with a substoichiometric amount of heme *b*, which suggests that in at least a fraction of purified HAS, the C-terminal heme binding site remains empty, leaving open the possibility that heme *o* could adventitiously bind to the cofactor heme binding site. Heme *o* is also very hydrophobic and could potentially bind non-specifically to the outside of HAS and convolute analysis of HAS turnover. This latter problem could potentially be solved by repurification of HAS after exogenous heme *o* addition. However, the hydrophobicity of heme *o* will complicate this separation, as using aqueous solvents to remove excess heme *o* from the surface of HAS will likely be inefficient. Another consideration is that release of the heme *a* product may be the rate-limiting step of the HAS reaction mechanism. If this is the case, a successful multiple-turnover *in vitro* activity assay would require addition of a second protein that could compete with HAS for heme *a*. Although overcoming these challenges will not be trivial, the development of an *in vitro* activity assay would be invaluable for studying the catalytic mechanism of HAS and strategically designed HAS variants.

Beyond the catalytic mechanism, another aspect of HAS function that is still under investigation is the role of this enzyme in prenylated heme trafficking. HAS co-purifies with heme *a*, suggesting that HAS may play a role in heme *a* delivery to cytochrome *c* oxidase. Consistent with this hypothesis, *Saccharomyces cerevisiae* HAS (*Sc*HAS) has been shown to interact with cytochrome *c* oxidase subunits and assembly factors (Chapter 2) (3,13,14).

Intriguingly, *Sc*HAS can also interact with cytochrome bc_1 subunits, even in the absence of fully assembled cytochrome *c* oxidase (Chapter 2) (3). This interaction with complex III could suggest that a fraction of HAS participates in assembly of complex IV that is already associated with complex III, one of the proposed methods of supercomplex formation. Additional investigations of supercomplex assembly and heme trafficking will be needed to validate this hypothesis.

In contrast to cytochrome *c* oxidase hemylation, the process of transferring heme *o* from heme *o* synthase (HOS) to HAS has not been investigated as thoroughly. Although it seems likely that the transfer of heme *o*, a redox active intermediate, would be a controlled process, the details of this transfer are unclear, especially in eukaryotes, where a stable interaction between HOS and HAS has never been demonstrated. Investigating the protein-protein interactions of HAS *in vivo* via Forster resonance energy transfer (FRET) might prove useful for determining if HOS and HAS interact transiently. Predicting protein-protein interaction interfaces of HAS computationally may also be possible once the structure of HOS is solved. Additionally, several fluorescent heme sensors have recently been developed for determining concentrations of labile intracellular heme *b* (15-18). In the future, these new techniques could potentially be adapted to study prenylated heme trafficking *in vivo*.

While the study of HAS is challenging, recent structural and technical advances promise to help move the field forward. The determination of the first structures of prokaryotic (type-1) HAS has confirmed the long-standing hypothesis that this enzyme has two heme binding sites and should prove useful for future experiments designed to probe the catalytic mechanism of HAS. Continued investigations of cytochrome *c* oxidase assembly and respiratory supercomplex assembly and function will likely contribute to our understanding of the role of HAS in heme *a* delivery to cytochrome *c* oxidase. Additional experimental and computational studies of the protein-protein interactions of HAS may also

help uncover the details of how heme *o* and heme *a* are transferred to and from HAS. Finally, new techniques for tracking labile heme concentrations *in vivo* also have the potential to broaden our understanding of prenylated heme transfer and its relation to intracellular heme trafficking as a whole. Thus, while there are still technical hurdles to overcome, the future of research into HAS promises to afford new insights into both metalloenzymology and heme metabolism.

REFERENCES

REFERENCES

1. Niwa, S., Takeda, K., Kosugi, M., Tsutsumi, E., Mogi, T., and Miki, K. (2018) Crystal structure of heme A synthase from *Bacillus subtilis*. *Proceedings of the National Academy of Sciences of the United States of America* **115**, 11953-11957

2. Zeng, H., Zhu, G., Zhang, S., Li, X., Martin, J., Morgner, N., Sun, F., Peng, G., Xie, H., and Michel, H. (2020) Isolated heme A synthase from *Aquifex aeolicus* is a trimer. *mBio* **11**

3. Herwaldt, E. J., Rivett, E. D., White, A. J., and Hegg, E. L. (2018) Cox15 interacts with the cytochrome bc_1 dimer within respiratory supercomplexes as well as in the absence of cytochrome *c* oxidase. *J. Biol. Chem.* **293**, 16426-16439

4. Brown, B. M., Wang, Z., Brown, K. R., Cricco, J. A., and Hegg, E. L. (2004) Heme O synthase and heme A synthase from *Bacillus subtilis* and *Rhodobacter sphaeroides* interact in *Escherichia coli*. *Biochemistry* **43**, 13541-13548

5. Svensson, B., Andersson, K. K., and Hederstedt, L. (1996) Low-spin heme A in the heme A biosynthetic protein CtaA from *Bacillus subtilis*. *European journal of biochemistry* **238**, 287-295

6. Sono, M., Roach, M. P., Coulter, E. D., and Dawson, J. H. (1996) Heme-containing oxygenases. *Chem Rev* **96**, 2841-2888

7. Hiner, A. N., Raven, E. L., Thorneley, R. N., García-Cánovas, F., and Rodríguez-López, J. N. (2002) Mechanisms of compound I formation in heme peroxidases. *Journal of inorganic biochemistry* **91**, 27-34

8. Poulos, T. L. (2010) Thirty years of heme peroxidase structural biology. *Archives of biochemistry and biophysics* **500**, 3-12

9. Hederstedt, L., Lewin, A., and Throne-Holst, M. (2005) Heme A synthase enzyme functions dissected by mutagenesis of *Bacillus subtilis* CtaA. *J Bacteriol* **187**, 8361-8369

10. Mogi, T. (2009) Probing structure of heme A synthase from *Bacillus subtilis* by site-directed mutagenesis. *Journal of biochemistry* **145**, 625-633

11. Hederstedt, L. (2012) Heme A biosynthesis. *Biochim Biophys Acta* **1817**, 920-927

12. Lewin, A., and Hederstedt, L. (2016) Heme A synthase in bacteria depends on one pair of cysteinyls for activity. *Biochim Biophys Acta* **1857**, 160-168

13. Taylor, N. G., Swenson, S., Harris, N. J., Germany, E. M., Fox, J. L., and Khalimonchuk, O. (2017) The assembly factor Pet117 couples heme *a* synthase activity to cytochrome oxidase assembly. *J. Biol. Chem.* **292**, 1815-1825

14. Bareth, B., Dennerlein, S., Mick, D. U., Nikolov, M., Urlaub, H., and Rehling, P. (2013) The heme *a* synthase Cox15 associates with cytochrome *c* oxidase assembly intermediates during Cox1 maturation. *Molecular and cellular biology* **33**, 4128-4137

15. Swenson, S. A., Moore, C. M., Marcero, J. R., Medlock, A. E., Reddi, A. R., and Khalimonchuk, O. (2020) From synthesis to utilization: the ins and outs of mitochondrial heme. *Cells* **9**

16. Abshire, J. R., Rowlands, C. J., Ganesan, S. M., So, P. T., and Niles, J. C. (2017) Quantification of labile heme in live malaria parasites using a genetically encoded biosensor. *Proceedings of the National Academy of Sciences of the United States of America* **114**, E2068-e2076

17. Hanna, D. A., Martinez-Guzman, O., and Reddi, A. R. (2017) Heme gazing: illuminating eukaryotic heme trafficking, dynamics, and signaling with fluorescent heme sensors. *Biochemistry* **56**, 1815-1823

18. Song, Y., Yang, M., Wegner, S. V., Zhao, J., Zhu, R., Wu, Y., He, C., and Chen, P. R. (2015) A genetically encoded FRET sensor for intracellular heme. *ACS chemical biology* **10**, 1610-1615